ERASMUS MUNDUS MSC PROGRAMME

COASTAL AND MARINE ENGINEERING AND MANAGEMENT
COMEM

# TYPHOON-INDUCED EXTREME WATER LEVELS NEAR SINGAPORE

## A NUMERICAL MODEL INVESTIGATION

Serene Tay Hui Xin

Delft University of Technology
June 2010

The Erasmus Mundus MSc Coastal and Marine Engineering and Management is an integrated programme organized by five European partner institutions, coordinated by Delft University of Technology (TU Delft). The joint study programme of 120 ECTS credits (two years full-time) has been obtained at three of the five CoMEM partner institutions:

- Norges Teknisk- Naturvitenskapelige Universitet (NTNU) Trondheim, Norway
- Technische Universiteit (TU) Delft, The Netherlands
- City University London, Great Britain
- Universitat Politècnica de Catalunya (UPC), Barcelona, Spain
- University of Southampton, Southampton, Great Britain

The first year consists of the first and second semesters of 30 ECTS each, spent at NTNU, Trondheim and Delft University of Technology respectively.
The second year allows for specialization in three subjects and during the third semester courses are taken with a focus on advanced topics in the selected area of specialization:

- Engineering
- Management
- Environment

In the fourth and final semester an MSc project and thesis have to be completed.

The two year CoMEM programme leads to three officially recognized MSc diploma certificates. These will be issued by the three universities which have been attended by the student. The transcripts issued with the MSc Diploma Certificate of each university include grades/marks for each subject. A complete overview of subjects and ECTS credits is included in the Diploma Supplement, as received from the CoMEM coordinating university, Delft University of Technology (TU Delft).

Information regarding the CoMEM programme can be obtained from the programme coordinator and director

Prof. Dr. Ir. Marcel J.F. Stive
Delft University of Technology
Faculty of Civil Engineering and geosciences
P.O. Box 5048
2600 GA Delft
The Netherlands

DELFT UNIVERSITY OF TECHNOLOGY
FACULTY OF CIVIL ENGINEERING AND GEOSCIENCE
SECTION OF HYDRAULIC ENGINEERING
DEPARTMENT OF COASTAL ENGINEERING

# TYPHOON-INDUCED EXTREME WATER LEVELS NEAR SINGAPORE

## A NUMERICAL MODEL INVESTIGATION

Serene Tay Hui Xin

Graduation committee

Prof.dr.ir. M.J.F. Stive (Chairman, Delft University of Technology)
Dr.ir. M. Zijlema (Delft University of Technology)
Ir. M. A. Burgmeijer (Delft University of Technology)
Ir. D. K. Vatvani (Deltares|Delft Hydraulics)

A dissertation submitted in partial fulfillment of the degree of
MSc Coastal and Marine Engineering and Management
June 2010

# Abstract

Due to the diminishing Coriolis force towards the equator, the equatorial zone is known to be cyclone-free. However, on 27th December 2001, a tropical cyclone Vamei was formed near Singapore; 1.4 degrees latitude North from the equator, and made a landfall about 60 km northeast of Singapore. Although this event did not cause any major destruction to Singapore, the neighbouring areas such as states of Johor and Pahang of Malaysia had suffered inland flooding and landslide caused by the heavy precipitation of the storm.

Chang et al. (2003) has suggested that the return frequency of a typhoon similar to Vamei is approximately 1 in 400 years, thus the possibility of a tropical storm occurring in Singapore could not be ignored. With the population density of over 7000 per square kilometer, the consequences of flooding due to storm surge can be devastating for Singapore.

This study aims to provide a quantitative assessment to estimate the possible storm surge induced by typhoon near Singapore using numerical hydrodynamic modeling tool Delft3D. In order to simulate the hydrodynamic condition of both the tide and the storm surge in the Singapore Strait, the so-called Singapore Regional Model (SRM) will coupled offline with the cyclone model; Wind Enhanced Scheme (WES), both developed by Deltares|Delft Hydraulics (2004 and 2009b). The hindcast of the typhoon Vamei event has been attempted in this report to examine the applicability of the model in Singapore waters. Then the sensitivity of different typhoon's tracks, forward speeds and radii of maximum winds on the storm surge will be examined closely to estimate the worst case scenario in terms of surge that could cause by a typhoon in this region.

This report also acts as a preliminary study of the possible extreme high water levels which includes storm surge, tide and sea level anomaly that could occur along the coast of Singapore. According to the result of this study, the extreme event with an estimated return frequency of 1 in 400 years can cause the water level to reach as high as 2.0 to 2.8 depending on location.

# Acknowledgements

I would like to extend my heartfelt appreciation and sincere gratitude to the following people, whom without their help, the completion of this study will not be possible.

Firstly, I am grateful to the members of my committee for their valuable inputs into this work. Individually, I would like to thank Prof.dr.ir. Marcel Stive for giving me the opportunity to work on this study in Delft, Dr.ir Marcel Zijlema for advising me on the important numerical modelling aspects, Ir. Madelon Burgmeijer who is also my coordinator for her organizational and moral support, and the last but not least, Ir. Deepak Vatvani for his guidance, constructive suggestions and understanding which have essentially given me the freedom to shape the whole scope of this study, and also perked up my interest in this subject.

Secondly, I would like to thank Dr. Herman Gerritsen, Dr. Ann Sisomphon, Ir. Daniel Twigt and Dr. Ferdinand Diermanse from Deltares for their valuable comments and suggestions on the various aspects of this study.

Thirdly, I like to thank Maritime Port Authority of Singapore (MPA) for their water level data provided within the framework of the Singapore-Delft Water Alliance (SDWA) programme.

Fourthly, I like to thank to my fellow CoMEM mate, Trinh Dieu Huong for her expertise in Fortran programming which has greatly helped me with the initial data processing. I would also like to thank the rest of my fellow CoMEM mates for making my past two years experience in Europe a pleasant one.

Finally, I would like to thank Deltares for providing me with a workspace, computer and communications for the duration of my MSc thesis work.

Last words of thanks go to my family and friends back in Singapore for their ‘ignorance’ of the details of this study which has given me the chance to take my mind off the thesis once in a while and enjoy their ‘virtual’ company.

# Contents

# List of Acronyms

| Acronyms | Definition |
|---|---|
| CBD | Central Business District Singapore |
| HURDAT | Atlantic Basin Hurricane Database |
| HAT | Highest Astronomical Tide |
| HHW | Highest High Water |
| IPCC AR4 | Intergovernmental Panel on Climate Change Fourth Assessment Report |
| JMA | Japanese Meteorological Agency |
| JTWC | United States' Joint Typhoon Warning Centre |
| LHW | Lowest High Water |
| MCVs | Mesoscale Convective Vortices |
| MHW | Mean High Water |
| MPA | Singapore Maritime Port Authority |
| NASA | National Aeronautics and Space Administration |
| NCEP | National Center for Environmental Prediction |
| NWP | Numerical Weather Prediction |
| QuikSCAT | Quick Scatterometer |
| RMW | Radius of Maximum Winds |
| SCSM | South China Sea Model |
| SLA | Seal Level Anomalies |
| TC | Tropical Cyclone |
| SRM | Singapore Regional Model |
| TRMM | Tropical Rainfall Measuring Mission |
| UHSLC | University of Hawaii Sea Level Centre |
| URA | Urban Redevelopment Authority Singapore |
| WES | Wind Enhanced Scheme |

## List of Symbols

| Symbols | Units | Definitions |
|---|---|---|
| $\lvert\vec{\tau}_s\rvert$ | kg/ms$^2$ | Magnitude of the wind shear-stress |
| $C_d$ | - | Wind drag coefficient |
| $U_{10}$ | m/s | Wind speed 10 meter above the free surface |
| $V_g$ | m/s | Gradient wind at radius $r$ |
| $v_{max}$ | m/s | Maximum sustained wind speed |
| $p_c$ | Pa | Central pressure |
| $p_{drop}$ | Pa | Pressure drop |
| $p_n$ | Pa | Ambient pressure |
| $u_s$ | m/s | Wind speed at height $z$ |
| $v_V$ | m$^2$/s | vertical eddy viscosity |
| $z_0$ | m | Roughness length |
| $\rho_0$ | kg/m$^3$ | Water density |
| $\rho_a$ | kg/m$^3$ | Density of air |
| $A$ | - | Scaling parameter of cyclone wind profile |
| $B$ | - | Scaling parameter of cyclone wind profile |
| $H$ | m | Total water depth |
| $RMW$ | m | Radius of maximum wind |
| $f$ | - | Coriolis parameter |
| $g$ | m/s$^2$ | Gravitational acceleration |
| $r$ | m | Radius of cyclone |
| $u$ | m/s | Flow velocities in the $\xi$ direction |
| $\beta$ | - | Charnock constant |
| $\theta$ | degree | Angle between wind stress vector and local direction of grid-line n |
| $\kappa$ | - | Von Karman constant |
| $\sigma$ | - | Scaled vertical coordinate |
| $v$ | m/s | Flow velocities in the $\eta$ direction |

# List of Figures

# List of Tables

# 1 Introduction

On 27th December 2001, a rare equatorial tropical cyclone event, typhoon Vamei had made landfall on the southeast coast of Malaysia Peninsular (approximately 60 km from Singapore). The tropical storm brought strong winds and intense rain which resulted in flooding and landslide to the states of Johor and Pahang of Malaysia, causing more than 17,000 people to be evacuated (Johnson and Chang, 2007). The storm event had also brought heavy precipitation to Singapore and caused disruptions to the air traffic at the Singapore Changi Airport (Williams, 2004). Fortunately this event took place during the period of neap tide and hence no severe coastal floods had occurred.

## 1.1 Problem description

Even though the 2001 event of typhoon Vamei described above did not caused much damage to Singapore and the probability of another similar cyclone event to hit Singapore with occurrence of higher water level is not zero. Chang et al, 2003, determined that the probability of occurrence of a tropical cyclone in Singapore is about once in 100 to 400 years. Uder more unfavourable circumstances than in Vamei case, the level of damage to Singapore could be devastating as the island is more densely populated. Infrastructures and buildings such as ports and skyscrapers could be heavily affected by the flood and coastal reservoirs which hold one of Singapore's scarce commodities, freshwater, will be affected due to the sea water intrusion. Being the sole cause of extreme water level conditions in Singapore it is essential to study and understand the possible level of the surge that can be induced by a tropical cyclone in the south of South China Sea and Strait of Singapore. If proven necessary preparation can then be taken to minimize the potential damage.

## 1.2 Objectives

The main objective of this study is to provide a quantitative assessment of the surge level along the coast of Singapore induced by a tropical cyclone similar to typhoon Vamei. Based on this and combined with the effect of high tide and the so-called Sea Level Anomaly (SLA) (Section 2.2.3) we aim to determine a realistic extreme water level conditions for Singapore with a recurring interval between 100 to 500 years.

The following issues are identified and studied to fulfill the stated objectives:

1. understand the surge propagation in the Singapore region during the 2001 typhoon Vamei event,
2. understand the sensitivity of different parameters of a typhoon on the induced surge level and how they will affect the propagation of the surge along the Singapore Strait,
3. study the effect of storm surge in different extremes of a tidal cycle; spring and neap,
4. determine a typhoon track that could produce highest surge level for Singapore and
5. estimate the return period of a near equatorial typhoon of similar intensity as typhoon Vamei in the Singapore region

## 1.3 Approach

In order to fulfill the objectives, an accurate numerical hydrodynamic model of the Singapore region is required and has been used to carry out this study. Using an application of the Delft3D modeling system, the so-called Singapore Regional Model (SRM) is forced with winds generated by a cyclone model, the so-called Wind Enhanced Scheme (WES) to reproduce the hydrodynamic condition of both the tide, Sea Level Anomaly (SLA) and the storm surge in the Singapore Strait. Both models

were, both developed by Deltares|Delft Hydraulics (2004 and 2009) to simulate the hydrodynamic condition of both the tide and the storm surge in the Singapore Strait

As a first step the hydrodynamic model, forced with synthesized typhoon winds generated for the typhoon Vamei, was run to hindcast the water level observations during the 2001 event. After the calibration of the hydrodynamic and wind models, the sensitivity of the surge in the Singapore Strait induced by different types of typhoons in terms of track, speed and size were examined. A track that could produce higher surge levels for Singapore was determined.

As the Vamei occurred during a neap tide in December 2001, the effect of tide (spring and neap) was investigated to investigate how the storm surge is affected.

The results are then combined to produce a water level conditions that could occur in Singapore region which can be categorized as an extreme event with a certain return period. For this purpose extreme wind analysis based on 13 years wind data of a station on land has been performed.

## 1.4 Assumptions and limitations

Due to time limitation and lack of detailed topographical data, the flooding extent and inundation along Singapore coast caused by storm surge will not be studied. For similar reasons, another important feature for typhoon-induced storm surge study, i.e. contribution of short waves on will also not be included.

The model also assumes that the effect of river discharge on water level is small in comparison with the tidal and wind-driven flows. The large scale wind effect in the model will be introduced at the boundaries.

## 1.5 Overview

Section 2 will briefly discuss the Singapore coast and sea climate, basics of typhoon in brief, and typhoon Vamei, which will provide the necessary knowledge and information to the subsequent sections.

Section 3 discusses the modeling aspects of the study focusing on the cyclone modelling approach in WES, configuration and setting of SRM, and processing of observation data for model result comparison in the hindcast of typhoon Vamei event.

Section 4 will describe and evaluate the results of sensitivity analysis of different typhoon parameters and effect of spring and neap tide on the surge level. A ‘worst’ track will then be proposed for the extreme scenario. The return period for the typhoon wind used in the simulation has been compared to the statistically derived return period by Chang et al. (2003).

Section 5 presents the conclusion and recommendations of this thesis.

# 2 Literature Review

## 2.1 Singapore coast

Singapore is a relatively small country in terms of land area; 710 km$^2$, currently (Statistics Singapore, 2010) with only 193 km long coastline (Singapore's National Climate Change Strategy, 2008). In many ways, the entire country of Singapore can be considered as coastal as nowhere on the Singapore main island is more there 12 km from the coast (Chia, 1998). Figure 2.1 shows the entire Singapore; the distance from the most northern point and southern point of Singapore is less than 23 km, and the distance between the most eastern and western point is less than 50 km.

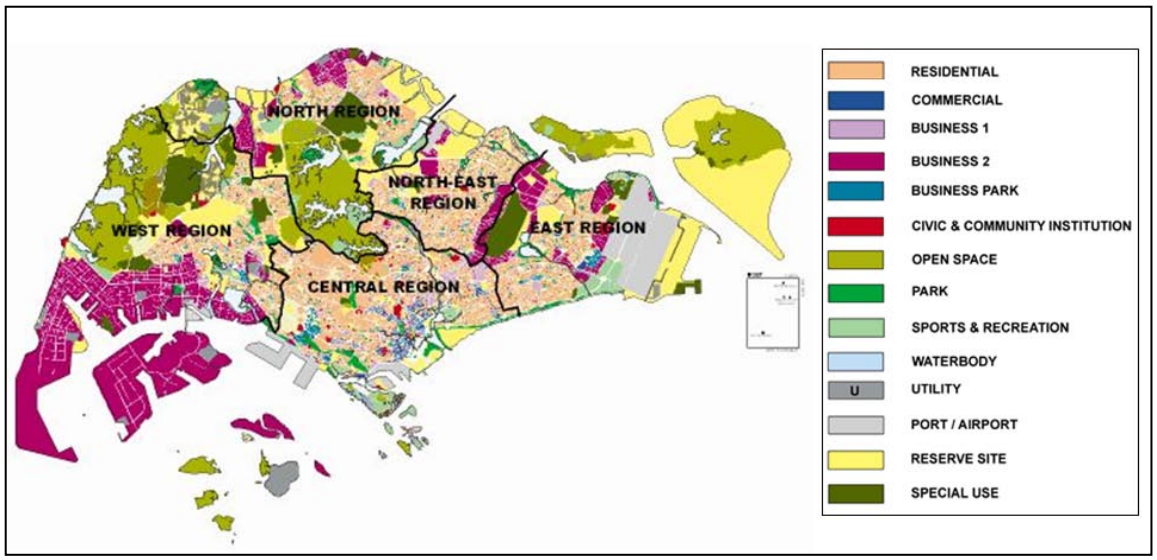


**Figure 2.1 Singapore and its land use (Adopted from URA, 2008)**

According to Chia et al. (1989), the Singapore coast, like other areas in the humid tropics, is characterised by accumulation rather than erosion; mainly due to the low wave and tidal energy conditions (Swan, 1971). During the Pleistocene Era where the sea level was low, large quantities of sediments were generated by the deep weathering of exposed continental shelf, and as the sea level rose, this eroded material was then reworked by the transgressing shore zone and re-deposited as extensive plain of coastal accumulation (Thomas, 1991).

In the past four decades, large-scale land reclamation projects have been carried out around the coast of Singapore main island. Though land reclamation in Singapore started as early as 1820s during the British colonial rule when the total land area was only 523 km$^2$ (Glaser and Walsh, 1991). Presently, there are still several ongoing land reclamation projects in the offshore islands around the main island such as Pulau Tekong.

Figure 2.1 also shows the land use of Singapore Island. Along the coast, the main air and sea ports are located on the east and south part of the main island, respectively. The southwest coast of Singapore and the offshore reclaimed Jurong Island consist mainly of marine industries such as ship building and petrochemical industry. The further offshore islands in the south such as Pulau Bukom and Semakau are used for petrochemical industry and landfill, respectively. In the south of the main island where the central business district (CBD) is located, consists also of Singapore's largest coastal freshwater reservoir, Marina Barrage. As Singapore is one of the water scarce cities in the world, freshwater is considered to be a national asset. Eleven freshwater reservoirs have been built from

damming the mouth of the rivers or estuaries along the northern coast of the main island. Other areas along to coast are mostly residential or nature reserve sites. The two offshore islands in the northeast are Pulau Ubin and Tekong respectively. Pulau Ubin which used to have numerous granite quarries until 1970 is one of the few un-urbanised areas in Singapore which still preserves the rich flora and fauna of its island. On the other hand, Pulau Tekong is currently undergoing land reclamation works in the southern part while other part of the island is temporarily used for military training purposes.


**Figure 2.2 Coastal water reservoirs of Singapore**

## 2.2 Singapore Strait climate

The topography and bathymetry of the Singapore Strait will be described in configuration of the Singapore Regional Model in Section 3.2. This section will focus on the sea climate of the strait such as hydrodynamic forces and water levels. Figure 2.3 shows the Singapore Strait and part of the large water bodies connected to it.

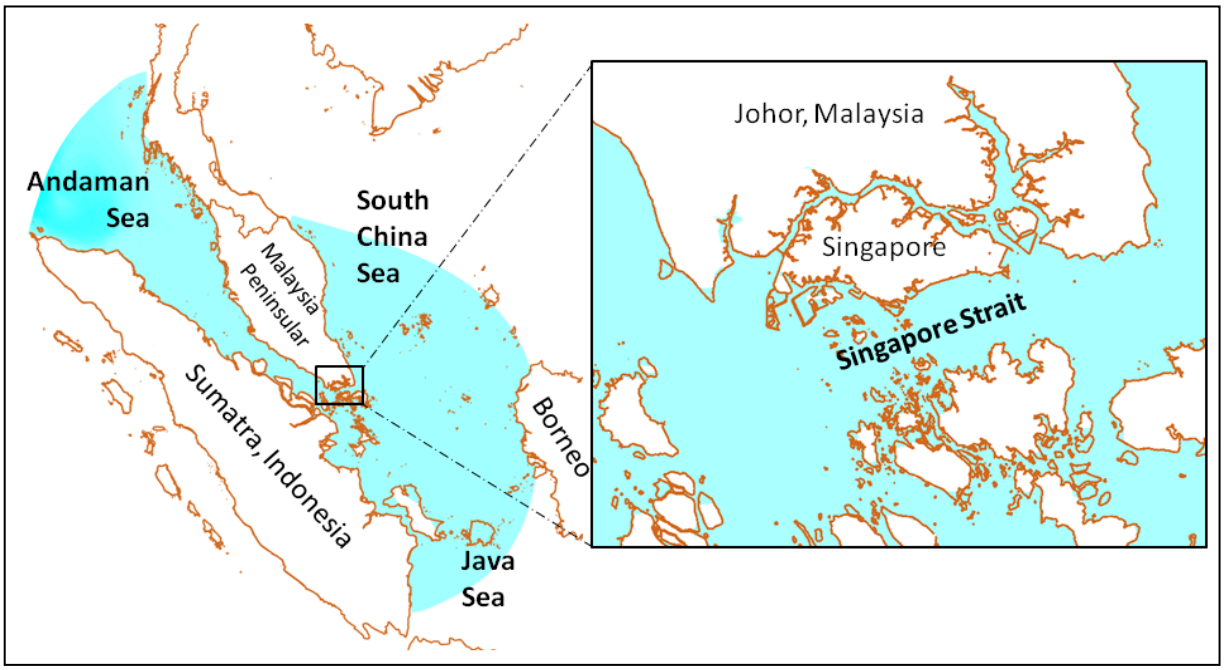


**Figure 2.3 Singapore Strait**

### 2.2.1 Waves

Around Singapore, the wave fetch is generally short, and the directions of maximum fetch rarely coincide with those of the strongest winds (Chia et al., 1989). A metre high openwater waves may be generated by the Sumatran squalls during the southwest monsoon and by swell from the South China Sea. However due to the obstruction by shallow waters and small offshore reefs, most of the energy from these waves are dissipated before they reach the coast of the main island (Wong, 1985 and Chew et al., 1975). Hence the average breaker height is less than 20 cm (Chew, 1974 and Swan, 1971).

### 2.2.2 Tides

The tide in the Singapore Strait is generated mainly from North Indian Ocean and South China Sea, in which the tidal characteristics of both water bodies are different from each other. The Indian Ocean is dominated by semi-diurnal tides while South China Sea is dominated by both diurnal and semi-diurnal tides (Chen et al., 2005). The major tidal constituents which dominate the tidal flow in the Singapore Strait are SE, K1, O1, M2, SW and N2 (Indonesia, Japan and Singapore, 1979). The tidal waves, especially M2 component (Indonesia, Japan and Singapore, 1979) generated from the Indian Ocean and South China Sea meet and interact approximately at the western part of the Singapore Strait which creates a complicated tidal dynamics along the strait (Chan et al., 2006). This also results a higher tidal range in the west compare to the east within the strait (Chen et al., 2005); 2.7 m and 1.4 m in the west and east respectively during spring tide, and 40 percent of spring tidal range across the strait during neap tide.

### 2.2.3 Sea level anomalies

Sea level anomalies (SLA) are variations of the sea level from the mean sea level which are not generated by tides. They are caused by several large scale oceanographic and meteorological parameters such as winds, atmospheric pressure gradient, sea surface temperature and fresh water run-off (Tkalich et al., 2009a). This non-stationary non-periodic ocean bahaviour of varying temporal and spatial scales is a characteristic observed in the shallow waters of Singapore Strait (Raghuraj et al., 2010). Both Tkalich et al. (2009b) and Raghuraj et al. (2010) found that the SLA in this region is strongly correlated with the monsoon winds of the seasonal monsoon seasons; Northeast monsoon from November to February and Southwest monsoon from May to August. Especially during the Northeast monsoon period, strong wind from the Asia continent prevails over the South China Sea and triggers the positive SLA events in the Singapore waters (Rahuraj et al., 2010). Tkalich et al. (2009b) concludes that the SLA is positive in the Singapore Strait and negative in the Taiwan (other end of South China Sea) during Northeast monsoon and the opposite stands for the case during the Southwest monsoon.

### 2.2.4 Sea level rise

According to the Intergovernmental Panel on Climate Change Fourth Assessment Report (IPCC AR4) (IPCC, 2007), the global mean sea levels are projected to rise by 34.3 cm over the 1990 levels by around 2100 based on the average of all global emission level scenarios in the future.

## 2.3 Basics of tropical cyclones

A tropical cyclone is the generic term for a non-frontal synoptic scale low-pressure system over tropical or sub-tropical waters with organized convection (i.e. thunderstorm activity) and definite cyclonic surface wind circulation (Holland, 1993). The terms hurricane and typhoon are regionally

specific names for a strong tropical cyclone (maximum sustained winds of 64 knots (34 m/s) or more). The maximum sustained winds of a tropical cyclone represent the highest winds expected over a one to ten minute time span anywhere within the tropical cyclone. The shape of a tropical cyclone over sea are determined by large scale weather pattern, but they are often more symmetrical compared to the pattern near landmass. Details about the formation of tropical cyclone can be found in many textbooks such as Anthes (1982) and Thurman (1999).

### 2.3.1 Classification

There are different terms to classify the different progressive levels of disturbed weather in the tropics that are less than a typhoon or hurricane status. The Saffir-Simpson Hurricane Scale which is widely used in the United States has classified these different levels of tropical cyclone by their maximum sustained winds (Table 2.1).

**Table 2.1 Saffir-Simpson Hurricane Scale**

| Category | Maximum sustained wind speed | |
|---|---|---|
| | m/s | knots |
| Tropical depression | 0-17 | 0-34 |
| Tropical storm | 18-32 | 35-63 |
| 1 | 33-42 | 64-82 |
| 2 | 43-49 | 83-95 |
| 3 | 50-58 | 96-113 |
| 4 | 59-69 | 114-135 |
| 5 | 70 and above | 136 and above |

In the Northwest Pacific region, the Japanese Meteorological Agency (JMA) and United States' Joint Typhoon Warning Centre (JTWC) have classified these different levels of tropical cyclone by their maximum sustained winds as shown in Table 2.2.

**Table 2.2 Tropical cyclone classifications of JMA and JTWC**

| Maximum sustained wind speed | | JMA | JTWC |
|---|---|---|---|
| m/s | knots | | |
| 0-17 | 0-33 | Tropical Depression | Tropical Depression |
| 18-24 | 34-47 | Tropical Storm | Tropical Storm |
| 25-33 | 48-63 | Severe Tropical Storm | Tropical Storm |
| 34-58 | 64-114 | Typhoon | Typhoon |
| 59 and above | 115 and above | Typhoon | Super Typhoon |

### 2.3.2 Storm Surge

Storm surge is water that is pushed toward the shore by the force of the winds generated by the strong winds. This rise in water level can cause severe flooding in coastal areas, especially when the storm surge coincides with the normal high tides.

The level of surge in a particular area is also determined by the slope of the continental shelf. A shallow slope off the coast will allow a greater surge to inundate coastal communities. Communities with a steeper continental shelf will not see as much surge inundation, although large breaking waves can still present major problems. Storm surges, waves, and currents in confined harbours severely damage ships, marinas, and pleasure boats.

In the northern hemisphere, the direction of the wind around the cyclone eye is anti-clockwise (cyclonic). When the cyclone approaches a shore, which projects from north to south, from the east to west, the surge will be higher on the right side than the left side of the eye (relative to the forward motion of the cyclone) (Figure 2.4a). As the cyclone makes the landfall, the wind on the right side of the eye is on-shore while the wind on the left side is off-shore. The on-shore wind will drive the water towards the shore and create a surge while the off-shore wind will push the water away from the shore generating negative surge. Hence the track of the cyclone plays an important role in the level of storm surge.

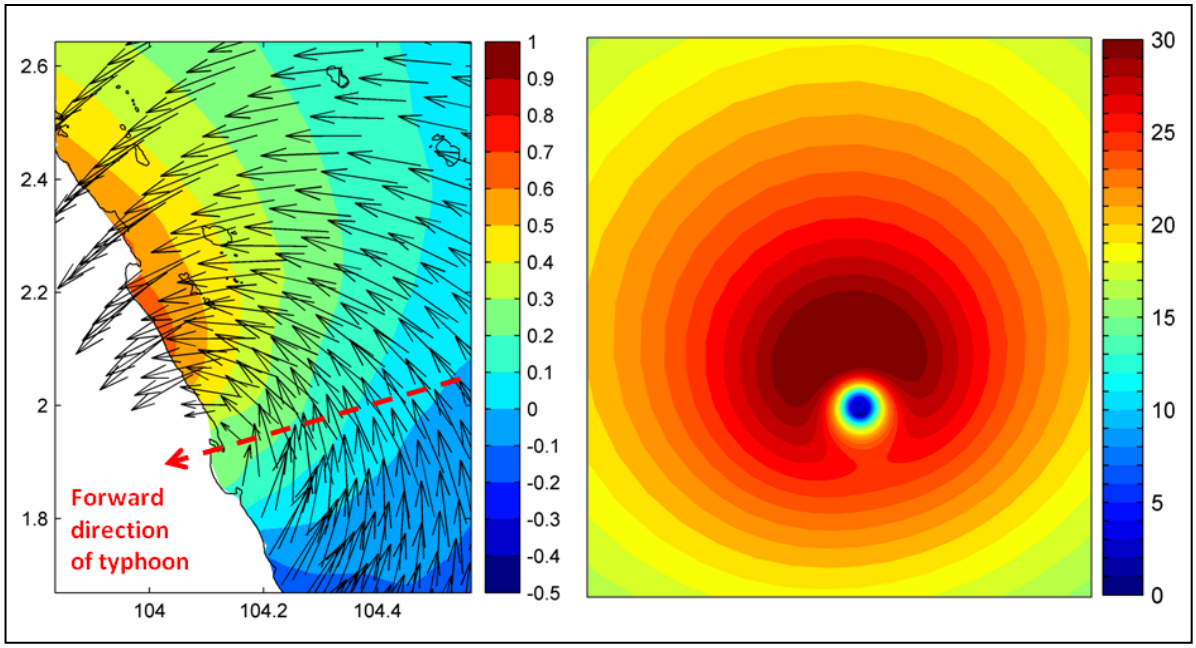


**Figure 2.4 (a) Contour map of surge level in metres of a typical typhoon (left) and (b) Wind distribution in metres per second of a moving typhoon (right)**

The forward speed of the cyclone also plays a part in the level of storm surge. The wind speed on the right side of the eye in Northern Hemisphere is increased with the translation speed of the typhoon (and decreased at the left side) (Figure 2.4b). Consequently, in an 'open' coast (coast which faces the ocean or sea), a fast moving cyclone will cause a higher surge than a slow moving one. However, in an enclosed basin such as the bay, estuary or river system, a slower moving cyclone will cause a higher surge. Slow moving cyclone will have more time to push the water inland than the fast moving one. In other words, the surge does not dissipate so long as the cyclone stays in the basin.

As for the case of Singapore Strait in which water area is only partially enclosed (Figure 2.3), the situation is more complex and highly depends on the track of the cyclone which will be discussed further in Section 4.

## 2.4 Typhoon Vamei

Historically, 300 km north and south of the equator is known to be cyclone-free (Anthes, 1982), because of diminishing Coriolis force. However, on 27$^{th}$ December 2001 a tropical cyclone Vamei had made an exception to this rule and was formed near Singapore; 150 km north from the equator. Its circulation circle was at 1.5 $^{o}$N and a near 200 km radius of convective cloud area (Figure 2.5). Naval ship reports had indicated up to 75 knots of wind sustaining within the small eyewall and 105 knots of gusts (JTWC, 2001).

NASA researchers found that a combination of topography and meteorology, rather than Earth's rotation triggered the cyclone. A strong monsoonal wind from Asia continent surged rapidly down over the South China Sea, reaching the equator in a narrow stretch of ocean between Malaysia Peninsula and Borneo Island.

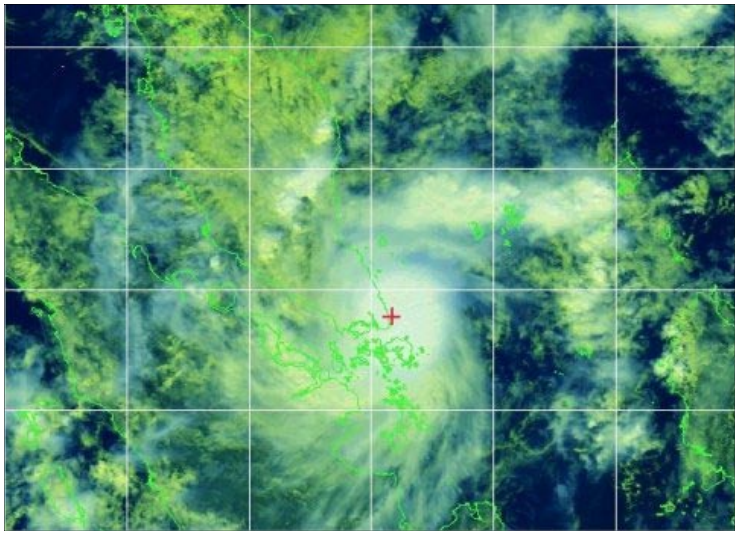

**Figure 2.5 05:30 (UTC) 27th December 2001 Multispectral image of typhoon Vamei located just Southeast of Malaysia Peninsula (Adopted from Chang et al, 2003)**

### 2.4.1 Formation

Chang et al. (2003) proposed that typhoon Vamei was the result of a weak Borneo vortex and a large background cyclonic vorticity at the equator. The Borneo vortex is a quasi-stationary low-level cyclonic circulation due to the deflection of persistent northeast monsoonal winds in the South China Sea caused by the mountainous topography of the northwestern Borneo Island (Johnson and Houze, 1987). On 21 December, the vortex drifted from the northwest coast of Borneo island to the open water in the southern tip of South China Sea and remained there for four days. During that time, the seasonal strong northeasterly surge which was persisting in the background was deflected slightly to the northwest of the vortex. This created a flow which wrapped around the vortex and triggered the spinning of a rapid anti-clockwise circulation, and led to the development of typhoon Vamei. In fact this is the main cause of typhoon in Singapore. At the end of the paper, Chang et al. (2003) has also presented the return frequency of a typhoon as 1 in 400 years and the method to achieve this value is summarized in Appendix A.

Chambers and Li (2007) have attempted to simulate the formation and intensification of Vamei by using a mesoscale model which involves the interactions between the scales of background cyclonic circulation (the Borneo Vortex of order around 100 km) and of mesoscale convective vortices (MCVs, of order around 10km), and vorticity budget analysis. From both observations and model results, Chambers and Li (2007) concluded that a near equatorial cyclone is only able to attain Category One intensity (64-82 knots, Saffir-Simpson Hurricane Scale).

Without the aid of navy ships and satellite images, typhoon Vamei, because of relatively low wind speed compared to other typhoons at landfall, would not have been detected (Chang and Wong, 2008 and Chambers and Li, 2007). Hence it is suggested that some near-equatorial cyclone events occurred in the past may have been missed, especially during the pre-satellite era.

### 2.4.2 Intensity and track

Both Joint Typhoon Warning Center (JTWC) and Japan Meteorological Agency (JMA) have reported on the best track information of typhoon Vamei (Table 2.3 and Figure 2.6). Note that JMA did not report the maximum sustained winds of less than 35 knots (tropical depression). JTWC continued to report on Vamei after 06:00 UTC 28th December 2001 when it was crossing North Sumatra and degrading to tropical depression. However, it attained energy when it moved offshore again into the Indian Ocean and sustained maximum winds of 35 knots. By 06:00 UTC 1st January 2002, Vamei had completed dissipated.

**Table 2.3 JTWC and JMA reports on Vamei**

| Date and Time UTC | Maximum sustained winds (knots) | | Radius of Maximum Winds (nm) | | Central Pressure (hPa) | |
|---|---|---|---|---|---|---|
| | JTWC | JMA | JTWC | JMA | JTWC | JMA |
| 26-Dec-2001 12:00 | 25 | - | 15 | - | 1005 | 1010 |
| 26-Dec-2001 18:00 | 35 | - | 20 | - | 997 | 1010 |
| 27-Dec-2001 00:00 | 65 | 40 | 30 | 100 | 976 | 1008 |
| 27-Dec-2001 06:00 | 65 | 45 | 20 | 120 | 976 | 1006 |
| 27-Dec-2001 12:00 | 45 | 35 | 30 | 100 | 991 | 1008 |
| 27-Dec-2001 18:00 | 40 | - | 30 | - | 994 | 1010 |
| 28-Dec-2001 00:00 | 30 | - | 30 | - | 1000 | 1010 |
| 28-Dec-2001 06:00 | 30 | - | 25 | - | 1000 | 1012 |
| 28-Dec-2001 12:00 | 25 | - | - | - | 1002 | - |
| 28-Dec-2001 18:00 | 25 | - | - | - | 1002 | - |
| 29-Dec-2001 00:00 | 20 | - | - | - | 1004 | - |
| 29-Dec-2001 06:00 | 20 | - | - | - | 1004 | - |
| 29-Dec-2001 12:00 | 25 | - | - | - | 1002 | - |
| 29-Dec-2001 18:00 | 25 | - | 35 | - | 1002 | - |
| 30-Dec-2001 00:00 | 25 | - | 35 | - | 1002 | - |
| 30-Dec-2001 06:00 | 25 | - | 35 | - | 1002 | - |
| 30-Dec-2001 12:00 | 25 | - | 35 | - | 1002 | - |
| 30-Dec-2001 18:00 | 35 | - | 35 | - | 1000 | - |
| 31-Dec-2001 00:00 | 35 | - | - | - | 997 | - |
| 31-Dec-2001 06:00 | 35 | - | - | - | 997 | - |
| 31-Dec-2001 12:00 | 35 | - | - | - | 997 | - |
| 31-Dec-2001 18:00 | 30 | - | - | - | 1000 | - |
| 01-Jan-2002 00:00 | 25 | - | - | - | 1002 | - |
| 01-Jan-2002 06:00 | 25 | - | - | - | 1002 | - |

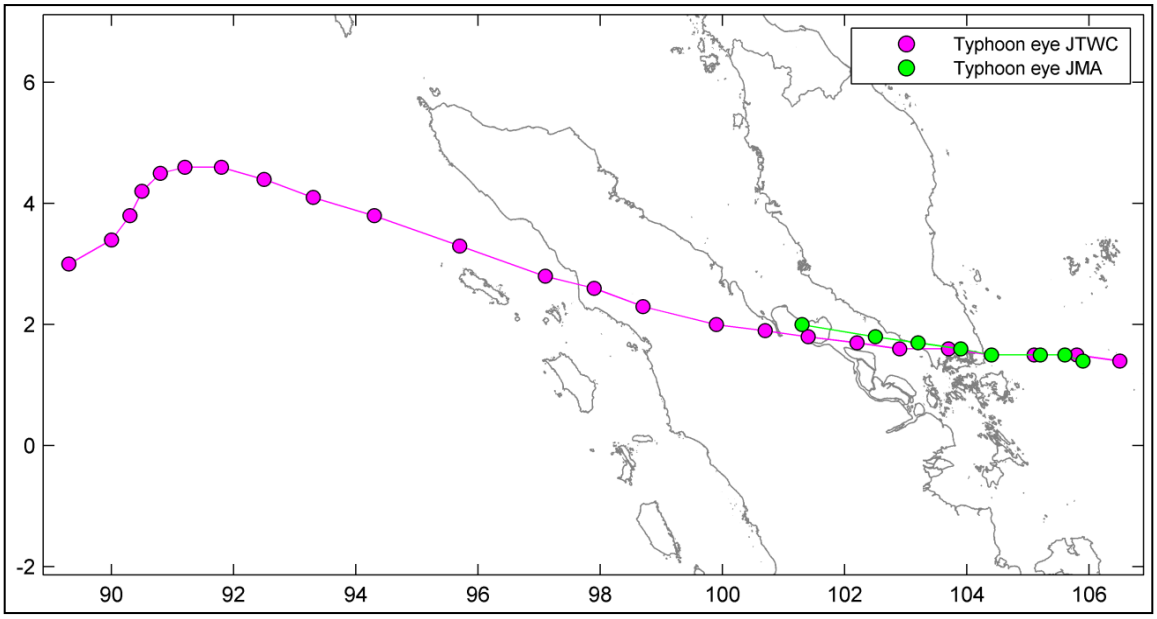


**Figure 2.6 JTWC and JMA Vamei track**

The conflicting reports on the typhoon wind speed from JTWC and JMA (Table 2.3) is caused by the fact that JTWC upgraded the intensity of the storm to that of a typhoon after the observation reported made by the ship (refer to earlier text). In Figure 2.6, the typhoon passed through the Malaysia Peninsular within two days (27$^{th}$ to 28$^{th}$ UTC), and suggested that the effect in Singapore only lasted two days. Section 3 will model the storm surge around Singapore caused by typhoon Vamei.

From the reports of JTWC and JMA, the typhoon Vamei is moving at about 3.5 m/s. However, according to the Atlantic basin hurricane database (HURDAT) the average forward speed of the hurricanes at this latitude (close to equator) is about 7 m/s (Atlantic Oceanographic and Meteorological Laboratory, http://www.aoml.noaa.gov/hrd/tcfaq/G16.html).

Figure 2.7 is an image of typhoon Vamei observed by Quick Scatterometer (QuikSCAT) in the South China Sea. It shows the distribution of wind of Vamei at 22:32 UTC 26$^{th}$ December. The wind distribution is clearly not a perfect symmetrical cyclone and more intense winds are located in the south of the eye. Interestingly, the observed wind speed is actually higher (more than 27 m/s) on the left side of the typhoon eye (relative to forward direction which is towards the west) than on the right side (about 20 m/s), this is an unusual phenomenon to observe from a tropical cyclone as the higher winds should usually be on the right side due to the additional speed contributes by the forward motion of the typhoon.

Also in Figure 2.7, there is a large scale meteorological weather pattern (northeast monsoon) in the north. This suggests that there is a 'mixture' of a classical typhoon and a large scale monsoon pattern, which could explain the inconsistency of the reports, including the radius of maximum winds and central pressure made by the two agencies. Therefore we have to be aware that the model result based on the agencies' information is of high uncertainty.

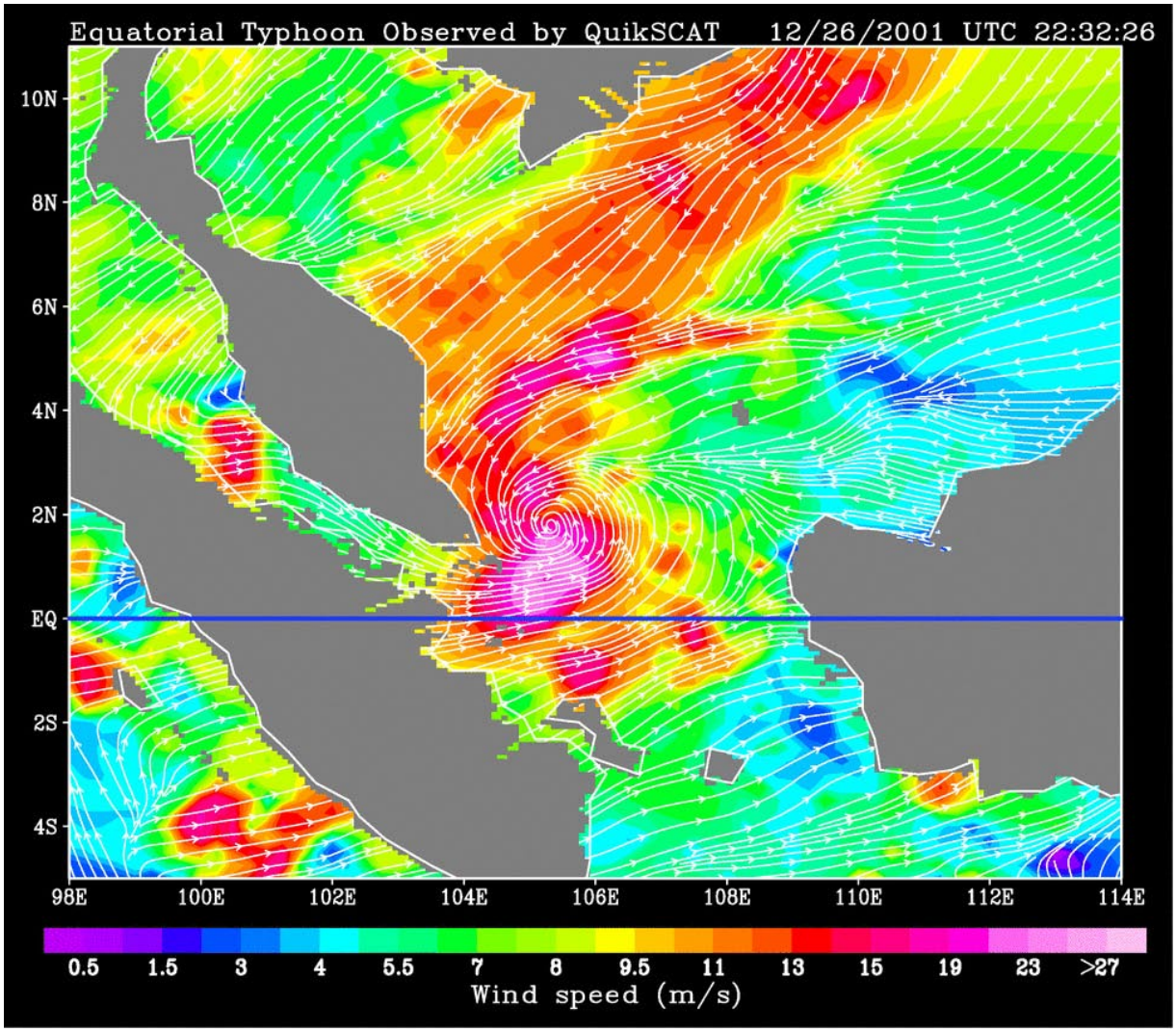


**Figure 2.7 22:32 UTC 26th December 2001 QuikSCAT observed wind speed contour map and streamlines at surface of South China Sea showing typhoon Vamei (Adopted from NASA Earth Observatory, 2003)**

# 3 Modelling aspects

## 3.1 Wind Enhanced Scheme (WES)

The WES model is developed by Deltares|Delft Hydraulics for cyclone modeling (Deltares|Delft Hydraulics, 2009b). Generally, the accuracy of storm surge computation depends on the accuracy of the wind forcing. However, in most Numerical Weather Prediction (NWP) models, cyclone winds, especially the strong variations of the wind gradients near the centre, are not accurately represented in the NWP models due to low grid resolution. Due to this and the lack of observations in many parts of the tropical oceans, many meteorological agencies used 'bogus' observations to define the cyclone's location and structure in the NWP model to bring out the cyclone in the analysis. Methods such as Rankine Vortex and synthetic vortex are used to illustrate cyclone winds. In the WES model, wind is generated based on the analytical model by Holland (1980) which is described in Appendix B, and further improved by introducing asymmetry. This asymmetry is brought about by the forward speed of the cyclone centre displacement as steering current and by introducing rotation of wind speed due to friction. For detailed description of the scheme, one may refer to Deltares|Delft Hydraulics (2009b).

## 3.2 Wind stress in Delft3D-FLOW

In Delft3D-FLOW, wind stress term is prescribed in the momentum equations at the free surface boundary condition (Deltares|Delft Hydraulics, 2009a) as shown

$$\frac{\nu_V}{H}\frac{\partial u}{\partial \sigma}\bigg|_{\sigma=0} = \frac{1}{\rho_0}|\vec{\tau}_s|\cos(\theta) \tag{3.8}$$

$$\frac{\nu_V}{H}\frac{\partial v}{\partial \sigma}\bigg|_{\sigma=0} = \frac{1}{\rho_0}|\vec{\tau}_s|\sin(\theta) \tag{3.9}$$

where $\nu_V$ is the vertical eddy viscosity, $H$ is the total water depth, $u$ and $v$ are the flow velocities in the $\xi$ and $\eta$ direction (in generalized Cartesian coordinate system) respectively, $\sigma$ is the scaled vertical coordinate (Phillips, 1957), $\rho_0$ is the referenced water density, $\theta$ is the angle between the wind stress vector and the local direction of the grid-line n, and $|\vec{\tau}_s|$ is the magnitude of the wind shear-stress. Without wind, the stress at the free surface is zero. The magnitude of the wind shear-stress is defined as

$$|\vec{\tau}_s| = \rho_0\,\vec{u}_{*s}|\vec{u}_{*s}| \tag{3.10}$$

where $\vec{u}_{*s}$ is the friction velocity at the surface. The magnitude is determined by the following widely used quadratic expression;

$$|\vec{\tau}_s| = \rho_a C_d U_{10}^2 \tag{3.11}$$

where $\rho_a$ is the density of air, $U_{10}$ is the wind speed 10 meter above the free surface (time and space dependent) and $C_d$ is the wind drag coefficient, dependent on $U_{10}$.

In this study, the $C_d$ used is based on Charnock relation (Charnock, 1955) as shown

$$z_0 = \frac{\beta u_{*s}^2}{g} \tag{3.12}$$

where $\beta$ is the Charnock constant and a value of 0.032 gives optimum results in the Dutch Continental Shelf model (Gerritsen et al., 1995), $g$ is the gravitational acceleration, and $z_0$ is the roughness length which is applied in a logarithmic wind profile

$$u_s(z) = \frac{u_{*s}}{\kappa} \ln\left(\frac{z}{z_0}\right) \tag{3.13}$$

where $u_s$ is the wind speed at height $z$ above the sea surface, $\kappa$ is the Von Karman constant (= 0.4).

The other formulation and conceptual description of Delft3D-FLOW module can be found in Lesser et al. (2004) or Deltares|Delft Hydraulics (2009a).

## 3.3 Singapore Regional Model

The SRM was developed by Deltares|Delft Hydraulics, the Netherlands in 2004, with the intent to provide reliable hydrodynamic information of the water surrounding Singapore (Deltares|Delft Hydraulics, 2004 (Zijl and Kernkamp)). The well calibrated and validated SRM could be used to accurately simulate large-scale tide and wind-driven flows. Large parts of the seas around Singapore; the Andaman Sea, the South China Sea and the Java Sea (Figure 2.3), have been covered in the model. Eight main tidal constituents; Q1, O1, P1, K1, N2, M2, SW and K2, are used to simulate the forcing at the open sea boundaries.

The model grid consists of around 36,500 grid cells, and the sizes of the grid cell vary from about 500 m to 600 m around Singapore Island up to over 15 km at the open sea boundaries. Singapore Strait, Malacca Strait, Selat Riau, Selat Durian, Johor Strait and Sungai Johor have been given a relatively high resolution (Figure 3.1) to obtain detailed hydrodynamic information in these areas which are near the area of interest. The bathymetry is based on Admiralty charts with maximum depth of about 2000 m in the Andaman Sea and 160 m in Singapore Strait (Figure 3.1). The SRM requires about 0.5 hour of computation time on a 2.0 GHz PC for a 10 day simulation period.

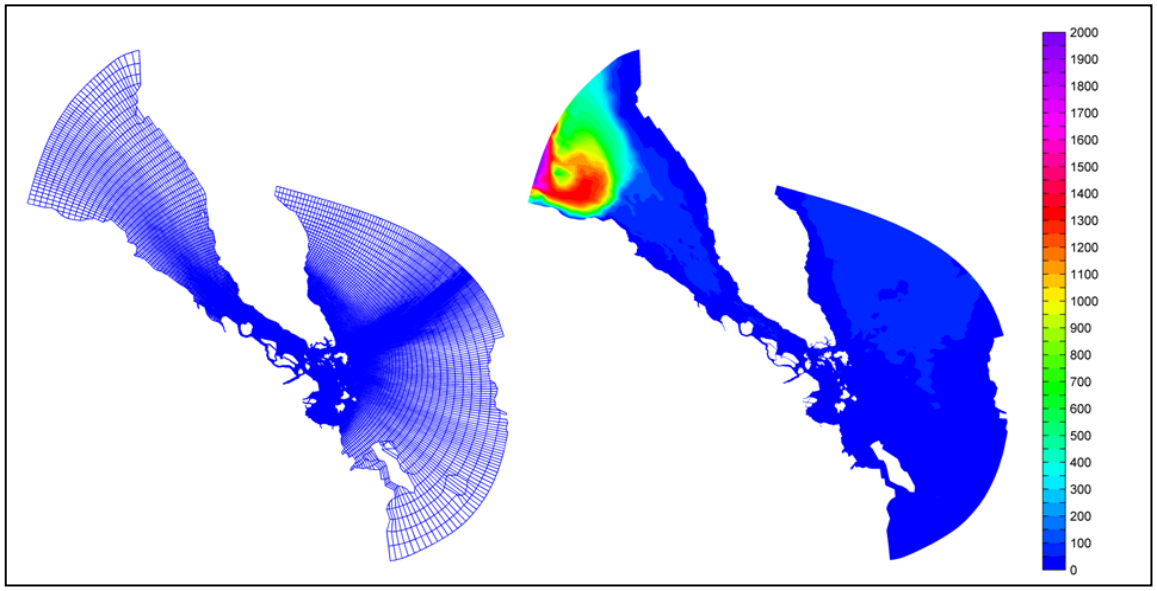


**Figure 3.1 Grid and Bathymetry of SRM**

In accordance to the land use of Singapore coast (Section 2.1), the coastline is divided into 13 segments with one station representing each segment (Figure 3.2). In the simulation, the surge level at any of the 13 stations will represent the surge of its respective segment.

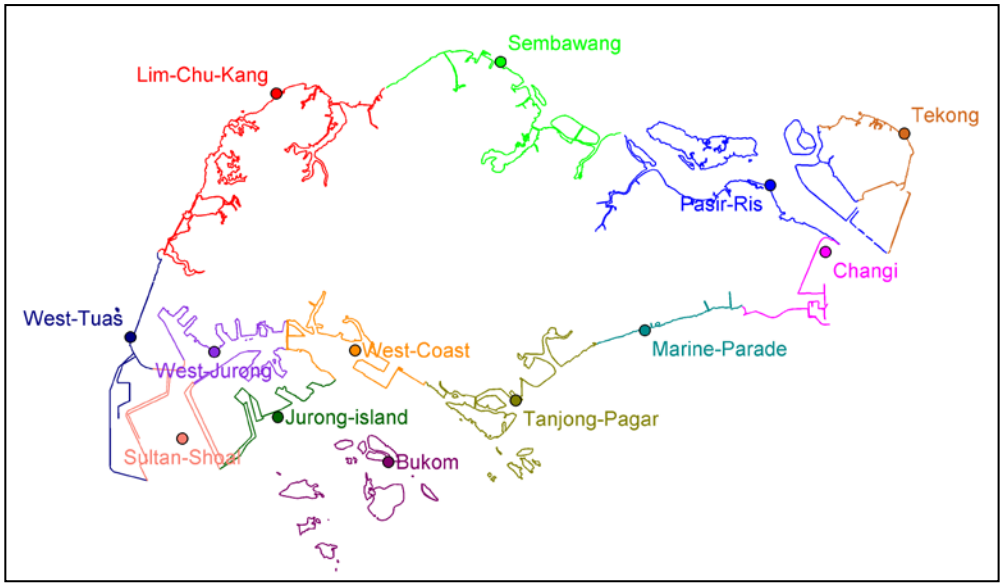


**Figure 3.2 Division of coastline into segment and the representative stations**

## 3.4 Determination of typhoon-induced surge

There are two types of typhoon-induced surge; observed and modelled. However, before either can be determined, the observation or modelled result has to be processed. The following describes the two methods on how the typhoon-induced surge, observed or modelled can be obtained.

### 3.4.1 Determine typhoon-induced surge in model

In the model, typhoon is simulated with tide to get the water level over the whole model domain. In order to obtain the typhoon-induced surge level only, the output of the model is subtracted with the output of another model which only simulated tide;

(Modelled typhoon-induced surge) = Model(Typhoon+Tide) – Model(Tide only)

### 3.4.2 Determine typhoon-induced surge in observation

Usually, measurement recorded by an in-situ gauge is the overall water level at a particular location. For waters around Singapore, the observation data contains several signals like tide, SLA and even typhoon induced surge if there is a presence of a typhoon. This section will describe how the tidal and SLA signals are removed from the observation data to distinguish the typhoon-induced surge which is summarized as follows:

(Observed typhoon-induced surge) = (Observed water level) - (Tidal prediction) - (Modelled SLA)

#### 3.4.2.1 Observation water level

Hourly water level data at various stations around Singapore are obtained from Singapore Maritime Port Authority (MPA) and University of Hawaii Sea Level Centre (UHSLC) (http://ilikai.soest.hawaii.edu/uhslc/data.html). Observations at four selected stations; Sedili, Tanjong Changi, Bukom and Kukup (Figure 3.3) will be used for calibration during the hindcast of Vamei later. Each of them represents the different sections of the affected region; Sedili is located on the east of Singapore Strait in the South China Sea, Tanjong Changi is located in the Johor Strait, Bukom is located near the middle of the Singapore Strait and Kukup is located in the western end of the Singapore Strait near Malacca Strait.

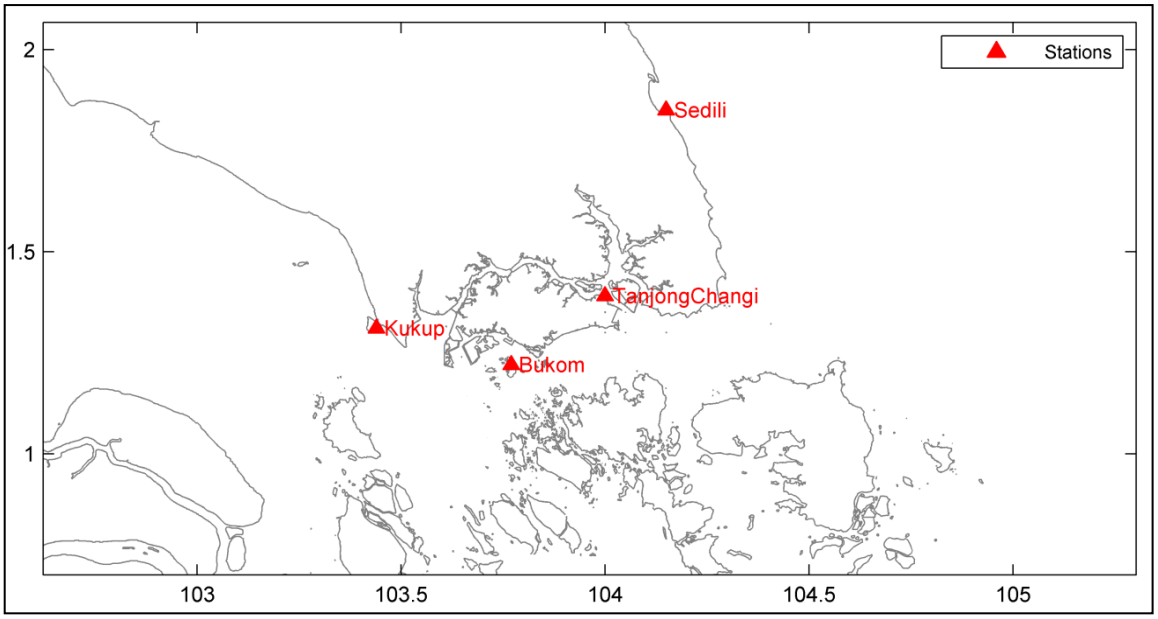


**Figure 3.3 Locations of the four selected stations**

Figure 3.4 shows the observed water level in December 2001 at Bukom station. The observed water level contains several signals like the tide, SLA and the typhoon-induced surge;

(Observed water level) = (Tide) + (SLA) + (Typhoon-induced surge)

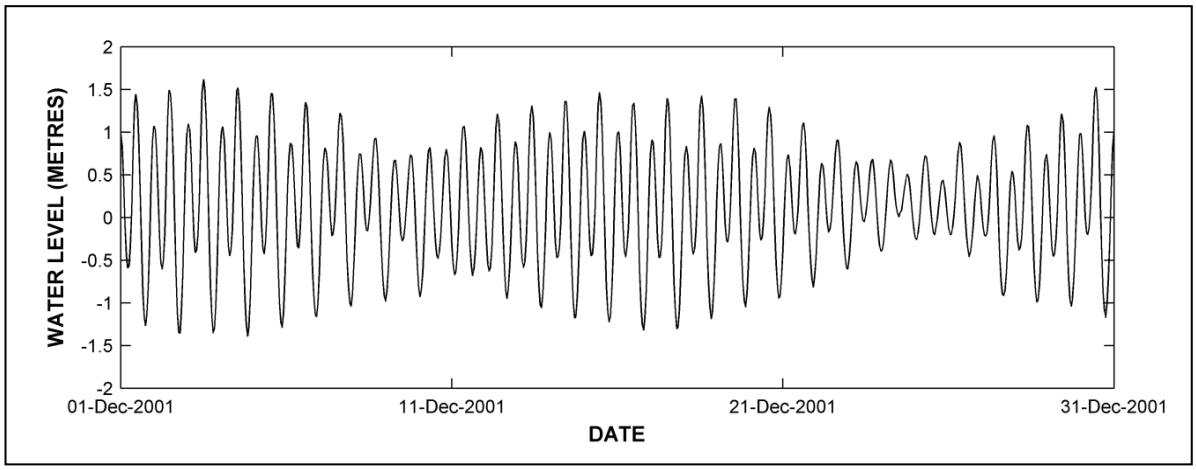


**Figure 3.4 Observed water level at Bukom station during spring and neap tides**

### 3.4.2.2 Residual water level

As the water circulation in the Singapore Strait is tide dominated, any water level anomaly is difficult to observe directly from the observation data (Figure 3.4). Therefore the influence of tide will be eliminated from the observation data by making a prediction using 65 dominant tidal constituents in this region and subtract it from the observation. The 65 tidal constituents used here can be found in Appendix C.

(Residual water level) = (Observed water level) - (Tidal prediction)

Figure 3.5 show the residual water level which represents the SLA and the typhoon-induced surge. Though the tide effect could also be achieved by a tide simulation in model (like in Section 3.4.1), a long term harmonic tidal analysis with many tidal constituents is able to provide a more accurate

tide effect which will then lead to better accuracy of the observed typhoon-induced surge determined later.

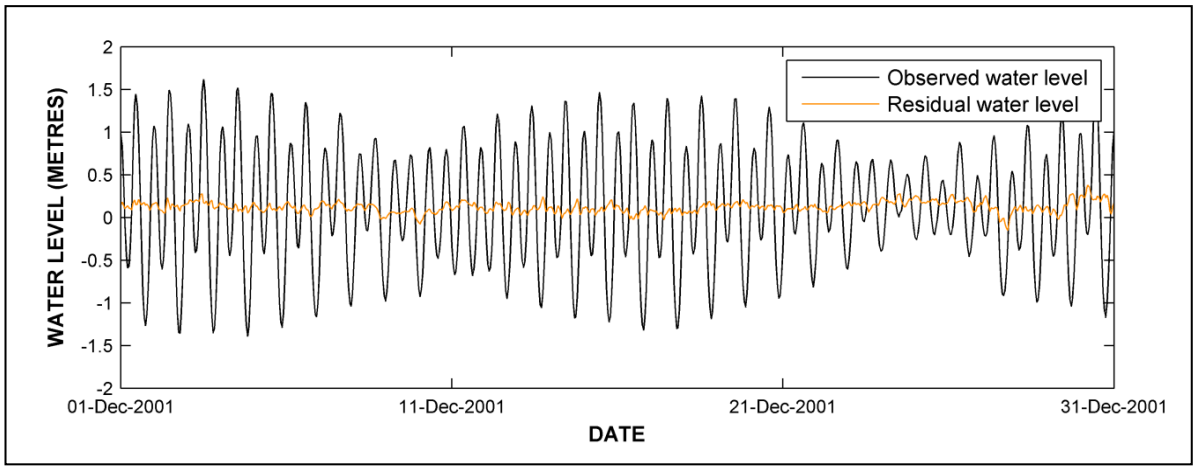


**Figure 3.5 Observed and residual water level at Bukom station**

### 3.4.2.3 Observed typhoon-induced surge

The residual water level above is still consisting of both the SLA and typhoon-induced surge. Unfortunately the SLA could not be well defined or predicted at the present moment. Several papers such as Tkalich et al. (2009b) and Raghuraj et al. (2009) have attempted to explain the cause, but none has able to predict the SLA in this region successfully. As presented earlier in Section 2.2.3, the SLA is highly correlated to large scale wind patterns associated with the monsoon. Therefore the determination of SLA can only be achieved with the help of numerical model.

There are two methods to account for SLA in the model. The first is by applying NCEP wind in a much larger model; South China Sea model (SCSM) (Gerritsen et al., 2003) to simulate the strong Northeast monsoonal wind over the South China Sea and then nest SRM in it. The second method is to correct the water level at the open boundaries of SRM which has been attempted by Twigt (2007) using satellite altimetry data. The latter has been decided to be used for this study to account for SLA in model which will then determine the 'modelled SLA' by:

(Modelled SLA) = Model(Tide+SLA) – Model(Tide only)

The residual water level from Section 3.4.2 is then subtracted by the modelled SLA to determine the typhoon-induced surge;

(Observed typhoon-induced surge) = (Residual water level) – (Modelled SLA)

Figure 3.6 shows the observed typhoon-induced surge for all the four selected stations during the two days (27$^{th}$ and 28$^{th}$ December 2001) when the typhoon is near Singapore. Note that the time is adjusted to Singapore local time (UTC+0800).

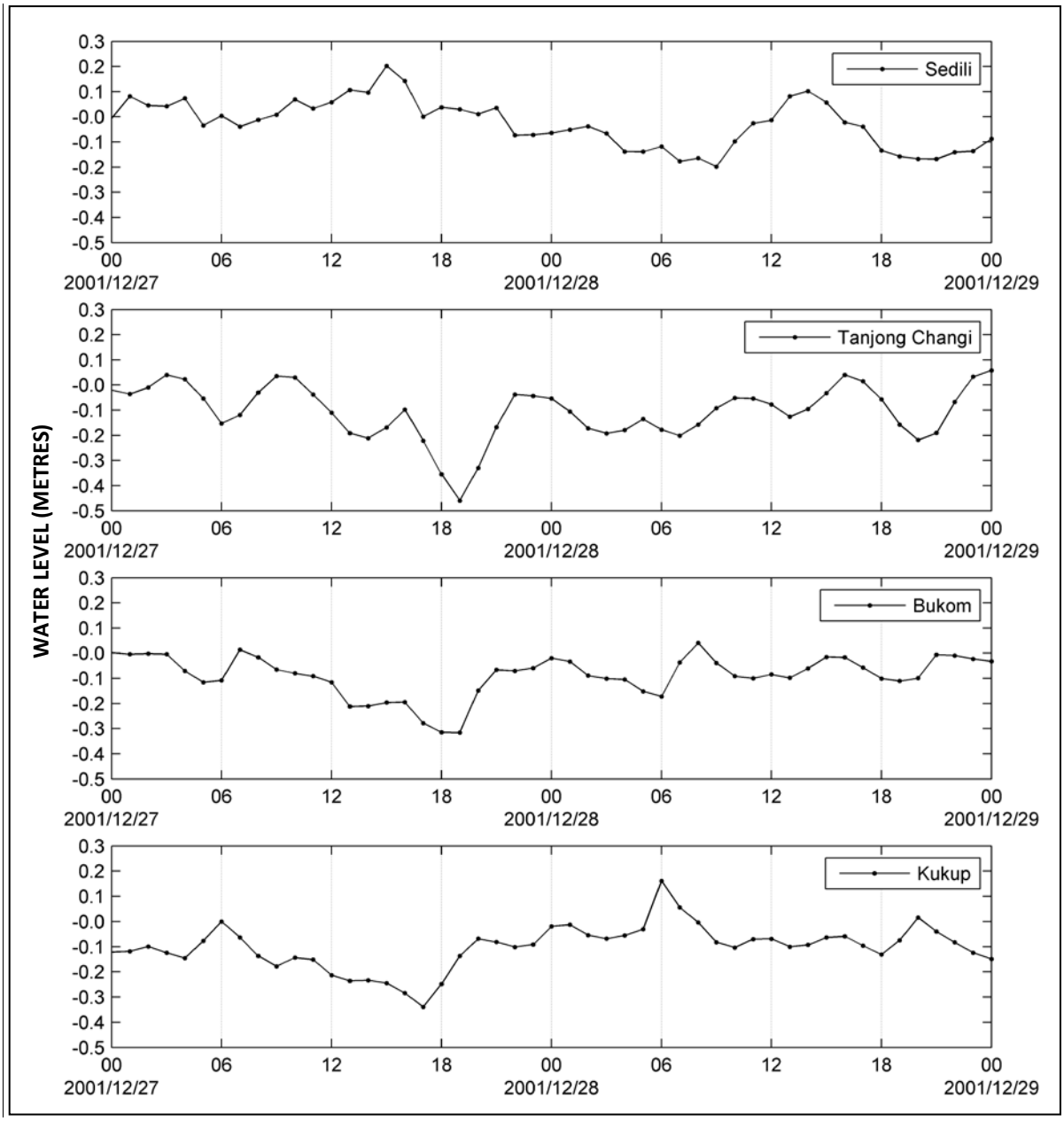


**Figure 3.6 Observed typhoon-induced surge level at four stations**

Referring to Figure 3.6, the observed surge during these two days at Sedili varies between -0.2 m and +0.2 m and highest surge is at 14:00 27th December. For Tanjong Changi and Bukom stations, there is a significant negative surge of -0.45 m and -0.32 m respectively at around 18:00 27th December. Other than this significant negative surge, both stations are experiencing only ±0.2 m surge. As for Kukup, a negative surge of 0.35 m is observed at 16:00 27th December and a positive surge peak of only 0.15 m at 06:00 28th December. The observed surge levels cannot be quantified as significant, as the surge levels are in the similar order of magnitude as SLA. The following section will attempt to perform a hindcast of the event using WES and SRM with the available information.

## 3.5 Hindcast of typhoon Vamei

This section describes the hindcast of typhoon Vamei event in 2001 using the information provided by JTWC and JMA, and water level observation. The purpose of this hindcast is to examine the

applicability of the model in the Singapore region, and determine the surge propagation during the event.

The position of the typhoon eye (track) provided by JTWC and JMA and the stations where the surge will be examined during the hindcast are shown in Figure 3.7.

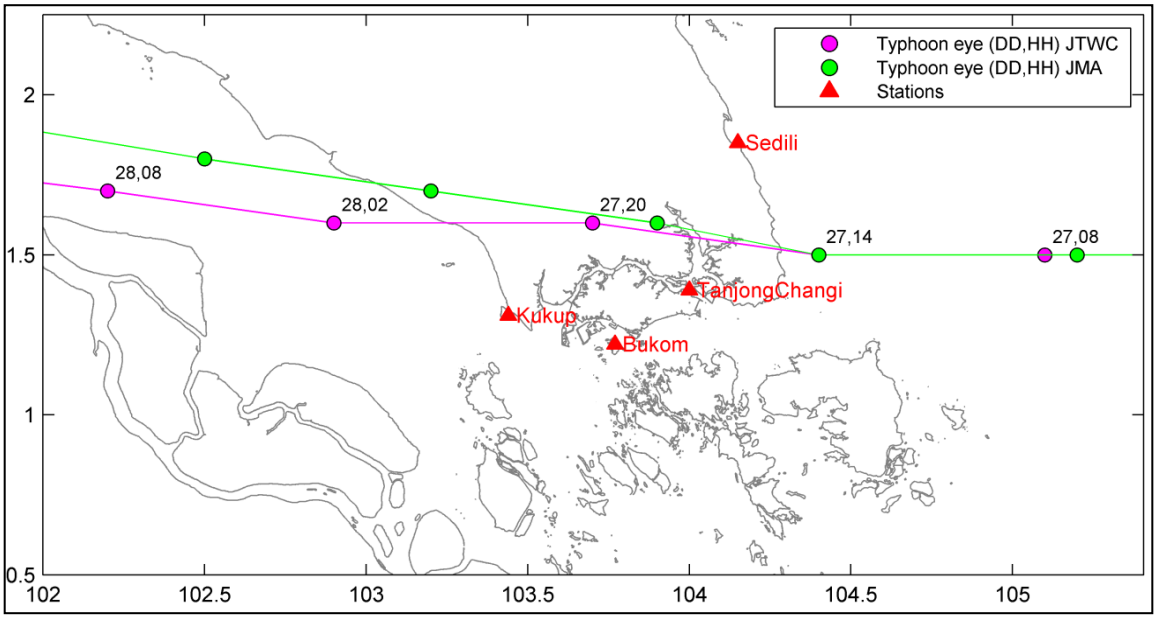


**Figure 3.7 Map of Singapore with 4 stations for calibration of typhoon Vamei with the original JTWC and JMA track**

Considering the original track given by JTWC or JMA both of which are similar in Figure 3.7, referring to Figure 3.6, the surge at Sedili is expected to be positive and at Tanjong Changi, Bukom and Kukup it is expected to be negative because of the high onshore winds on the right side (relative to the typhoon's forward motion) of the typhoon where Sedili is located and opposite wind direction for the left side of the typhoon where eastern opening of the Singapore Strait (Section 2.3.2). However, the strange thing here is that the negative surge of Kukup occurred earlier than that of Tanjong Changi and Bukom which are located nearer to the approaching typhoon from the east.

### 3.5.1 Hindcast approach

As presented in Section 2.4, both JTWC and JMA have provided information for the central position, $v_{max}$, $p_{drop}$ and $RMW$ of typhoon Vamei. Besides the central position (Figure 3.7), all other tropical cyclone (TC) parameters differ substantially. JTWC provides a larger $v_{max}$ and $P_{drop}$ but smaller $RMW$ than JMA.

Because of this it was not easy to construct a TC wind and pressure field to properly force the hydrodynamic correctly. Observation data for winds are insufficient (temporally and spatially) to calibrate the winds generated by the WES program. Moreover the WES program was initially designed to produce winds for strong hurricanes sufficiently far away from the equator. Finally typhoon tracks are usually specified as pair of geographical coordinates (latitude, longitude) with one decimal behind the comma. It is therefore accurate within ± 0.1 degrees in both direction - approximately 15 km (see Section 2.4), explaining the difference between JMA and JTWC track.

Consequently we were unable to check the quality of the winds generated by the WES program. Hence we decided to play with some input parameters of the WES program, generate a number of winds and then use the hydrodynamic simulation results (i.e. storm surge results) to select the appropriate typhoon characteristics that matches the surge produce by the hydrodynamic model.

As WES provides the options to choose which parameters to input for the wind and pressure distribution, the following presents the result of using two different input options of WES for both JTWC and JMA. After some tests, we decided to use the standard option of WES to hindcast Vamei as shown in the following. The results of using other options have been presented in Appendix D.

### 3.5.2 First attempt using JTWC and JMA's information (Simulation 1)

WES and Delft3D simulation results for typhoon Vamei based on the data from two meteorological agencies' are shown in Figure 3.8 using the standard option; $v_{max}$ and $P_{drop}$. Based on JTWC's data, the simulation results show larger surge ranges in terms of positive and negative peak surges than that using JMA's data.

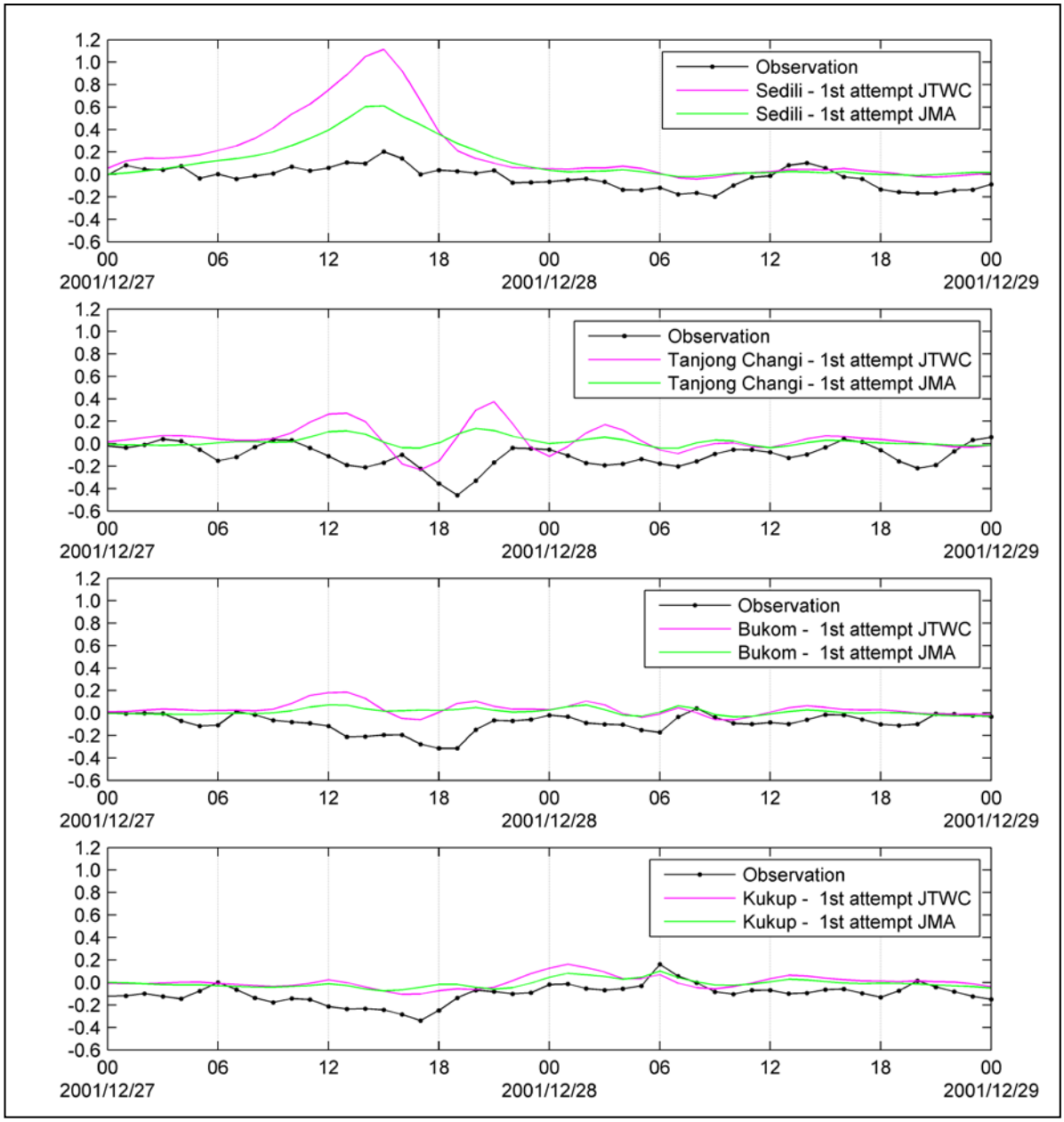


**Figure 3.8 Simulated surge level (metres) using typhoon information provided by JTWC and JMA**

The results in Figure 3.8 represents the effect of surge of different typhoon intensities (JTWC and JMA), the positive and negative surge peaks are not only differed in scale but also in phase from the observation. As both agencies have provided the central position of typhoon with one decimal behind the comma (i.e. accuracy of ± 0.1 degrees in both direction - approximately 15 km), and due to large radii of the typhoon specified, it is decided to calibrate the model is by adjusting the typhoon's track instead of intensity.

In the given track (central positions), only 14:00, 20:00 and 02:00 (27$^{th}$ to 28$^{th}$ December) are the time where the typhoon is near Singapore. Hence positions of these three points will be adjusted with the intensities ($v_{max}$ and $p_{drop}$) provided by JTWC at these three points remain unchanged. During the calibration process, the position of these three points will be adjusted one by one systematically in four directions (North, South, East and West). More than forty simulations have been made before arriving at the final one. The following will only present the two main simulations

of progressive improvement relative to the original one (first attempt) and then the final simulation which is concluded as the model for typhoon Vamei. Note that the first attempt made using the original track by JTWC will be named 'Simulation (1)'. The track of the simulations is shown in Figure 3.9 and results are described in the following sections.

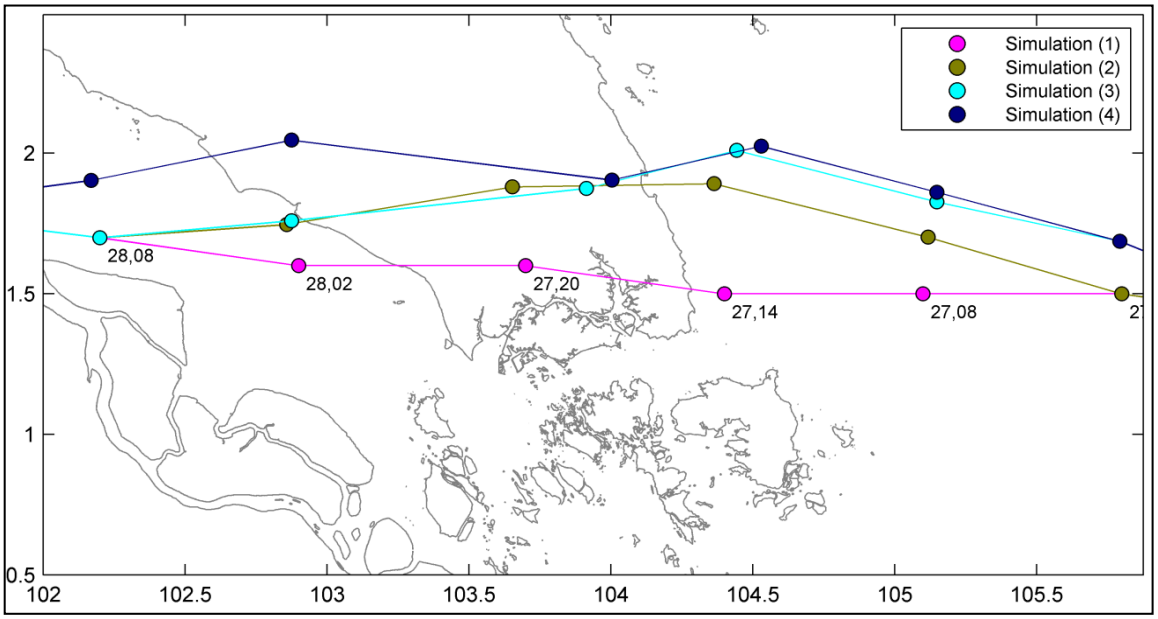


**Figure 3.9 Tracks of the four simulations for Vamei hindcast**

### 3.5.3 Simulation (2)

Looking at result of Simulation (1) (Figure 3.8), the positive surges at Sedili is too high. Tanjong Changi and Bukom show 'undesired' positive surge peaks at 12:00 and later at 21:00 and 04:00 for Tanjong Changi only. The position surge peak at Kukup is in the wrong phase; 02:00 instead of 07:00. As discussed in Section 2.3.2, storm surge is high at the right side (relative to forward motion) of the typhoon especially during landfall. In order to reduce the surge at Sedili, the track before landfall is shifted to the North which makes Sedili on the left of the typhoon during landfall. Positions of 14:00, 12:00 and 02:00 have been moved to the North by 20 to 45 km (Figure 3.9). The result is shown in Figure 3.10.

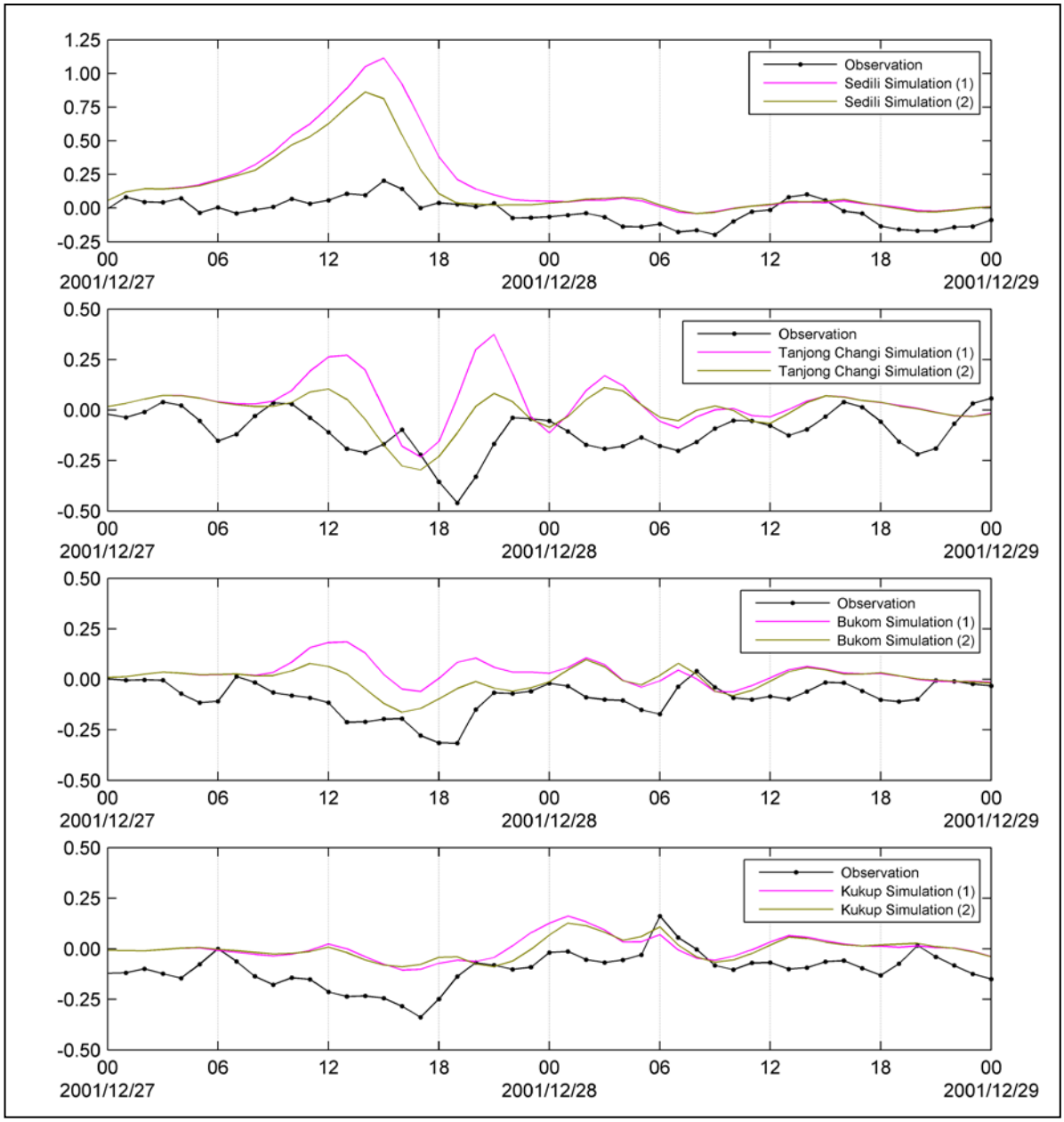


**Figure 3.10 Surge level (metres) of Simulation (2)**

As seen in the result above, Sedili shows a significant decrease in surge (around 30 cm) at the positive peak, and the positive surge peaks at Tanjong Changi and Bukom have reduced significantly. However there is no improvement for Kukup.

### 3.5.4 Simulation (3)

Simulation (3) will have the landfall later by two hours at 18:00 instead of 16:00 in Simulation (2) by adjusting the 14:00 and 20:00 (27$^{th}$ December) points to the east (Figure 3.9). Also, the landfall is shifted slightly further North. The result is shown in Figure 3.11.

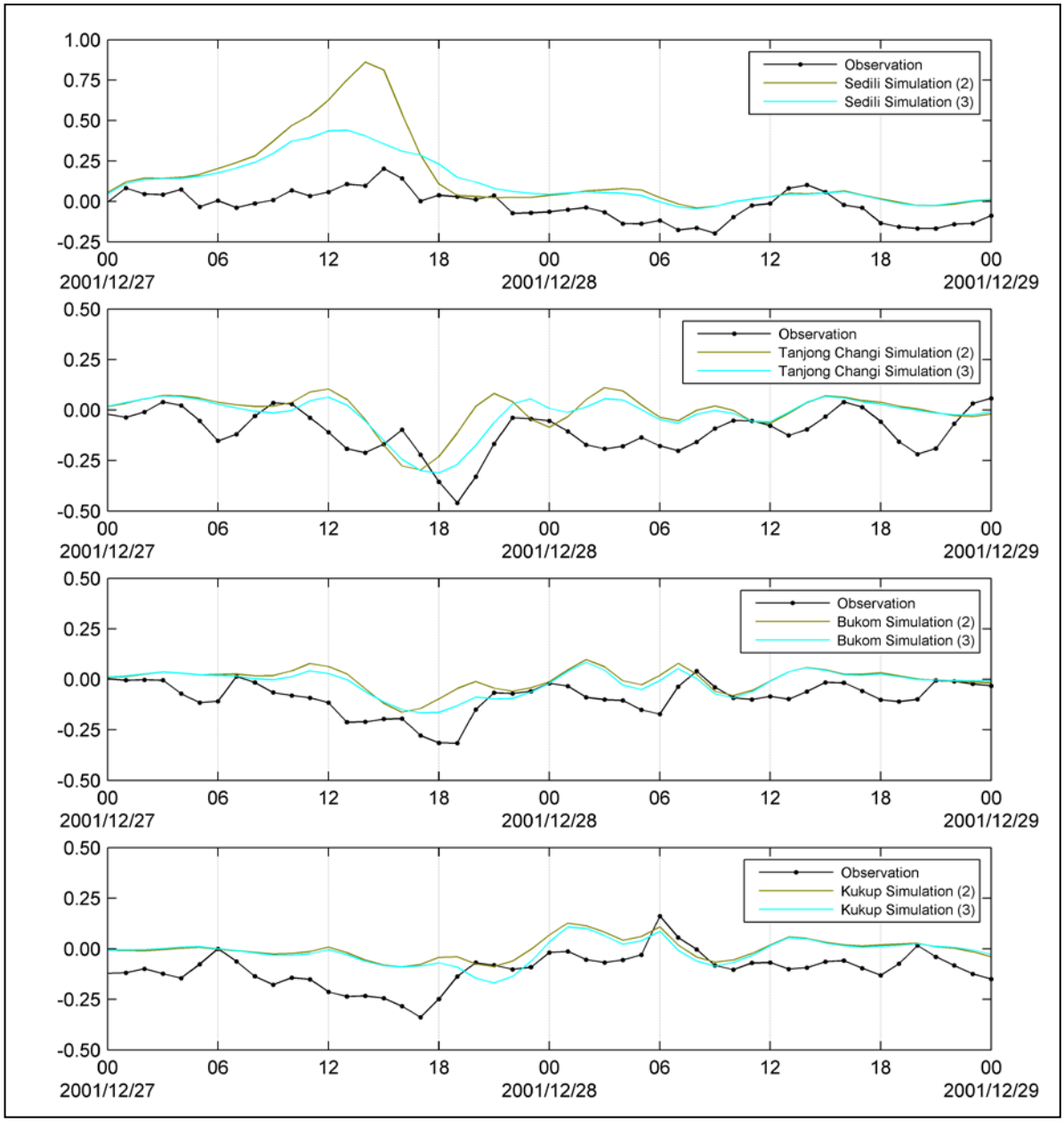


**Figure 3.11 Surge level (metres) of Simulation (3)**

Referring to Figure 3.11, the positive surge peak at Sedili is reduced to 0.43 m and Kukup finally shows a negative surge peak, though the phase is still incorrect; 21:00 instead of 16:00 27th December. However, there is no improvement for Tanjong Changi and Bukom stations.

### 3.5.5 Simulation (4)

In this simulation, the 14:00 and 20:00 (27th December) points are moved further east by 10 km compared to Simulation (3) which delays the landfall by another hour to 19:00. The 02:00 and 08:00 (28th December) are also moved to the North by about 25 km (Figure 3.9). The result is shown in Figure 3.12.

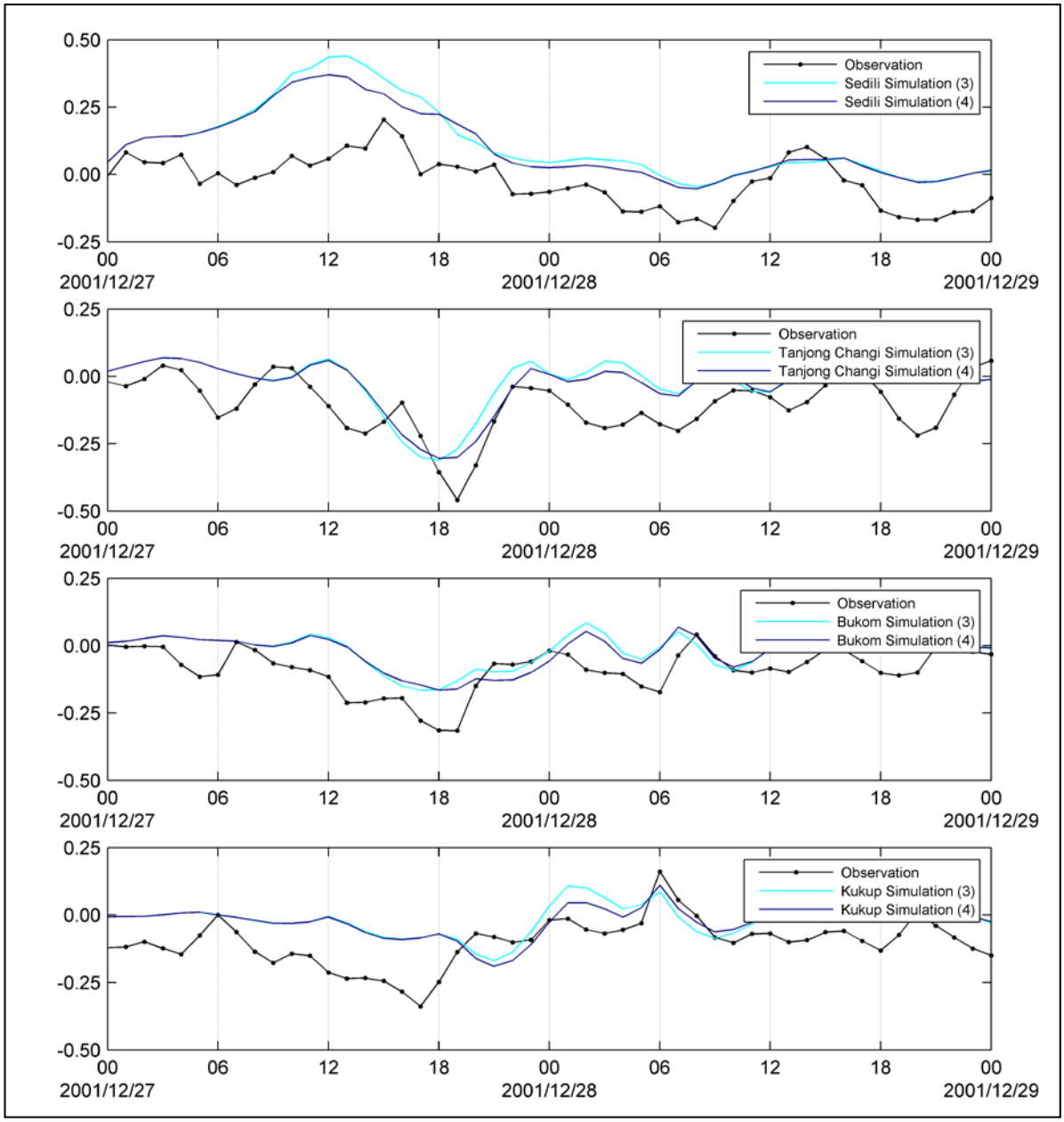


**Figure 3.12 Surge level (metres) of Simulation (4)**

The positive surge peak in Sedili has been further reduced to just 0.38 m, the negative surge peak at Tanjong Changi is also in phase with the observation, and the 06:00 (28th December) positive surge peak at Kukup is more 'pronounced' than the previous simulations. As for Bukom, no significant improvement is observed.

Among all the four simulations above, Simulation (4) has proven to give the best results particularly when the observation is added with a constant 0.1 m as shown in Figure 3.13. This may be due to the difference between the mean sea level of recorded in the field tidal gauge and the mean sea level in model which apparently is about 0.1 m. The propagation of the surge is shown in Appendix E.

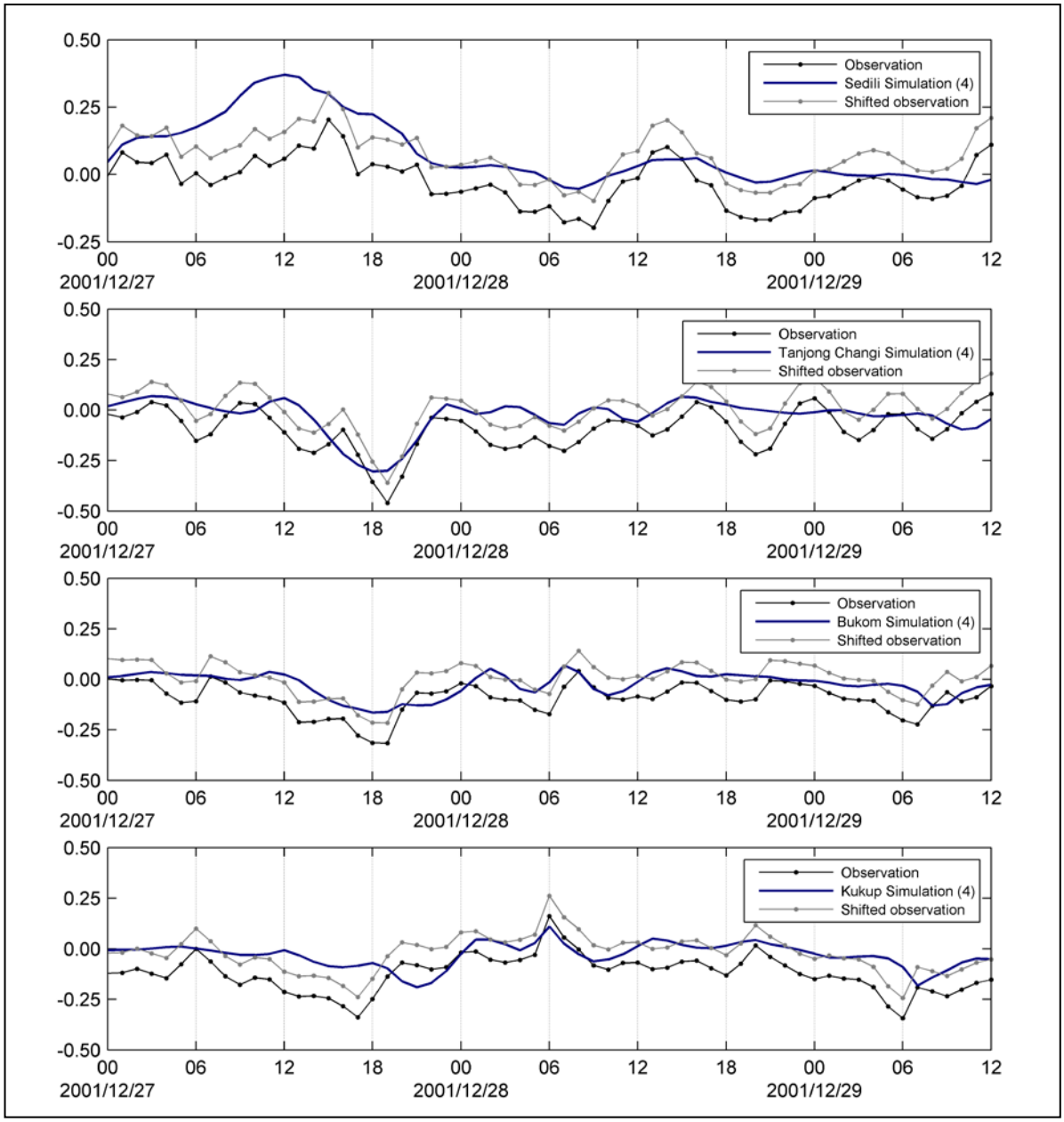


**Figure 3.13 Surge level of simulation (4) and the adjusted (shifted) observation**

### 3.5.6 Discussion

As presented above, Simulation (4) shows the best result among the other simulations by comparing the storm surge at the four stations of the observations. Comparing to Simulation (1) which uses the track provided by JTWC, Simulation (4) has showed great improvement in the surge level. The track used in Simulation (4) may have deviated from the one reported by JTWC which can also be seen in the TRMM (Tropical Rainfall Measuring Mission) imagery (Figure 3.14).

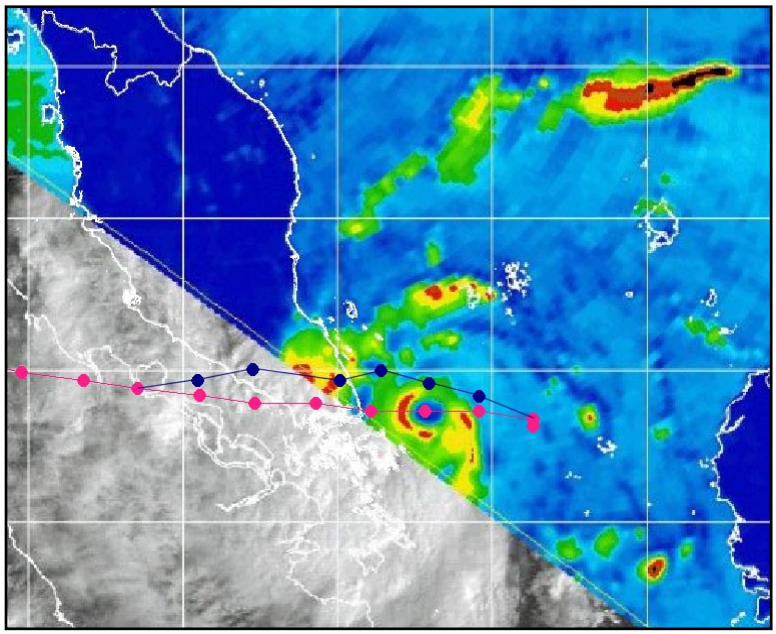

**Figure 3.14 Comparing JTWC track (pink) and model track (blue) with TRMM image which reveals the eye of Vamei on 08:00 (UTC+0800) 27th December 2001 (Adopted from JTWC, 2001)**

Due to insufficient detailed and low temporal resolution information of the typhoon Vamei, the cyclone wind distribution could only be modelled as an almost symmetrical cyclone's, which is not the case in reality as observed in Figure 2.7 and 3.14.

# 4 Defining the extreme water condition

This section will determine the height of water level caused by an extreme event which involves the typhoon, tide, SLA and sea level rise. Being the primary source of surge level, the assumed typhoon maximum intensity will be checked against available wind data for Singapore. This is followed by examination of the surge induced by the typhoon by carrying out sensitivity analysis of the typhoon parameters on the surge in Singapore waters. Secondly, the 'worst' track that will give a high surge level relative to the wind intensity will be proposed and the effect of spring and neap tide on the surge will be briefly investigated. Thirdly, the intensity of the cyclone wind will be estimated using extreme wind prediction based on local wind data. Finally, the water level of the extreme event will be approximately computed.

In short the following steps are taken to determine the extreme water level condition for Singapore:

1. Extreme wind analysis using wind data at Changi station
2. Sensitivity analysis on track, forward speed and RMW
3. Derive the 'worst track'
4. Run the worst track in both spring and neap tide
5. Extreme case scenario
    a. Surge (from worst track) + High tide + SLA

## 4.1 Extreme wind event estimation

The return period of typhoon Vamei proposed by Chang et al. (2003) did not convey the intensity of the typhoon (Appendix A). As typhoon Vamei was the first and only typhoon found in this region, there is only one record of typhoon. Hence, in this section an attempt is made to estimate the wind intensity with recurrence interval of 1 in 400 year based on wind data of 13.5 years at Changi Airport Station (Figure 4.1). The data is obtained from the (Weather Underground, http://www.wunderground.com/history/). A priori it is known that the duration of the data is too short to produce a desirable result. Nevertheless, this is the only data that is available.

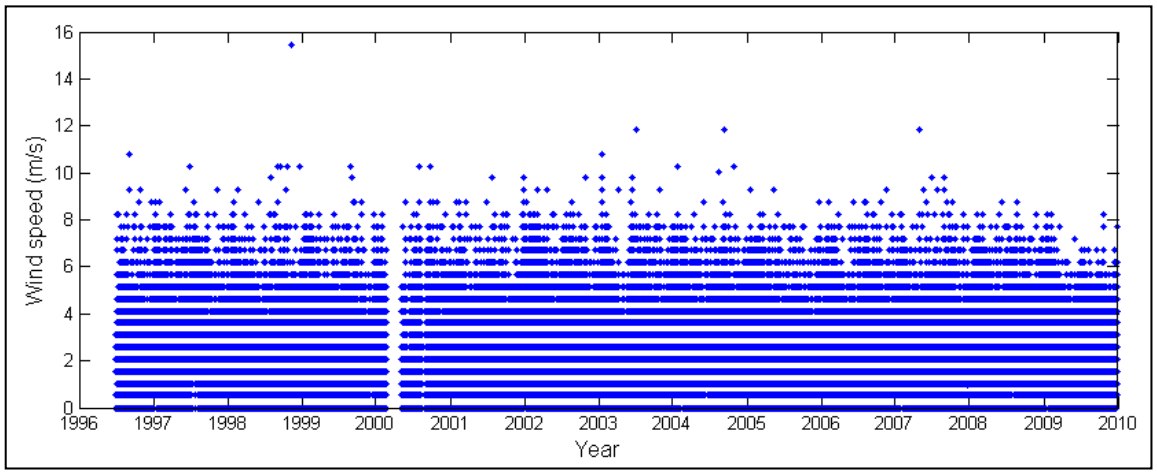


**Figure 4.1 Wind data 13.5 years (1996 July till end of 2009)**

Figure 4.1 show the wind speed every 30 minute. As the focus of this exercise is to determine extreme wind, only records that are higher than 8.5 m/s will be used in the analysis. Because high wind speed occurrences under storm conditions usually last for few hours, two or more consecutive

extreme value records will be considered as one event. Table 4.1 shows the number events of each extreme wind speed

**Table 4.1 Data of events with wind speed greater than 8.5 m/s in 0.5 m/s bins**

| Wind speed (m/s) | Number of events |
|---|---|
| 8.5 – 9.0 | 41 |
| 9.0 – 9.5 | 16 |
| 9.5 – 10.0 | 9 |
| 10.0 – 10.5 | 11 |
| 10.5 – 11.0 | 2 |
| 11.0 – 11.5 | 0 |
| 11.5 – 12.0 | 4 |
| 12.0 – 12.5 | 0 |
| 12.5 – 13.0 | 0 |
| 13.0 – 13.5 | 0 |
| 13.5 – 14.0 | 0 |
| 14.0 – 14.5 | 0 |
| 14.5 – 15.0 | 0 |
| 15.5 – 15.5 | 1 |

Weibull distribution (Weibull, 1951) has been commonly used, accepted and recommended in most literatures (Eskinazi and Cramer, 1982 and Garcia et al, 1998) to express the wind speed frequency. This distribution has been applied here to fit the 13.5 years of wind data based on maximum likelihood estimation method. The Weibull distribution is a two-parameter model: the shape parameter $k$ that defines the shape of the distribution and mainly depends on the regularity of the wind regime and the scale parameter $c$ which is a measure of the mean wind speed. The probability density function of a Weibull random variable $x$ is

$$f(x;c,k) = \begin{cases} \frac{k}{c}\left(\frac{x}{c}\right)^{k-1} e^{-(x/c)^k} & x \geq 0 \\ 0 & x < 0 \end{cases} \qquad (6.1)$$

Based on the extreme events within the 13.5 years (Table 4.1), $k$ and $c$ are found to be 6.891 and 10.162 respectively. With these values, a return period of 1 in 400 years yields only a wind speed of 13.8 m/s (27 knots) which according to the tropical cyclone classification of both JTWC and JMA is considered to be a tropical depression, not a typhoon. As mentioned earlier, we already anticipated that 13.5 years of wind data is not sufficient to estimate very high wind speed. The result of this analysis should therefore regard as the lower limit for the wind speed with a recurrence interval of 1 in 400 years. It is to be expected that this analysis would have yield a higher wind intensity if longer historical wind data would have been available

Although this exercise did not confirm the conclusion presented by Chang et al. (2003) (Appendix A) for an occurrence of a 1 in 400 years typhoon of intensity similar to Vamei, but given the lack of wind data we can assume that Chang's conclusion may still be applied for this study.

## 4.2 Sensitivity analysis of typhoon parameters on storm surge in the Singapore region

Typhoon Vamei, as shown earlier, did not produce high storm surge levels for Singapore. Our earlier investigation suggests that with a slightly different track the effect for Singapore could have been much worse.

For the determination of an extreme water level condition we decided to perform sensitivity tests of the surge levels in Singapore region as a function of a number of typhoon parameters. However, as the extreme wind analysis performed in previous section did not provide a conclusive indication for the wind speed that we could apply for a typhoon with 1 in 400 years return period it was decided to fix the wind intensity and pressure drop during the tests, respectively at 28.3 m/s (55 knots) and 2200 Pa[1]. Both of which are obtained simply by taking the average of the highest record of JTWC and JMA (Section 2.4)

Consequently the sensitivity tests will focus on the effect of other three typhoon parameters in the Singapore region (see also earlier discussions in Section 2.3):

- track,
- forward speed and
- radius of maximum wind

At the end of this systematic sensitivity tests, a 'worst' track will be proposed based on the test results. Then the effect of spring and neap tide on the surge will be investigated using the proposed worst track.

The water level behavior at Tanjong Pagar station will be presented as part of the sensitivity tests as an indication of the surge in the Singapore Strait (see Figure 4.2). However, the main analysis will be carried out focused on the map of the surge contour levels. The inflow and outflow of water in the strait (see Figure 4.2) will also be examined in this context. Note that the cross sectional discharge is inclusive of tidal flow fluxes of the model, but all the case runs in a parameter test will have the same tidal flux (consistent simulation time frame), and the discharge of simulation without typhoon (tide only) will also be presented to see enhancement or weakening of fluxes caused by the different typhoons.

[1] The effect of the barometric pressure drop is straightforward and linked to intensity. The level of the sea surface is inversely proportional to the pressure drop. A pressure drop of 1 mbar (100 Pa) is equivalent to 0.01 m rise in water column.

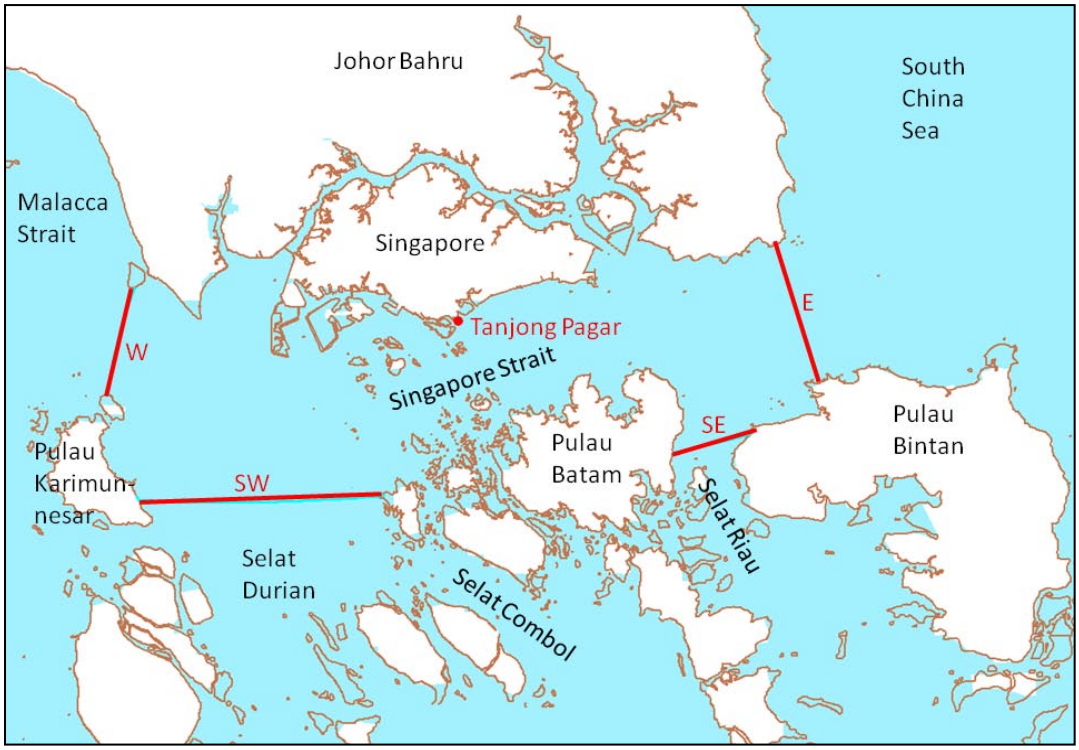


**Figure 4.2 Location of Tanjong Pagar station and various cross sections in the Singapore Strait**

### 4.2.1 Sensitivity of surge level as a function of the track

Three horizontal tracks at 1.00 °N, 1.25 °N and 1.5 °N will be defined to check the sensitivity of the surge on for the prescribed typhoon track (Figure 4.3). A typhoon of constant $RMW$ of 25 km and 3.5 m/s travelling speed will be used here.

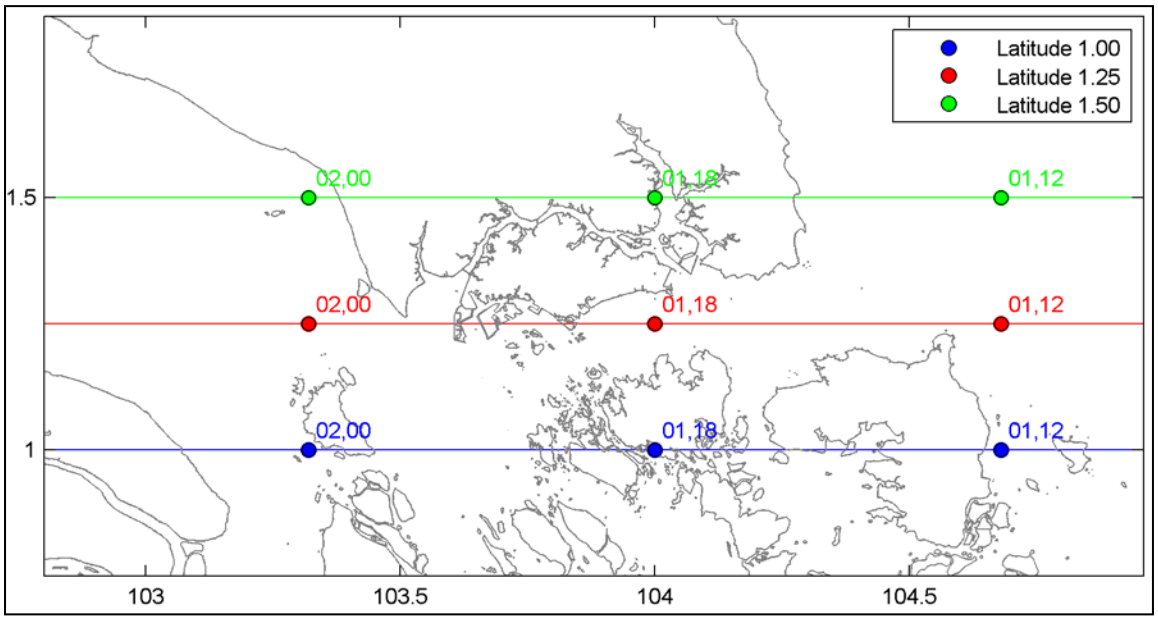


**Figure 4.3 Tracks at different latitude with day and time (from reference date) of the typhoon eye (DD,HH)**

From the result in Figure 4.4 the track 1.00 °N and 1.25 °N gave a much higher surge than track 1.50 °N at Tanjong Pagar. The reason for this is the same as the case of typhoon Vamei. While the typhoon is approaching Singapore Strait from the east, the cyclonic character of the typhoon caused the water to pile up at the north of the storm eye and push the water away at the south of the eye

(Figure 4.7). Hence, for the case of 1.00 $^{o}$N (Figure 4.5a and b) and 1.25 $^{o}$N (Figure 4.6a and b), water is forced into the Singapore Strait by the typhoon.

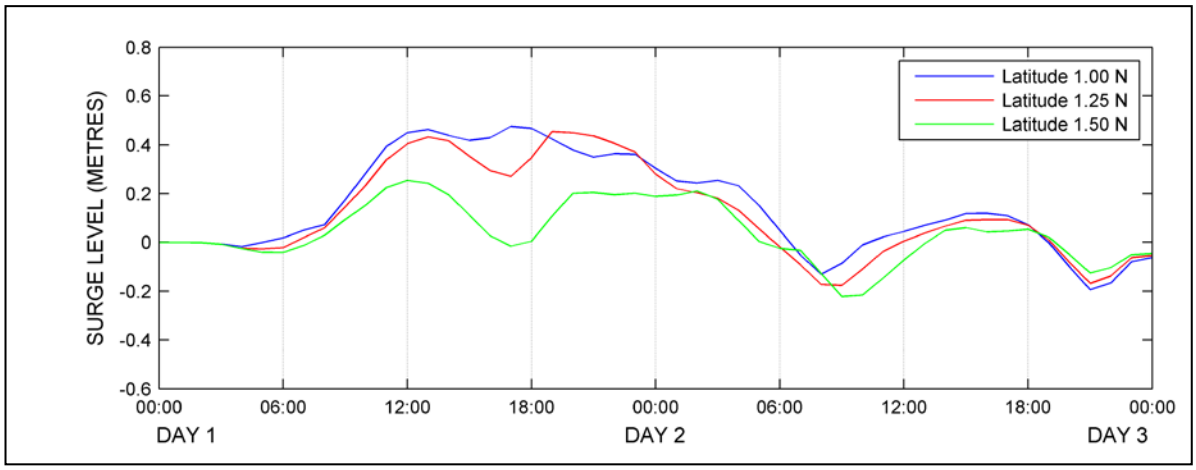


**Figure 4.4 Surge level at Tanjong Pagar caused by typhoon track of different latitudes**

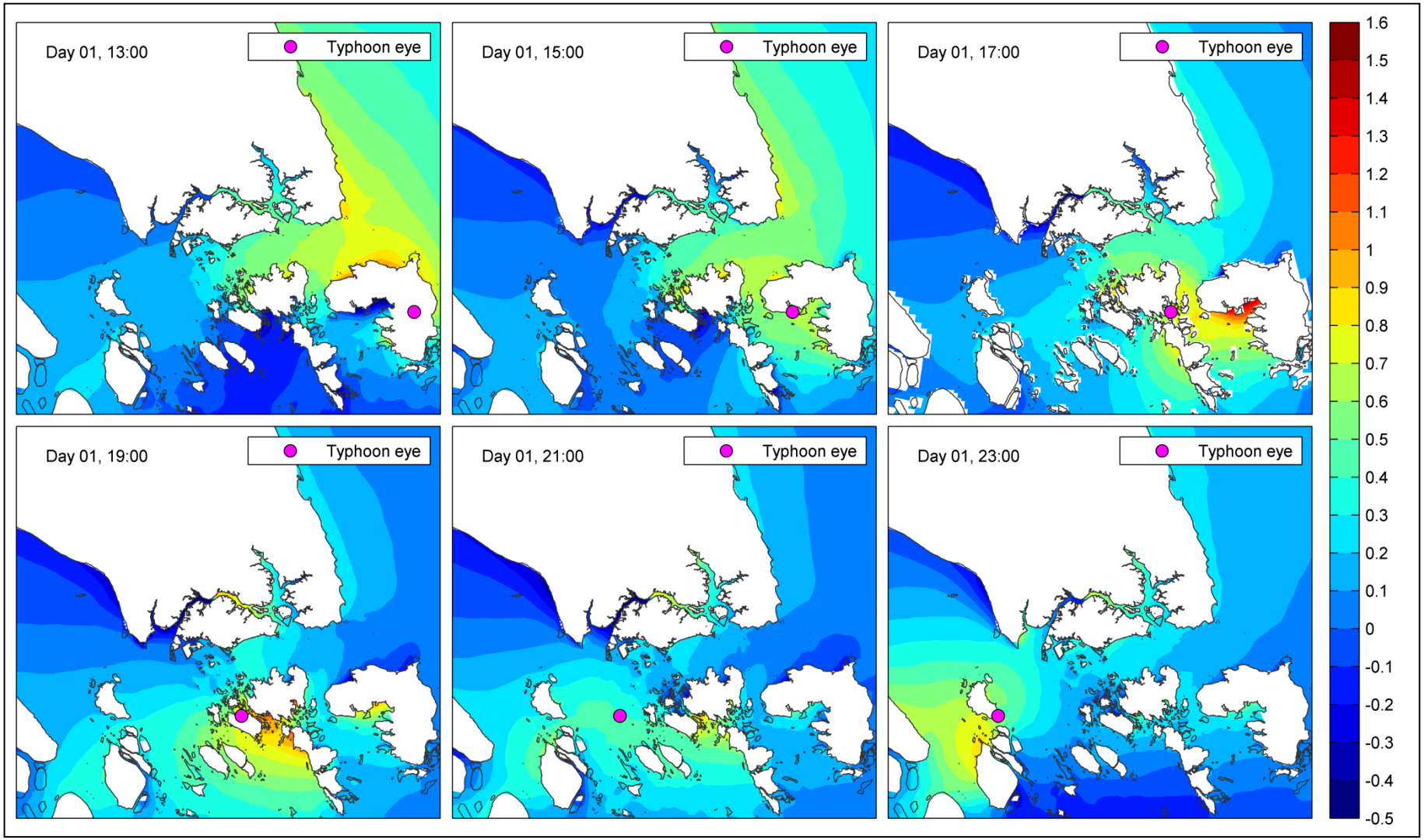


**Figure 4.5 Surge level in metres caused by typhoon track at 1.00 degree North (a) top left, (b) top middle, (c) top right, (d) bottom left, (e) bottom middle and (f) bottom right**

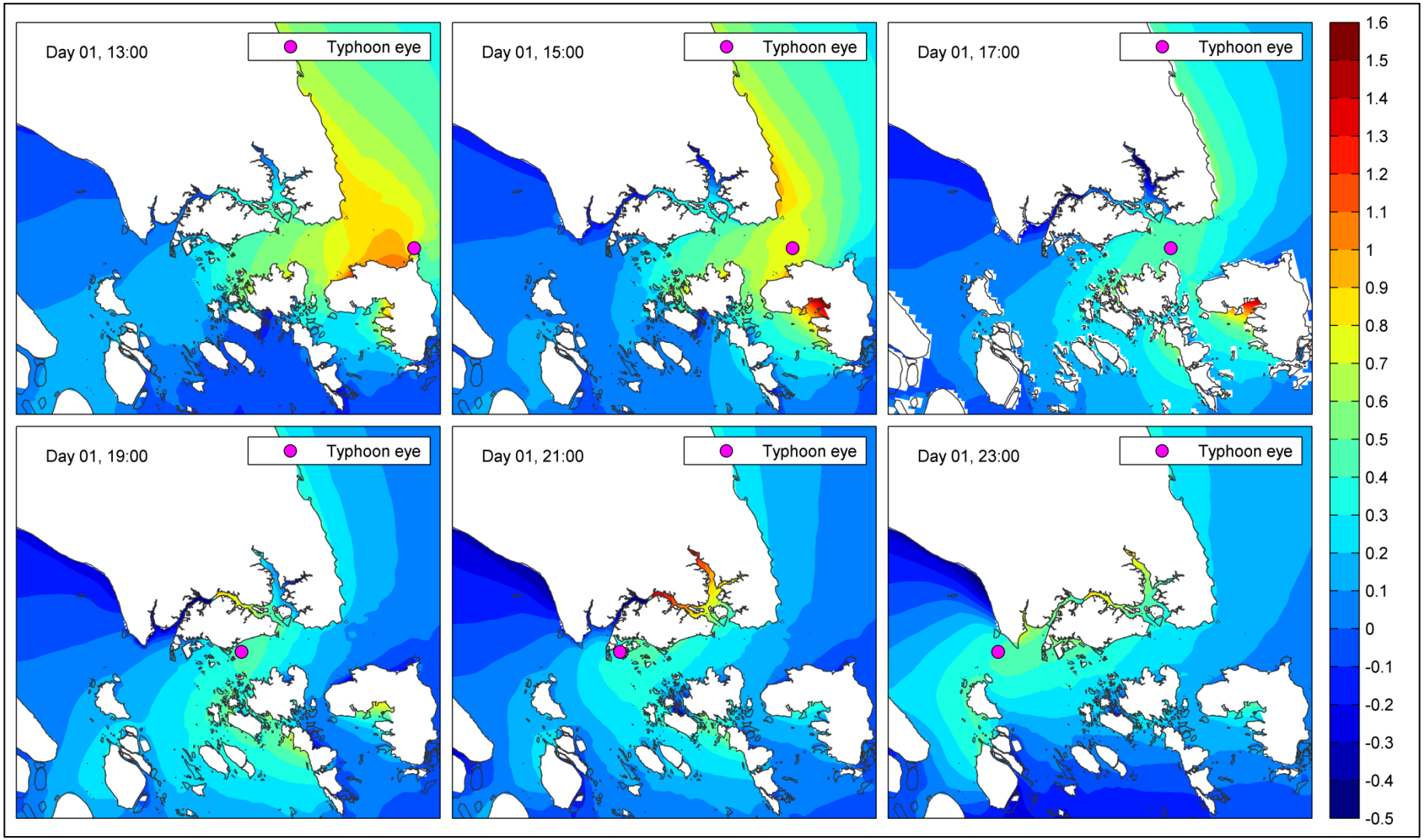


**Figure 4.6 Surge level in metres caused by typhoon track at 1.25 degree North (a) top left, (b) top middle, (c) top right, (d) bottom left, (e) bottom middle and (f) bottom right**

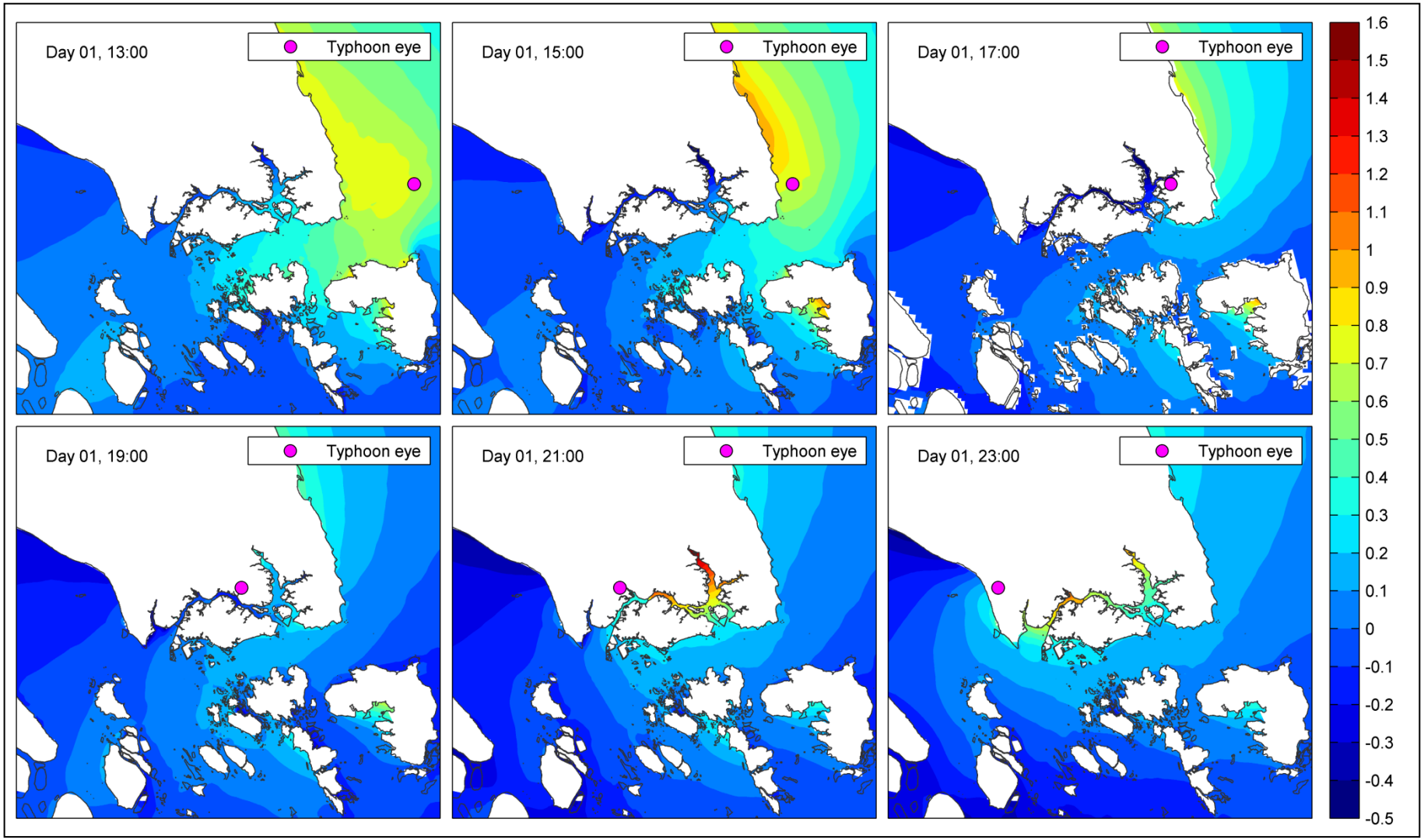


**Figure 4.7 Surge level in metres caused by typhoon track at 1.50 degree North (a) top left, (b) top middle, (c) top right, (d) bottom left, (e) bottom middle and (f) bottom right**

The momentary discharge of water into the strait via cross-section E is shown in Figure 4.8. The inflow of water of track 1.50 °N is smaller than the other two at 07:00 of Day 1, and at around 13:00 of Day 1 high volume of the water is flowing outwards from the strait into the South China Sea. For the other two tracks, the flow through this cross section is kept in one direction (into the strait). This is especially true for track 1.00 °N, as the entire time the typhoon is in or near the strait (12:00 to 23:00 of Day 1).

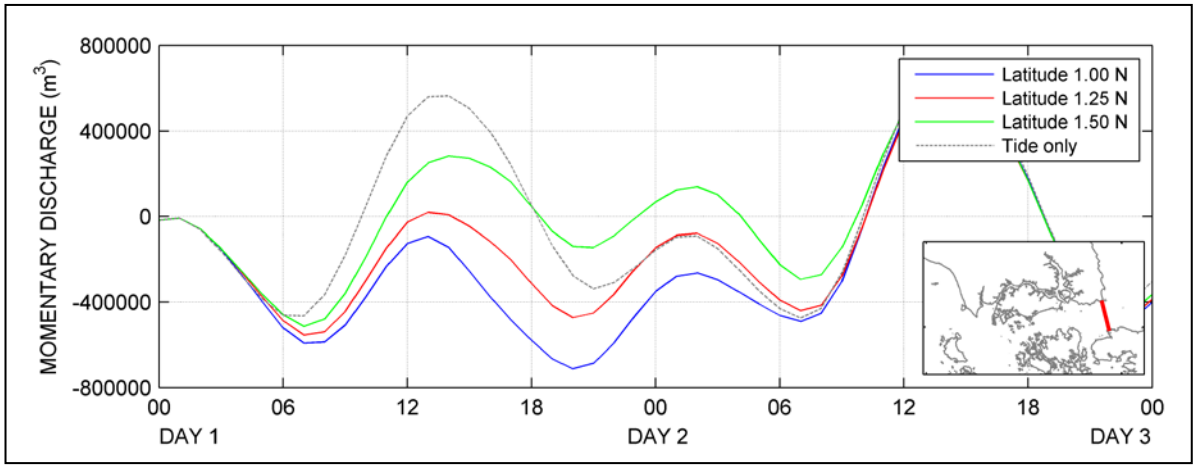


**Figure 4.8 Momentary discharge at cross section E for different typhoon tracks (positive indicates eastward discharge and negative indicates westward discharge)**

Interestingly for track 1.00 °N, because of the presence of Pulau Bintan at the east entrance of the strait, more water has been forced into the strait after the typhoon made a landfall on the eastern coast of Pulau Bintan when compared to track 1.25 °N (Figure 4.8). This is again due to the cyclonic character where the wind is forcing the water along the eastern coast of the island northwards and into the strait after landfall (Figure 4.5b). After making landfall water is continuously being pushed towards the west due to the west blowing wind at the north of the eye as the typhoon moves westward on land. However, when the typhoon is approaching the west of Pulau Bintan, water starts flowing into Selat Riau between Pulau Bintan and Pulau Batam, which can be observed at cross section SE (Figure 4.9). In Figure 4.9, the flow discharge out of Singapore Strait through cross-section SE is higher for track 1.00 °N compared to track 1.25 °N at around 15:00 of Day 1.

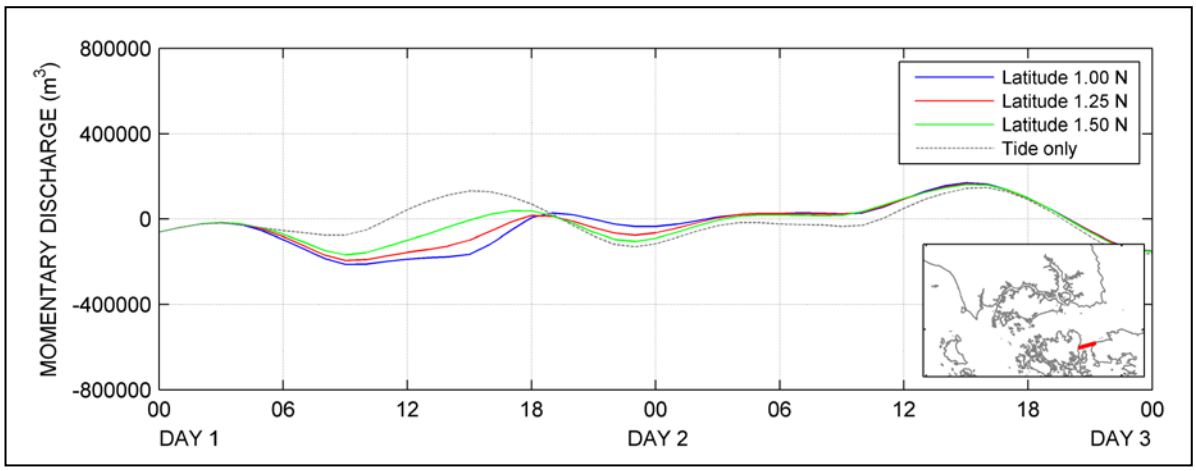


**Figure 4.9 Momentary discharge at cross section SE for different typhoon tracks (positive indicates northward discharge and negative indicates southward discharge)**

At around 21:00 of Day 1, under the influence of track 1.25 °N, water from the Malacca Strait is directly being forced by the wind into the Singapore Strait via cross-section W (Figure 4.6e) which however is not the case for track 1.00 °N (Figure 4.5e). Evidence can be observed from the discharge at cross-section W in Figure 4.10.

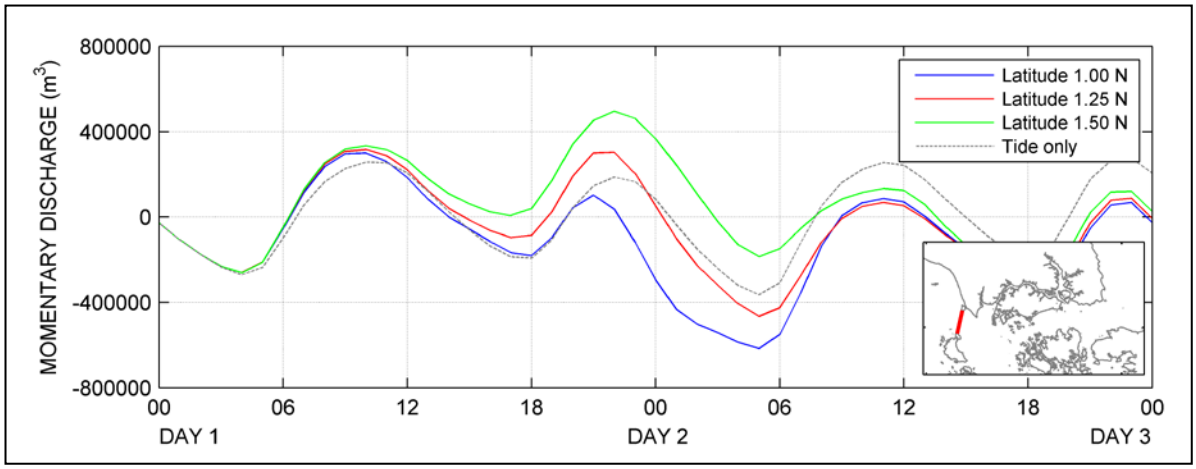


**Figure 4.10 Momentary discharge at cross section W for different typhoon tracks (positive indicates eastward discharge and negative indicates westward discharge)**

The results above leads to the observation that the typhoon-induced surge in the Singapore Strait is the greatest for track 1.00 °N initially and then for tracks 1.25 °N or 1.50 °N mid-way in the strait; much of the water from the South China Sea contributes to the surge initially, and after midway of the strait the main water source becomes the Malacca Strait. However, in reality, the strength of the typhoon weakens when it moves on land due to lack of moisture source. Unlike in the model, a real typhoon is unable to sustain its strength while travelling on land. Also, the track which will give the highest surge is partially dependent on the $RMW$; if the $RMW$ is 25 km, the highest surge will most probably occur at 25 km away from the eye at that point of time.

### 4.2.2 Forward speed

As the forward speed of the only known typhoon in this region is about 3.5 m/s, the values used in the sensitivity test will centre around 3.5 m/s by ± 2.0 m/s.

Figure 4.11 shows the position of the typhoon at different times for the different forward speed; 1.0 m/s, 3.5 m/s and 5.0 m/s. The point in the far east indicates the first position of the typhoon in the Singapore Strait while the point in the far west marks the last position of the typhoon in the strait before it moves to the Malacca Strait.

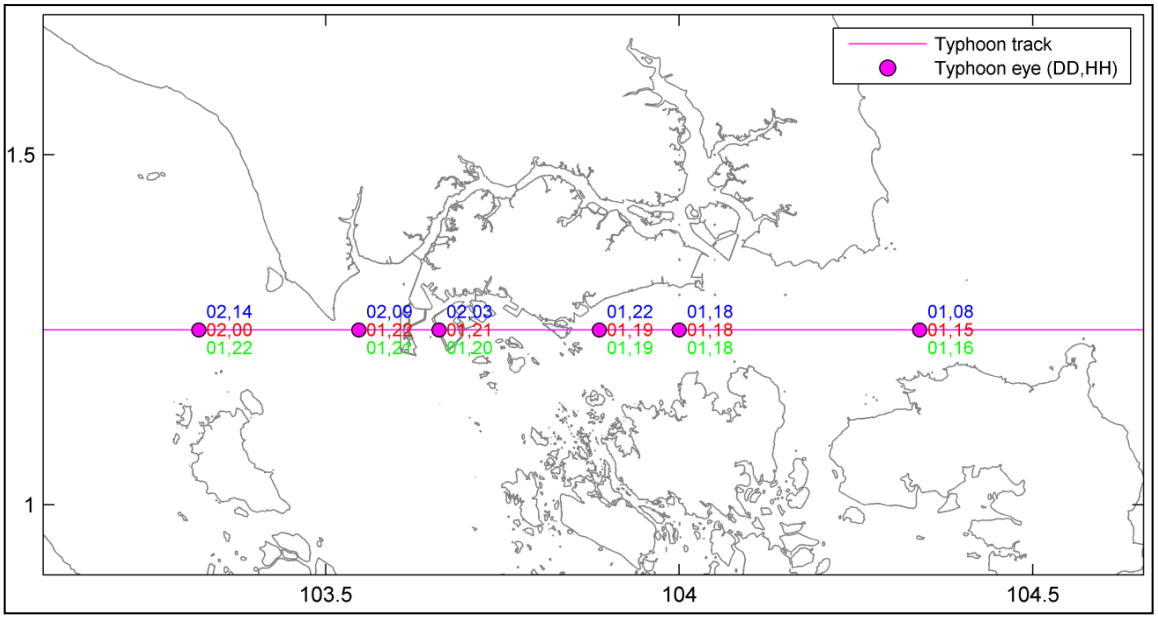


**Figure 4.11 Positions of typhoon eye with typhoon propagating at different speeds 1.0 m/s (Blue), 3.5 m/s (Red) and 5.0 m/s (Green)**

Figure 4.12 shows the surge level of the three cases at Tanjong Pagar. For the three different propagation speed the surge level at this station is more or less similar.

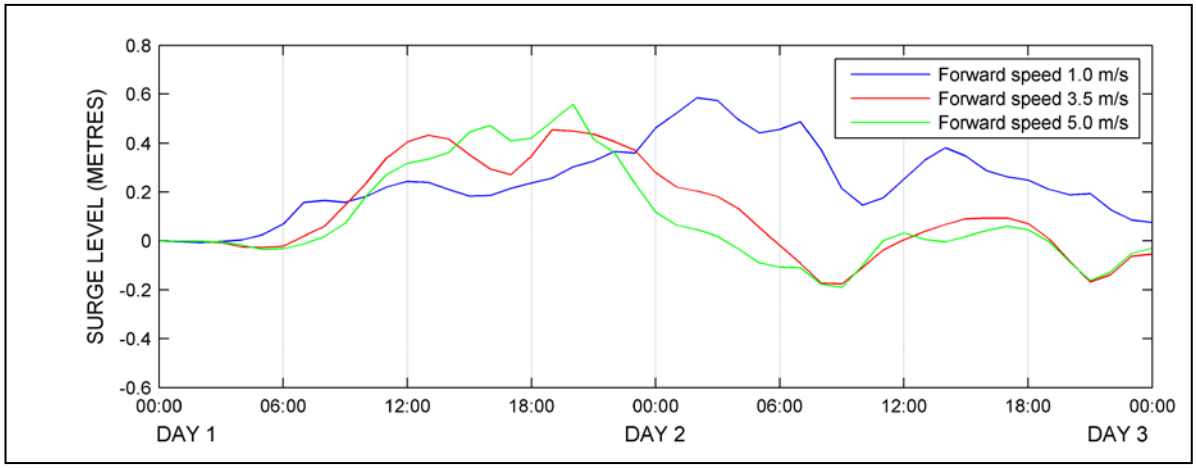


**Figure 4.12 Surge level at Tanjong Pagar caused by typhoon track of different forward speeds**

At the times that the typhoon reaches at the points indicated in Figure 4.8, the contour map of the surge levels are depicted in Figure 4.14a, 4.15a and 4.16a, respectively.

From the figures one can conclude that the surge level is generally higher as the propagation speed increases. This can be explained by the fact that the actual wind speed on the right of the typhoon (relative to forward direction) is enhanced with this propagation speed when it coincides with the propagation direction and vice versa (see Figure 4.13) Higher propagation speed in the westerly direction enhances the westerly wind in the typhoon and hence the higher surge level in the strait and along the East Coast of Malaysia.

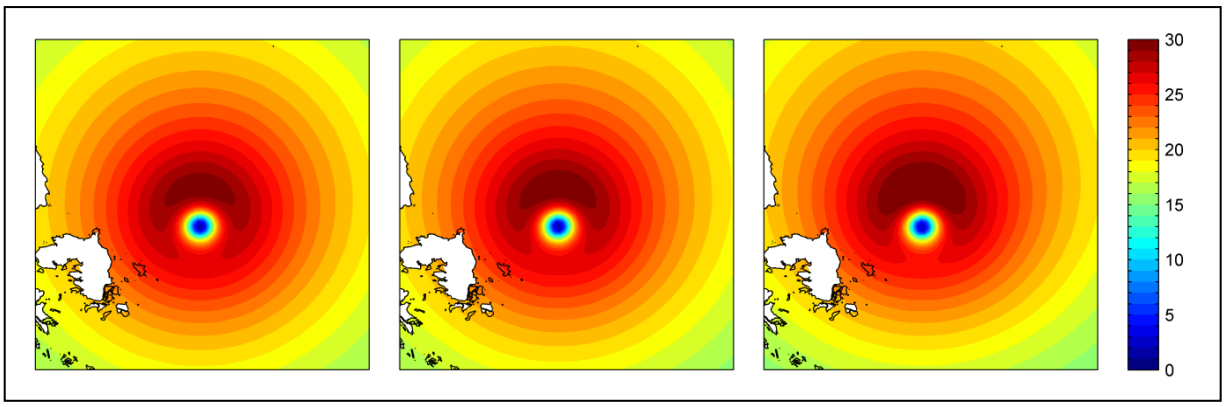


**Figure 4.13 Wind distribution in metres per second of typhoon with (a) forward speed = 1.0 m/s (left), (b) forward speed = 3.5 m/s (middle) and (c) forward speed = 5.0 m/s (right)**

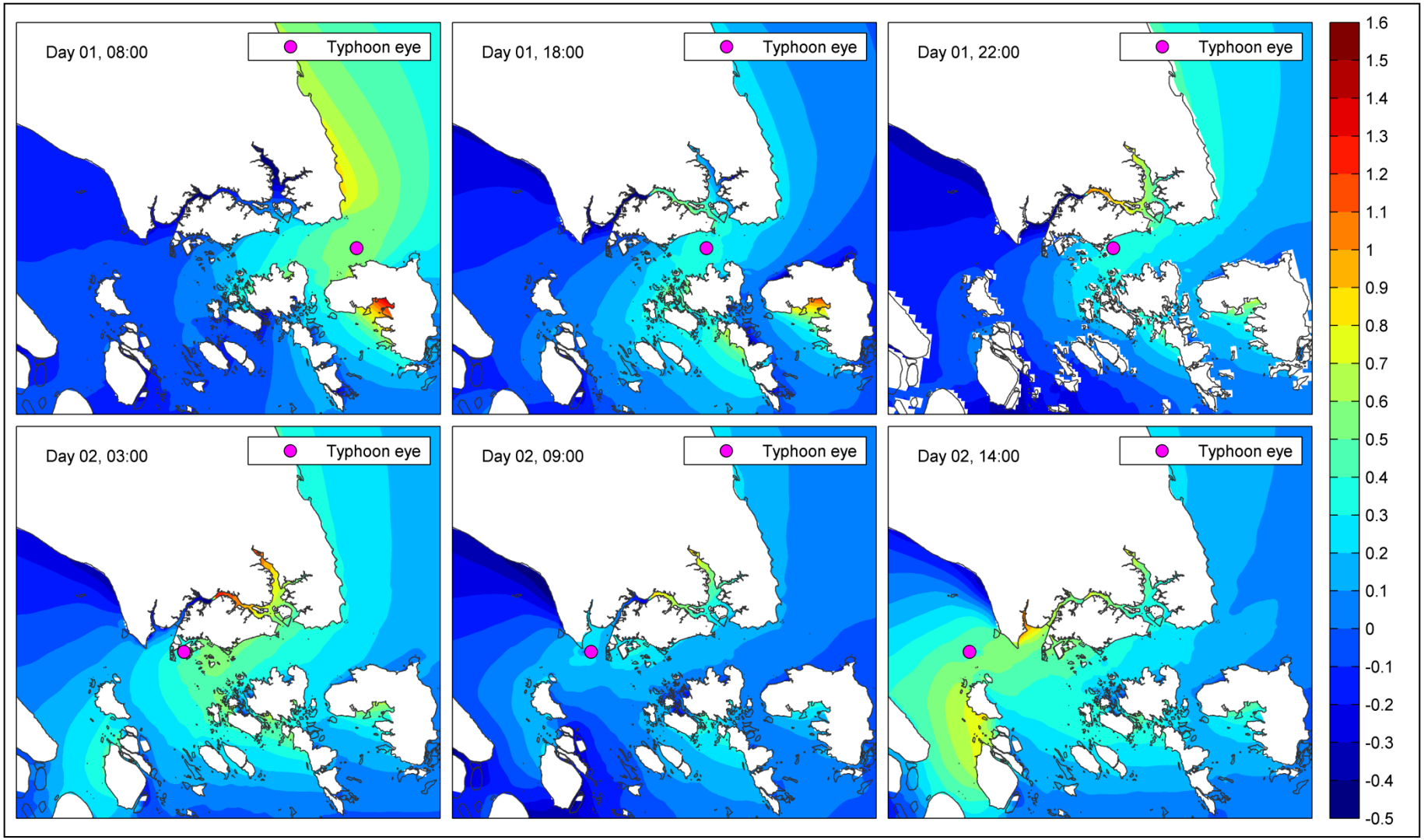


**Figure 4.14 Surge level in metres caused by typhoon track of forward speed 1.0 m/s (a) top left, (b) top middle, (c) top right, (d) bottom left, (e) bottom middle and (f) bottom right**

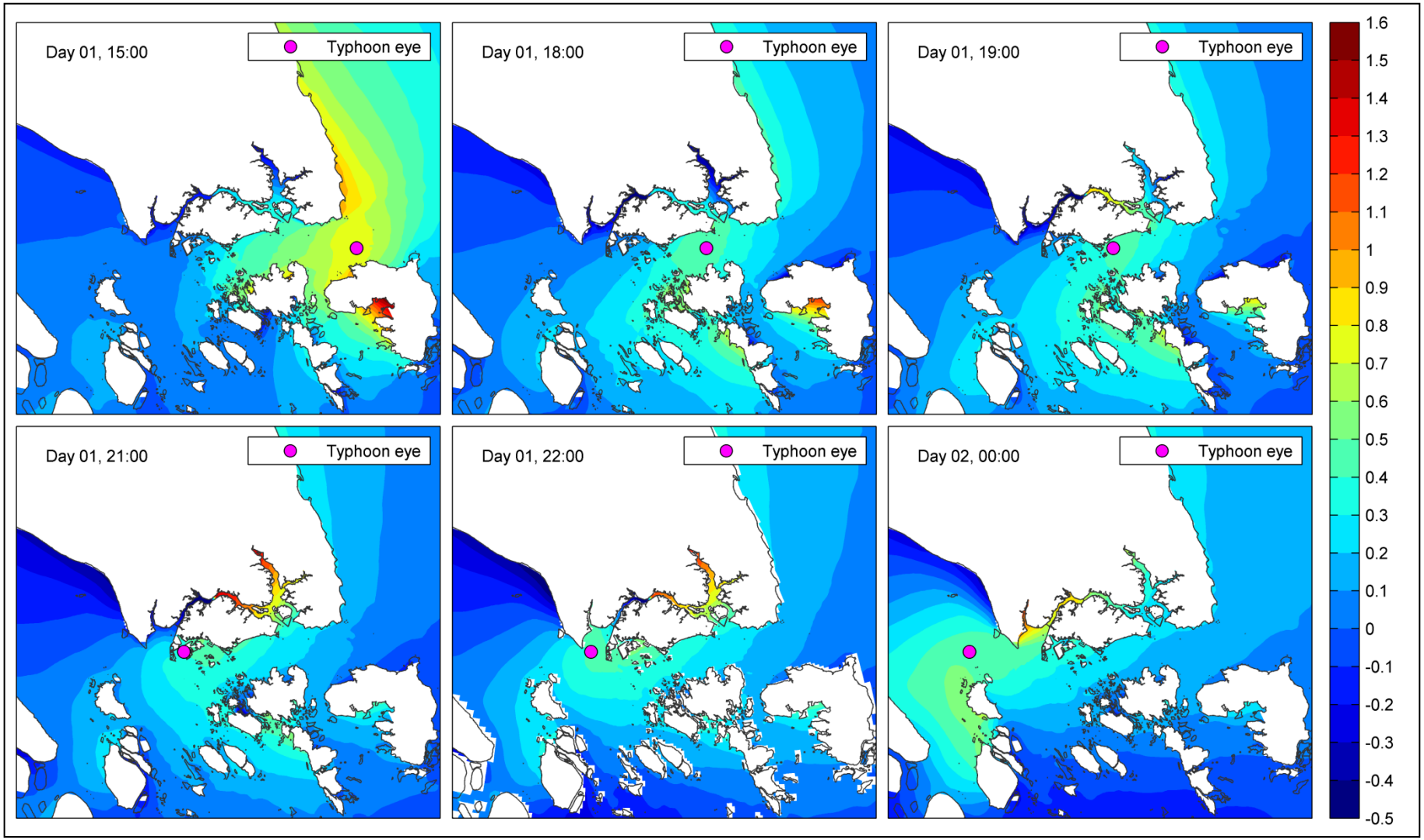


**Figure 4.15 Surge level in metres caused by typhoon track of forward speed 3.5 m/s (a) top left, (b) top middle, (c) top right, (d) bottom left, (e) bottom middle and (f) bottom right**

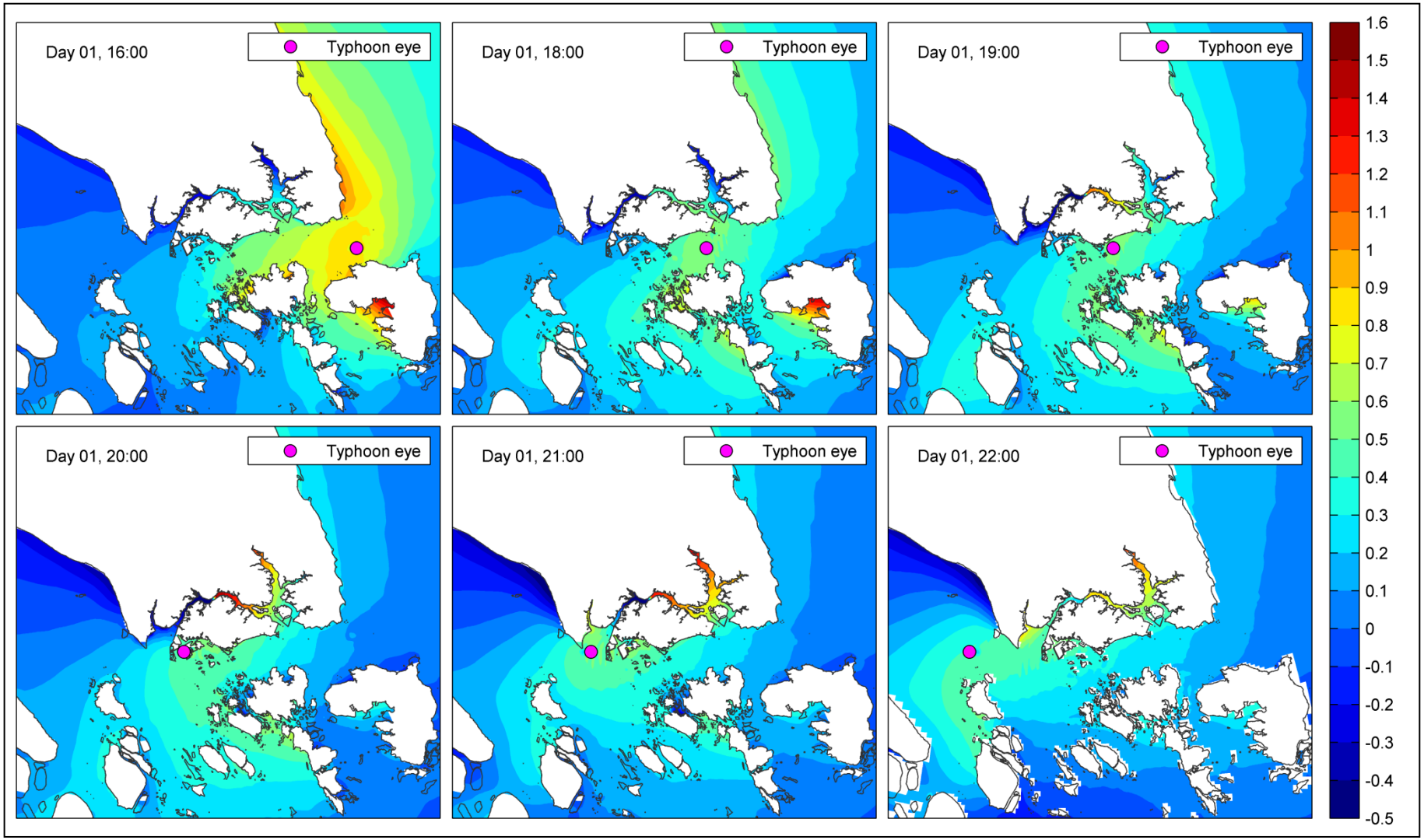


**Figure 4.16 Surge level in metres caused by typhoon track of forward speed 5.0 m/s (a) top left, (b) top middle, (c) top right, (d) bottom left, (e) bottom middle and (f) bottom right**

Figure 4.17 and 4.18 show the momentary discharge at cross-section E and SE respectively. Both figures suggest that water is flowing out of the strait during the period from 08:00 to 18:00 of Day 1 for the case of forward speed 1.0 m/s. For the forward speed 5.0 m/s, Figure 4.17 also shows that there is constant flow of water into the strait via cross section E from the beginning (16:00 of Day 1) to the end (22:00 of Day 1) of the time the typhoon is in the strait, which is also the case for forward speed 3.5 m/s from 15:00 of Day 1 to 00:00 of Day 2.

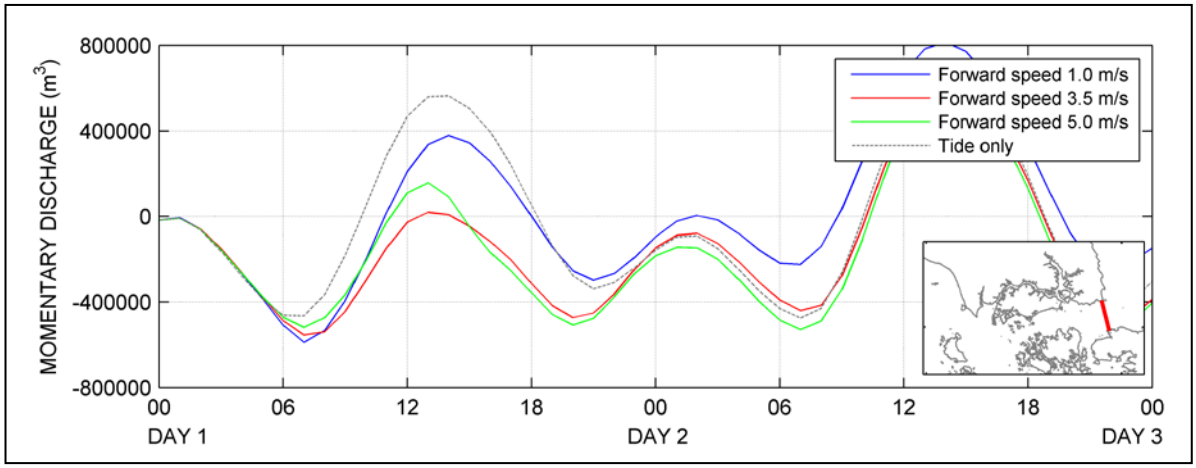


**Figure 4.17 Momentary discharge at cross section E for different forward speeds (positive indicates eastward discharge and negative indicates westward discharge)**

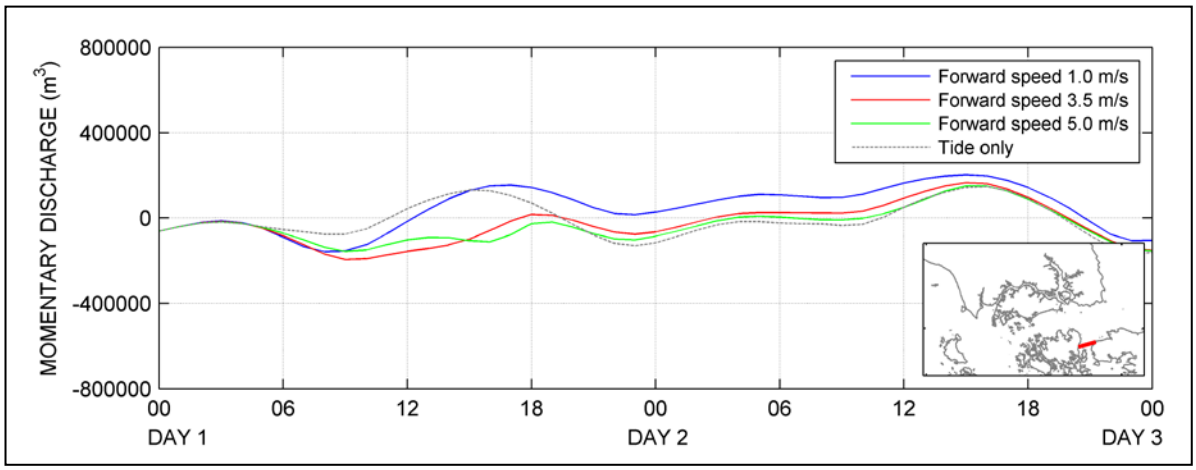


**Figure 4.18 Momentary discharge at cross section SE for different forward speeds (positive indicates northward discharge and negative indicates southward discharge)**

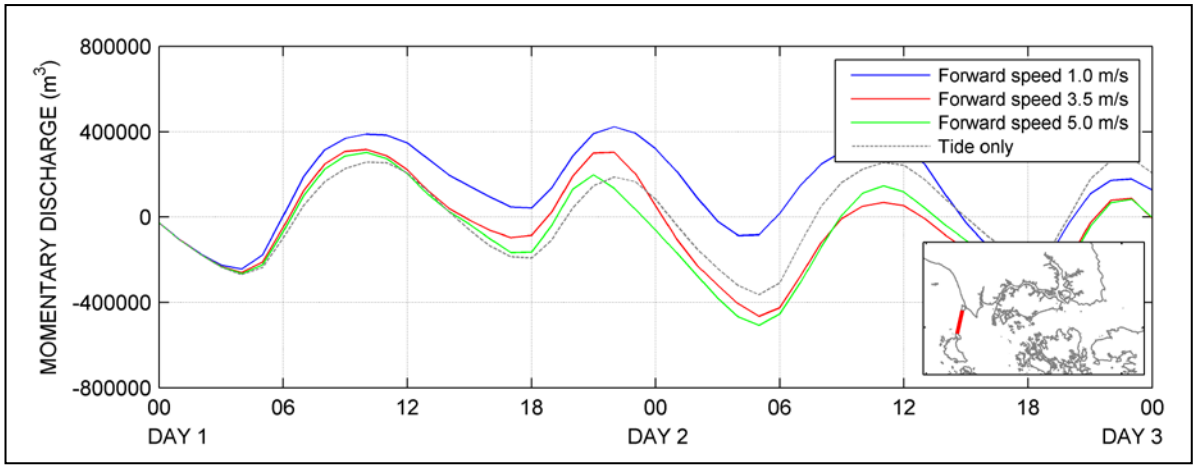


**Figure 4.19 Momentary discharge at cross section W for different forward speeds (positive indicates eastward discharge and negative indicates westward discharge)**

After 18:00 of Day 1, surge around the eye begins to increase for forward speed 1.0 m/s (Figure 4.14c and d). This can be supported by Figure 4.17, 4.18 and 4.19 which show the momentary discharge via cross sections E, SE and W, respectively and all illustrate an inflow of water fluxes from 18:00 of Day 1 to 03:00 of Day 2.

At the final position of the typhoon in the strait, the surge around the eye is highest for the case of forward speed 1.0 m/s, followed by 3.5 m/s and then 5.0 m/s (Figure 4.14f, 4.15f and 4.16f), especially at the western coast of Pulau Karimunbesar due to the on-shore wind contributed by the typhoon at that moment. This is caused by the same mechanism explained earlier but in opposite direction. In the southern part of the typhoon, the easterly wind is least affected (reduced) by the propagation speed of the typhoon. The wind speed in the Easterly direction in the typhoon for fast moving typhoon is the lowest.

In conclusion, for a moving typhoon, wind speed in the typhoon is enhanced when the wind is blowing in the same direction as the typhoon propagation direction and vice versa. However, the land topography in the region that may obstruct water flow affects the rate of receding of surge. It determines how fast the water can move out.

### 4.2.3 Radius of maximum wind

Three different typhoon's radii of maximum wind, $RMW$ equals to 15 km, 25 km and 50 km has been simulated using the same typhoon track and speed, i.e. along 1.25 $^{o}$N and 3.5 m/s respectively (see Figure 4.20). The wind and pressure drop field for typhoon with three different $RMW$ 15 km, 25 km and 50 km are shown in Figure 4.21 and 4.22 respectively. Referring to Figure 4.21, the area with high wind speed (> 25 m/s) is largest for $RMW$ 50 km, followed by $RMW$ 25 km and 15 km. Similar feature can be observed for the pressure drop distribution (see Figure 4.22).

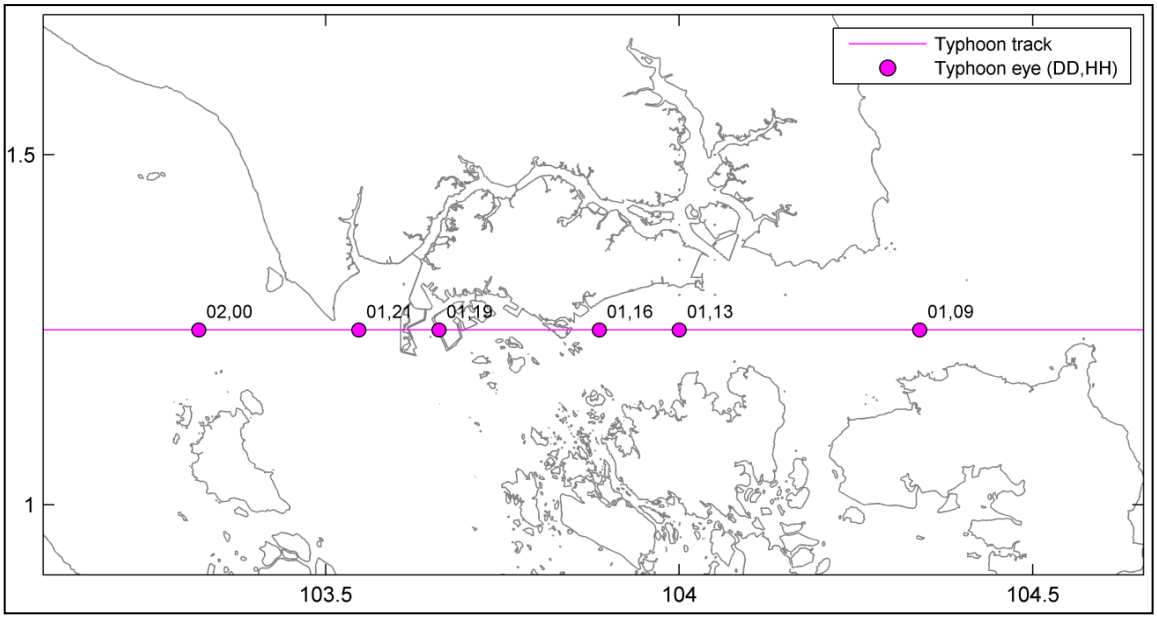


**Figure 4.20 Position of typhoon eye with day and time (from reference date) for RMW 15 km, 25 km and 50 km**

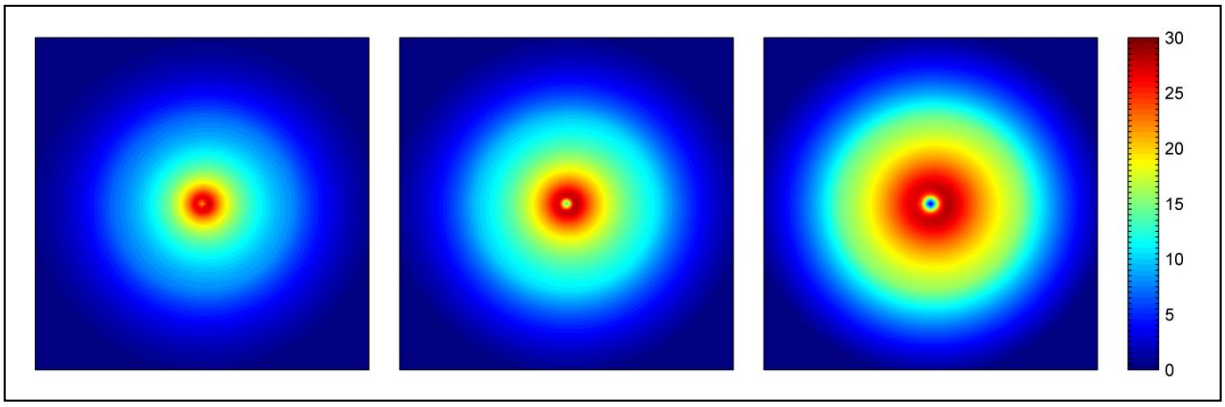


**Figure 4.21 Wind distribution in metres per second of typhoon with (a) RMW 15 km (left), (b) RMW 25 km(middle) and (c) RMW 50 km(right)**

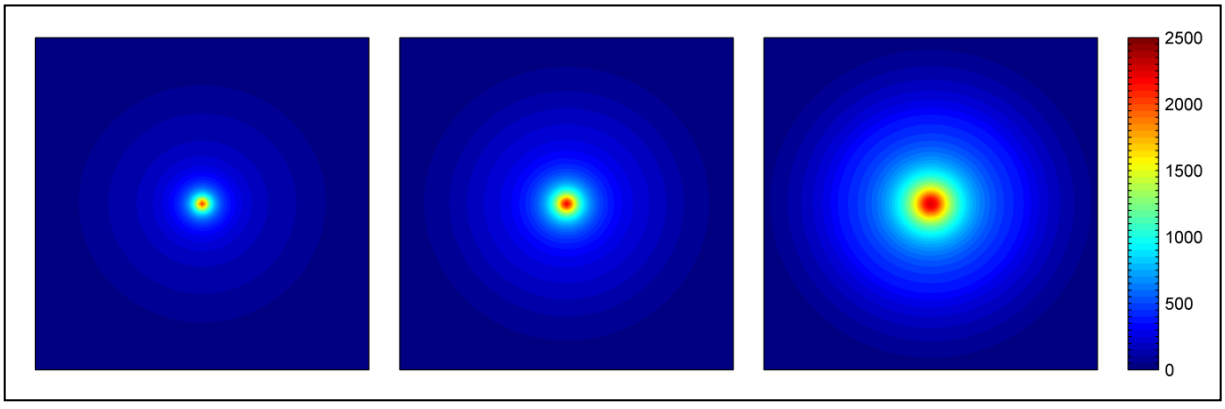


**Figure 4.22 Pressure drop distribution in Pascals of typhoon with (a) RMW 15 km (left), (b) RMW 25 km(middle) and (c) RMW 50 km(right)**

In general, by observing the surge levels for these three different cases for identical positions of the (Figure 4.25, 4.26 and 4.27), the surge around the eye is simply intensified with increasing $RMW$. At 09:00 of Day 1, $RMW$ 50 km has caused a great effect on the surge outside the strait and at the east coast of Johor Bahru (Figure 4.27a) compared to $RMW$ 25 km and 15 km (Figure 4.26a and 4.25a,

respectively). As intense wind of $RMW$ 50 km covers a larger area (Figure 4.21c), the surge begins to build up even when the eye is still far away. So while the typhoon is approaching nearer and nearer to the strait, the surge accumulates further and piles up in front of the east coast of Johor and Pulau Bintan. Figure 4.23 shows the momentary discharge through the cross section E of the three cases. Obviously, the flow into the strait is the highest for $RMW$ 50 km from 09:00 to 19:00 of Day 1. The surge level at Tanjong Pagar station is shown in Figure 4.24. $RMW$ 50 km gives surge of more than 0.4 m and lasted for 16 hours (10:00 of Day 1 to 04:00 of Day 1) which is the longest lasting surge among the three cases.

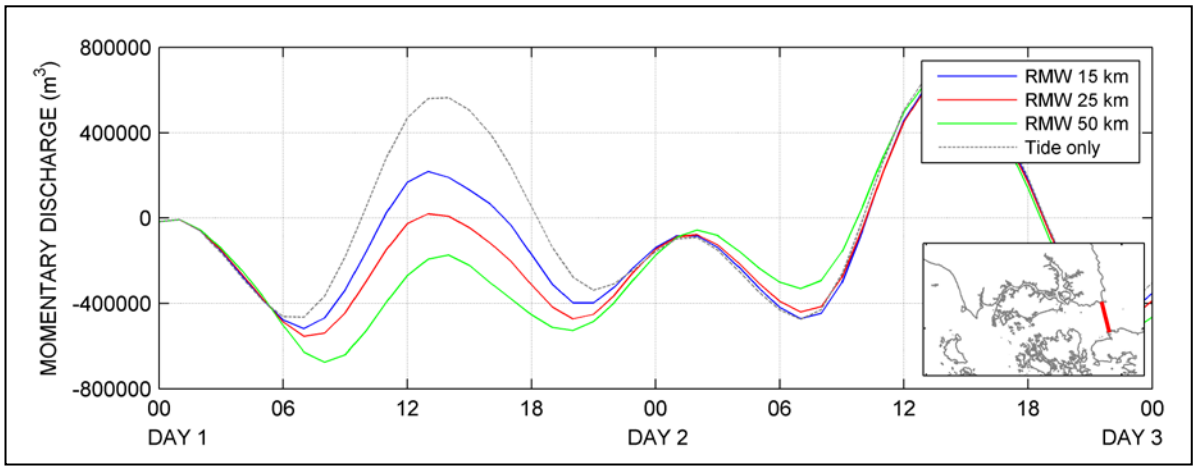


**Figure 4.23 Momentary discharge at cross section E for typhoon with different RMWs (positive indicates eastward discharge and negative indicates westward discharge)**

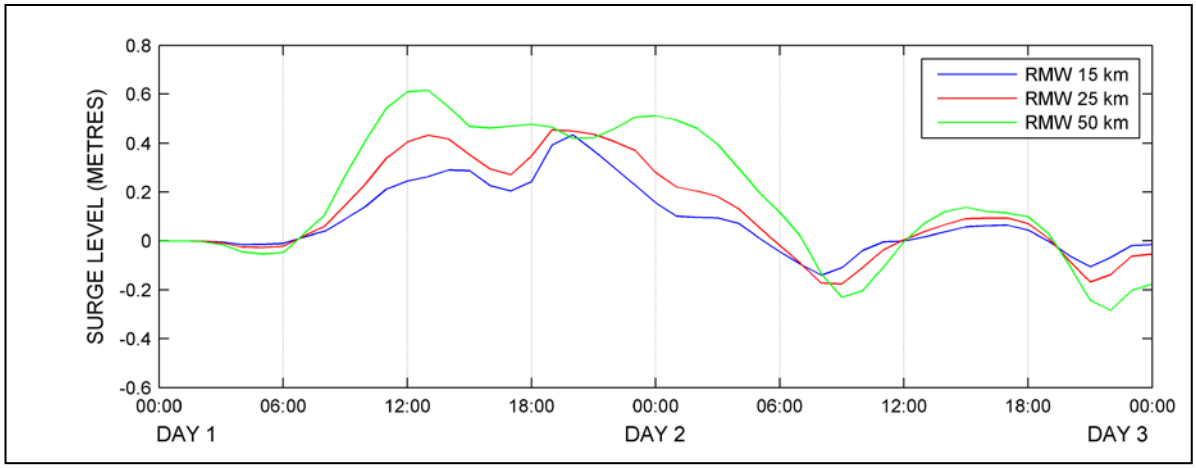


**Figure 4.24 Surge level at Tanjong Pagar caused by typhoon with different RMWs**

In conclusion, the surge level is positively influenced when $RMW$ is increased. A larger area of intense wind (large $RMW$) will have a longer lasting surge effect in the strait.

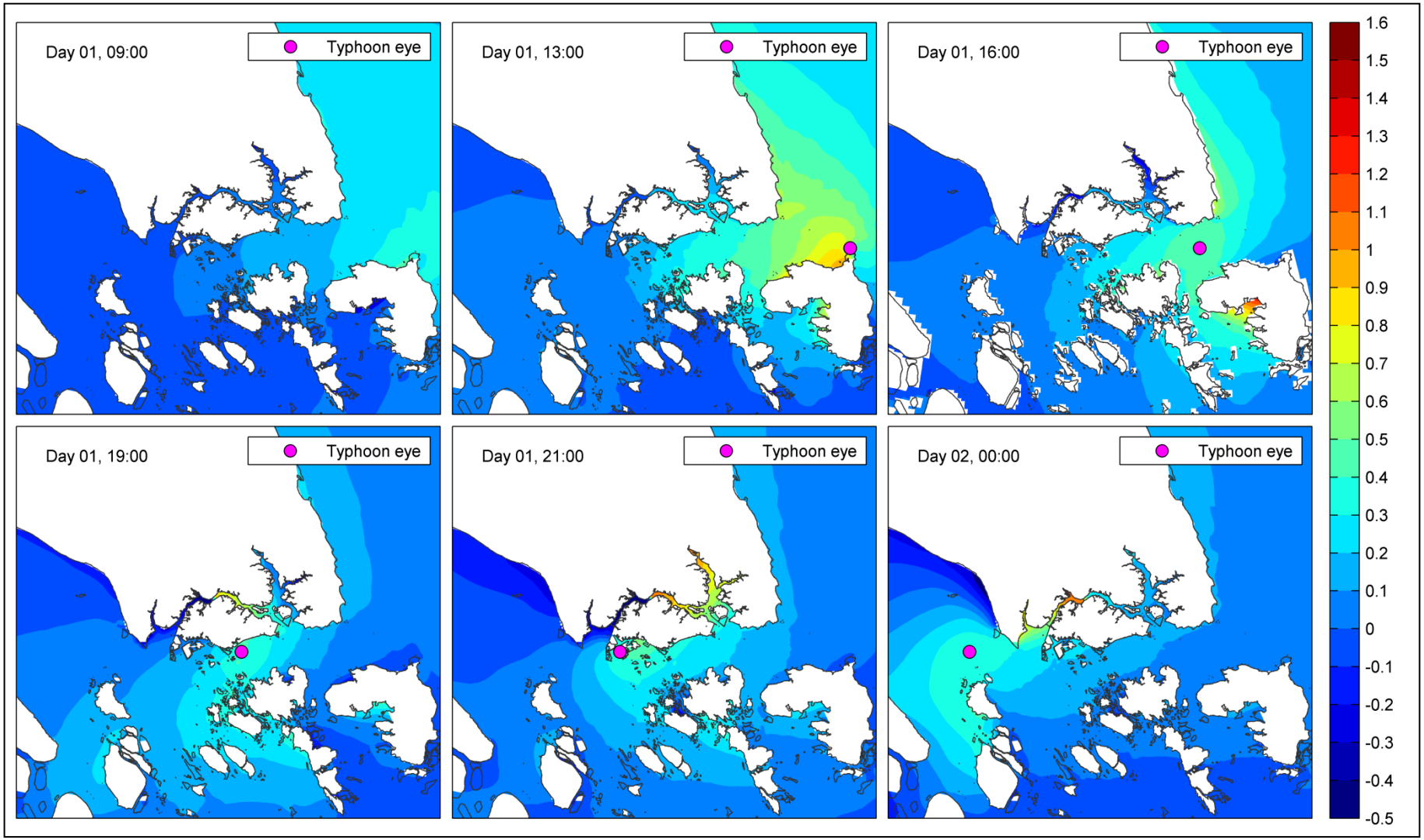


**Figure 4.25 Surge level in metres caused by typhoon with RMW 15km (a) top left, (b) top middle, (c) top right, (d) bottom left, (e) bottom middle and (f) bottom right**

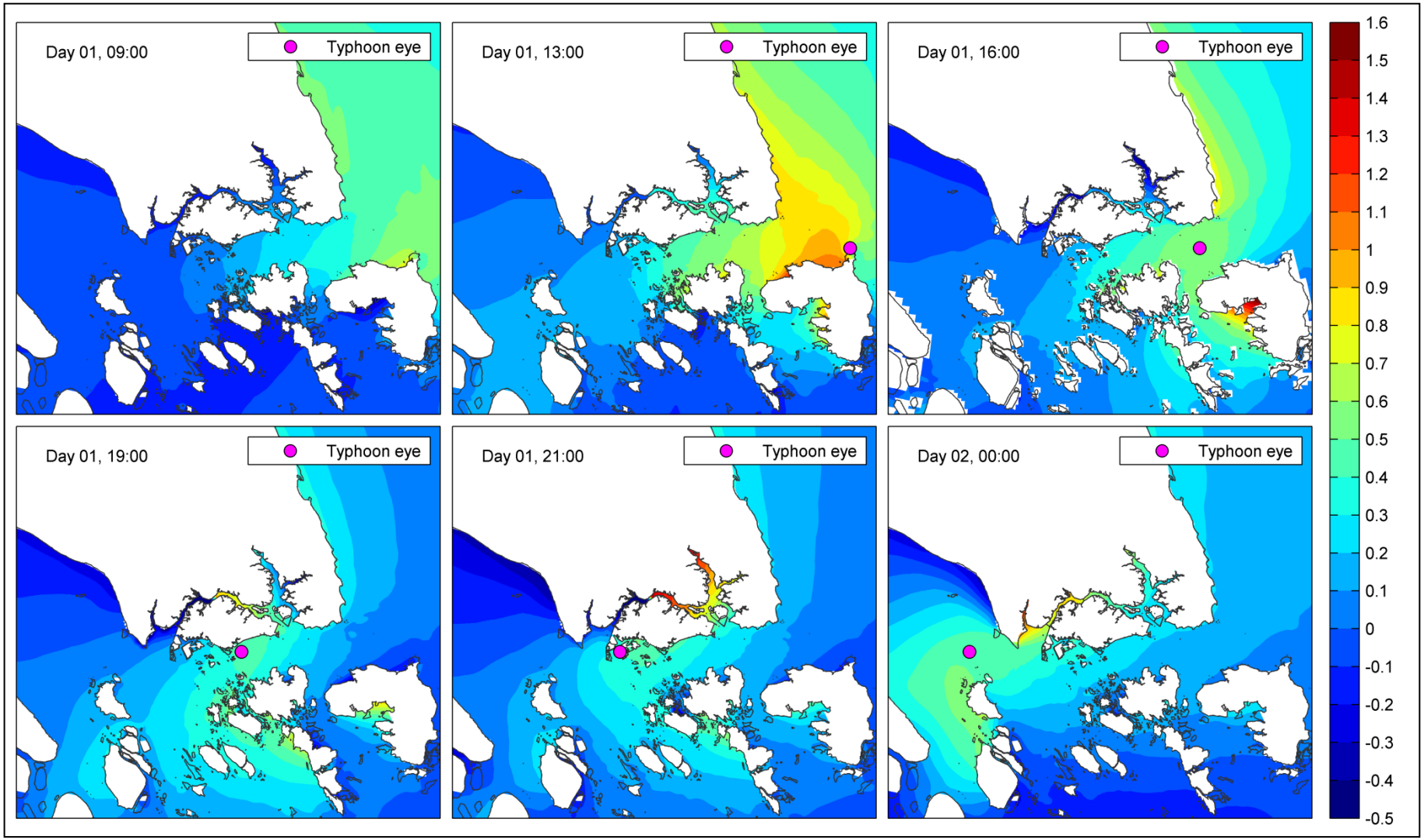


**Figure 4.26 Surge level in metres caused by typhoon with RMW 25 km (a) top left, (b) top middle, (c) top right, (d) bottom left, (e) bottom middle and (f) bottom right**

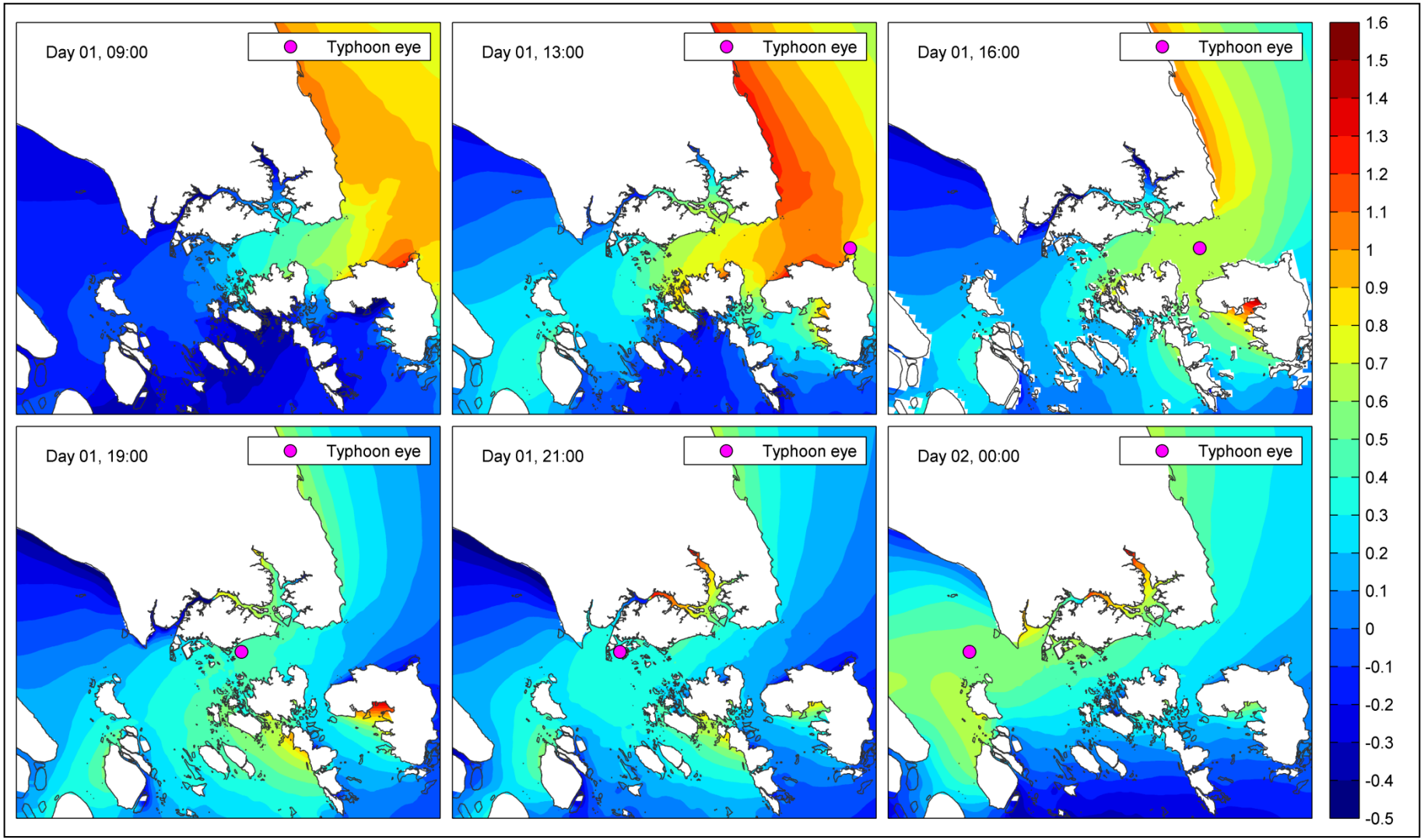


**Figure 4.27 Surge level in metres caused by typhoon with RMW 50 km (a) top left, (b) top middle, (c) top right, (d) bottom left, (e) bottom middle and (f) bottom right**

### 4.2.4 Worst track

Without implicating the physical typhoon formation and its evolution characteristics, based on the finding in the sensitivity tests on $RMW$, the highest surge is yielded by the 50 km $RMW$ which is also consistent with the report of JTWC on typhoon Vamei. As for forward speed, though both 1.0 m/s and 5.0 m/s give s higher surge than 3.5 m/s, these values may be too slow or too fast to apply. The 3.5 m/s forward speed which was the speed of the real typhoon event in this region has been applied for this 'worst track' simulation. Again here the wind speed and pressure drop are maintained at 55 knots and 2200 Pa throughout the whole course of the typhoon.

About sixteen tracks (Figure 4.28b) are simulated before concluding the worst track. A priori we anticipated that given a certain value for $RMW$, the surge will be the highest when the distance between the typhoon and the land is identical to $RMW$. For $RMW$ equals 50 km then for the coast of Singapore this track is depicted in (Track 1 in Figure 4.28a).

Final analysis however showed that Track 2 produced the highest surge level (Figure 4.28a).

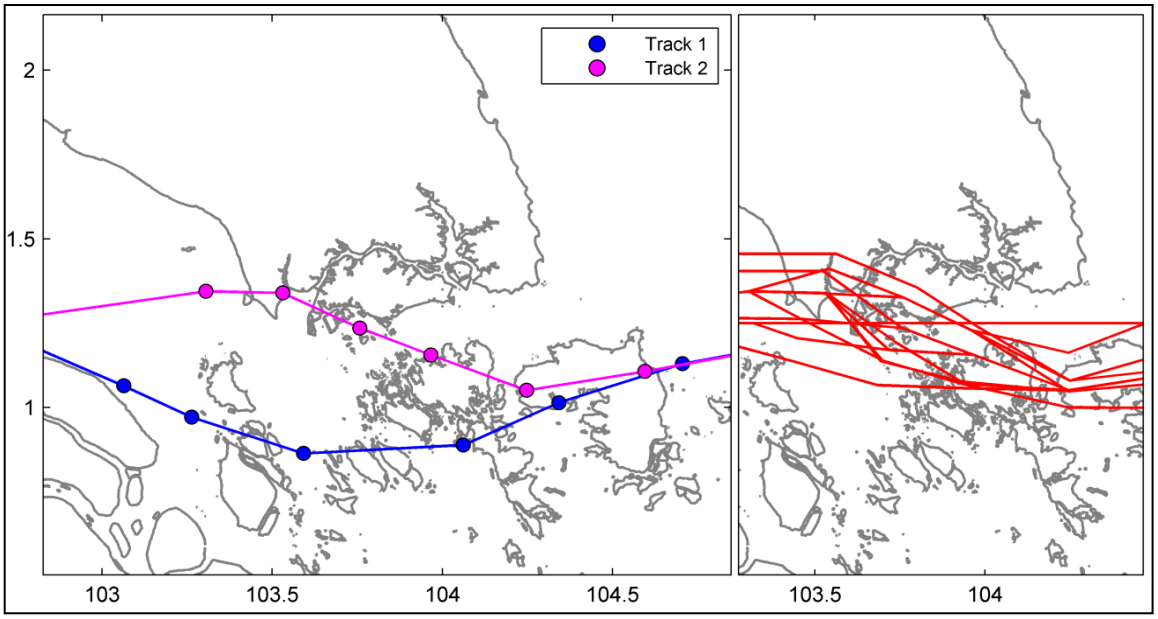


**Figure 4.28 (a) Position of typhoon eye in track 1 and 2 (left) and (b) other tracks attempted (right)**

For this track 2, the typhoon approaches the Singapore Strait from the east and makes a landfall on the eastern coast of Pulau Bintan. This track allowed more water to enter the strait. Then when the typhoon gradually moves towards the north while travelling westward mid-way in the strait, it forces water from the Malacca Strait to flow into the Singapore Strait. Figure 4.29 shows the surge generated by two tracks at all 13 stations around Singapore (Figure 3.2). All stations except Pasir Ris and Changi have greater surge for Track 2 than in Track 1. Therefore it was concluded Track 2 is the worst track that gives the highest surge ranging from 0.64 to 1.60 m. The surge propagation characteristic for of the worst track scenario is presented in Figure 4.30.

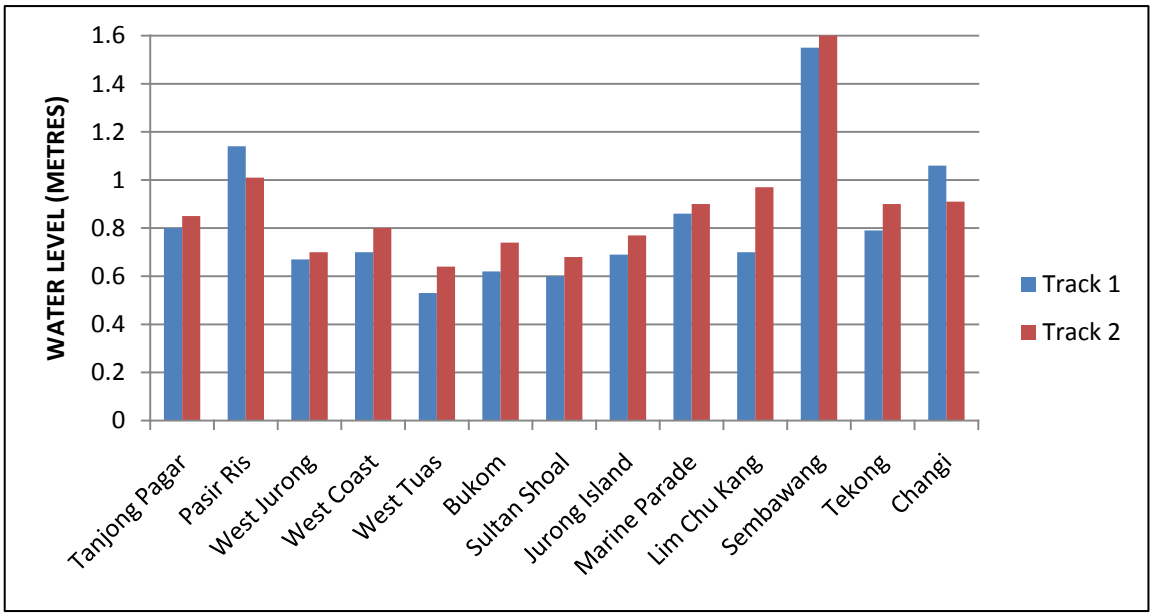


**Figure 4.29 Surge at 13 stations for track 1 and 2**

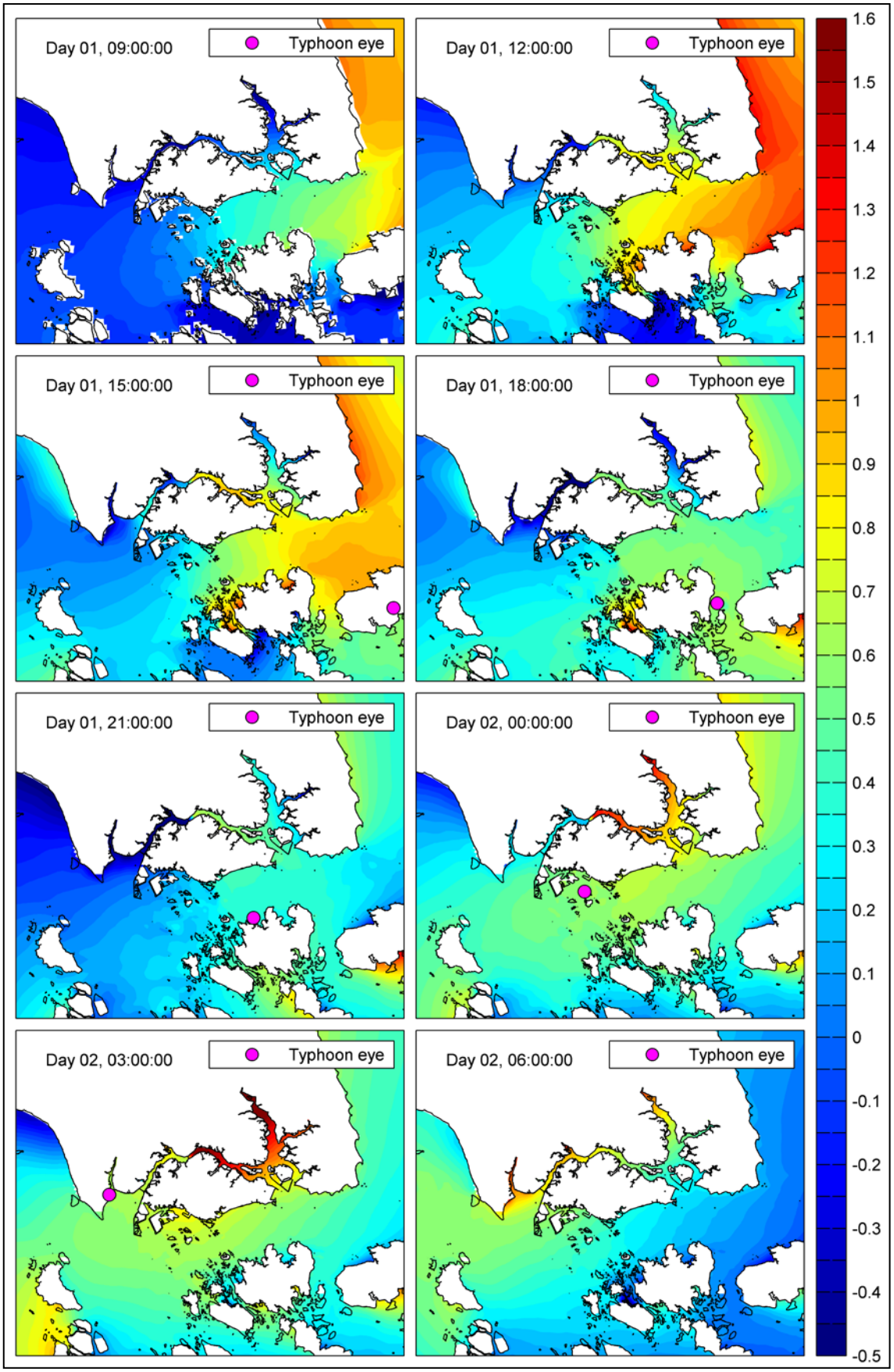


**Figure 4.30 Surge level in metres of 'worst track' scenario**

### 4.2.5 Effect of spring and neap tide on storm surge

The simulations until now are focused on the neap tide of December 2001 which is the period when typhoon Vamei occurred. The water level during spring and neap tide in the Singapore Strait differs about 1.2 m. In large scale hydrodynamic condition, the water depth is often associated with the resistance of water flow; the shallower the area will impart more resistance to the flow. Hence this section will examine the effect of spring neap on the storm surge propagation. The following shows the highest surge induced by the typhoon of the worst track at the 13 stations in spring and neap tide.

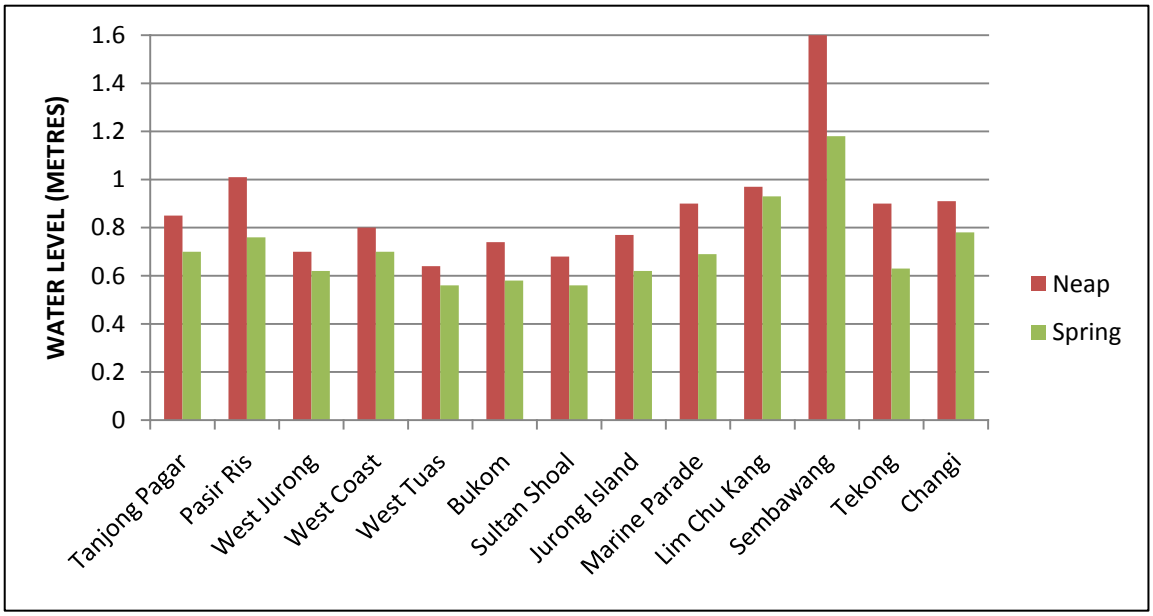


**Figure 4.31 Surge (metres) of 13 stations during spring and neap tides**

It can be observed that the maximum surge during the spring tide is lower than in the neap tide (Figure 4.31).

Figure 4.32 and 4.33 show the plots of surge of all 13 stations during spring and neap tides respectively. During spring tide, the surge is lower than that of neap tide but the envelope (duration) is wider (longer). This shows that during spring tide the surge propagate into the strait at a faster rate that enables the surge to flow in earlier than during neap tide whose envelope is higher and narrower; surge is experiencing resistance to flow into the strait. This mechanism has been described in numerous literatures (e.g. Rego and Li, 2010).

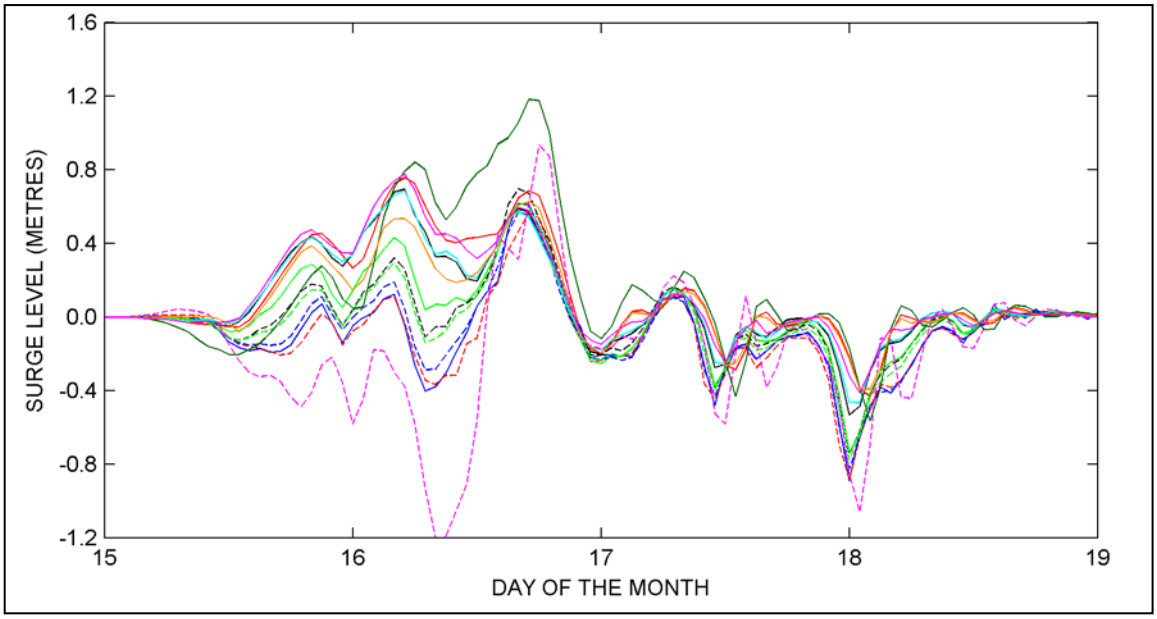


**Figure 4.32 Envelope of surge (measurement at all 13 stations) during spring tide**

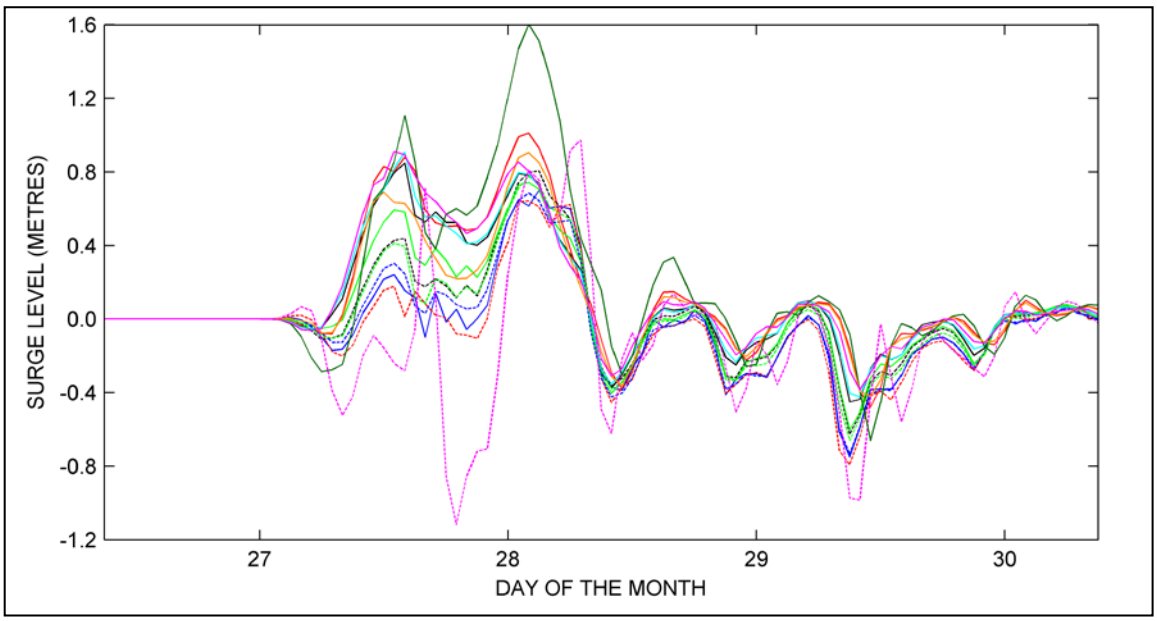


**Figure 4.33 Envelope of surge (measurement at all 13 stations) during neap tide**

## 4.3 Estimation of water level for extreme scenario

The extreme scenario here referred to the extreme high water level around Singapore. This will include extreme values of typhoon-induced surge and other hydrodynamic influences in the region (Section 2.2); tide, SLA and sea level rise. In this study, the occurrence of all these four hydrodynamic influences are assumed to be independent of each other and the extreme effect of each will be superimposed on one another to give the extreme high water level.

### 4.3.1 Typhoon-induced surge

As discussed earlier, a typhoon of the same maximum intensity as typhoon Vamei (around 55 knots, average of maximum winds recorded by JTWC and JMA) has a return frequency of 1 in 400 years (0.25 % of a year). The maximum surge induced in the region by this extreme event; typhoon that is moving on the route of the worst track is shown in Figure 4.28a. As discussed in Section 4.2.5, the induced surge during the spring and neap are slightly different (surge in neap is greater than in spring) and this effect on the surge in the Singapore Strait is still not very well understood. Therefore the average of surge during both spring and neap will be considered in this extreme event, with both upper- and lower-bound uncertainties as the difference between average surge and the one in neap, and the difference between the average surge and the one in spring, respectively (Figure 4.34).

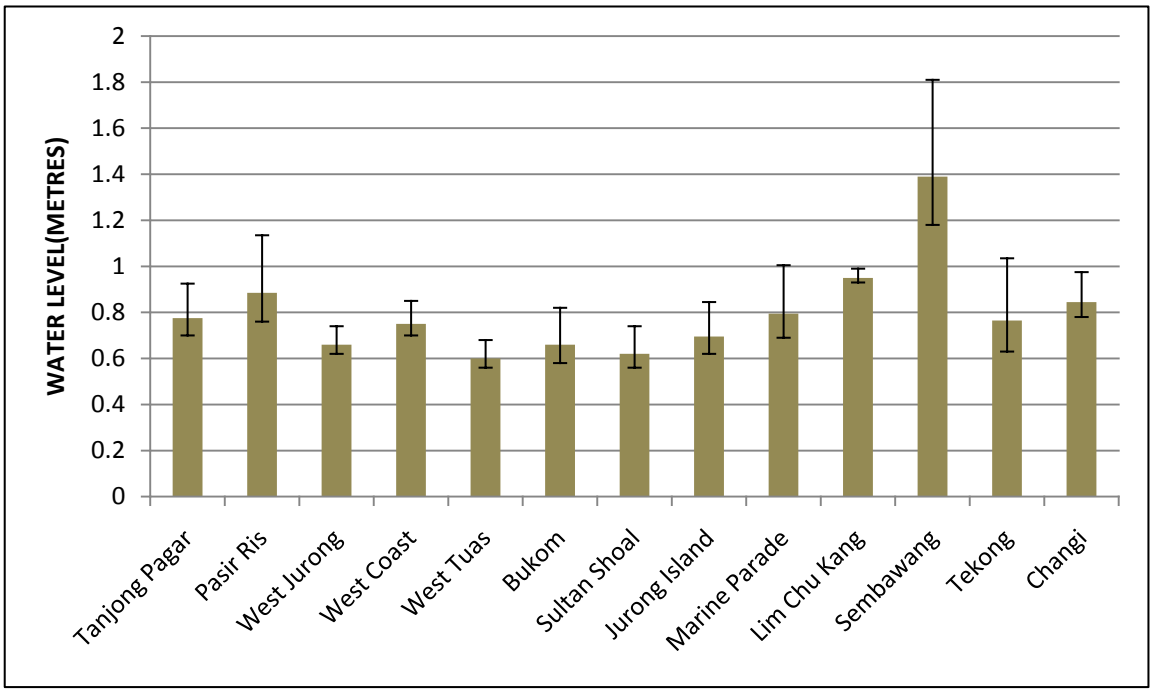


**Figure 4.34 Mean typhoon-induced surge during spring and neap and its uncertainty at 13 stations**

### 4.3.2 Tide

For this extreme scenario, high water of the tide will be considered. As the typhoon is estimated to last longer than 12 hours in the Singapore Strait (Figure 4.30), the possibility of it occurring during one of the two high waters of the day (mixed diurnal and semi-diurnal tide) is certain.

A 19 year tidal prediction of 65 constituents (Appendix C) has been carried for all of the 13 stations except Jurong Island and Tekong as there is no available observation data for those two stations. However the tidal prediction of nearer stations such as West Coast and Changi will each represent Jurong Island and Tekong respectively.

From the 19 years tidal prediction, we obtain the highest high water (HHW), mean high water (MHW) and lowest high water (LHW) at each station. The HHW here is also the highest astronomical tide (HAT). Figure 4.35 shows the MHW at each station with its respective upper- and lower-bound uncertainty which is the difference between HHW and MHW, and the difference between LHW and MHW, respectively.

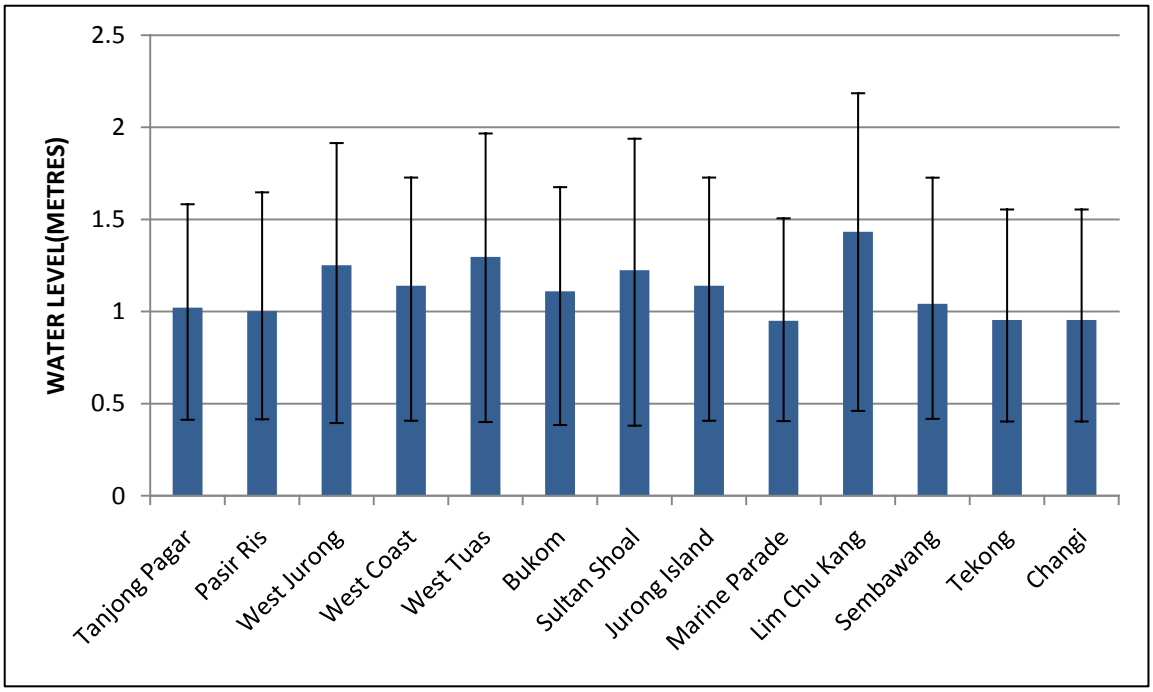


**Figure 4.35 Mean high water (tide) and its uncertainty at 13 stations**

### 4.3.3 Sea level anomaly

According to Tkalich et al. (2009a) and Raghuraj et al. (2010), the SLA is highly correlated with the northeast monsoon. Chang et al. (2003) also suggests that the occurrence of typhoon in this region greatly depends on the strong winds of northeast monsoon and bases his approximation of the return frequency of the typhoon (1 in 400 years) on the duration of the strong winds of more than 10 m/s. Hence the SLA in this extreme scenario with typhoon is dependent on the strength of the northeast monsoon winds at this time. Looking at Figure 2.7, during the occurrence of typhoon Vamei, the northeast winds prevailing in the South China Sea near Vietnam is about 14 m/s which is approximately the same value presented by Chang et al. (2003) (Table A.1 in Appendix A).

Tkalich et al. (2009a) proposed an empirical relationship between the wind off Vietnam (based on NCEP wind analysis) and the SLA near Singapore during northeast monsoon (Figure 4.36). By applying the wind-SLA empirical relationship (Figure 4.36), the predicted SLA with a wind speed of 14 m/s is about 0.37 m (mean), 0.68 m (upperbound) and 0.05 m (lowerbound).

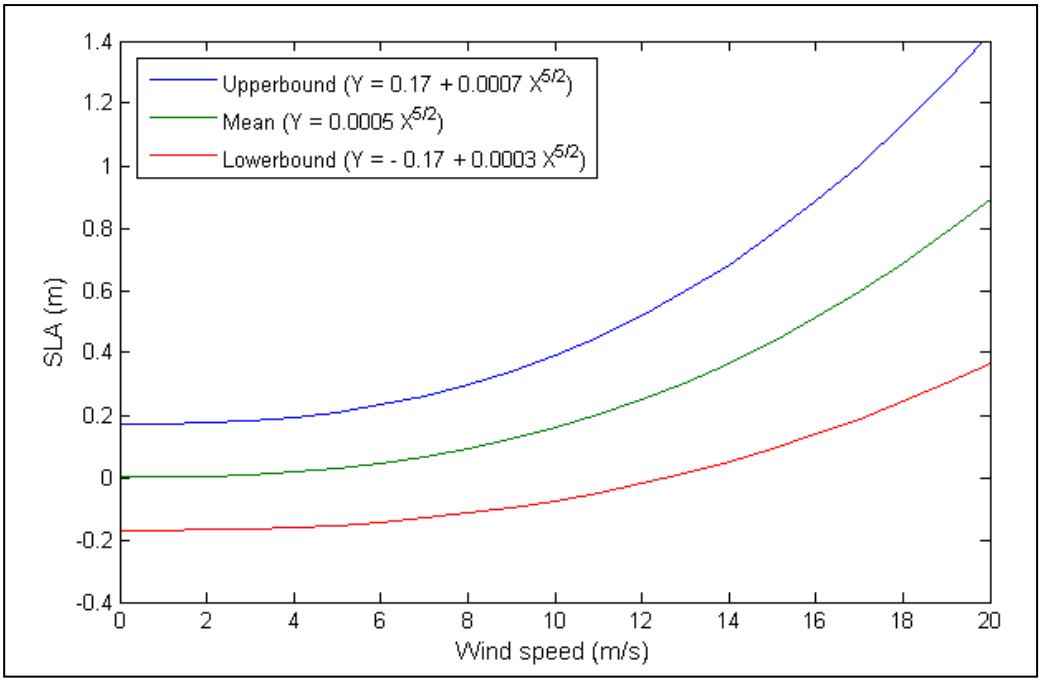


**Figure 4.36 Empirical relationship between SLA in the Singapore Strait and winds off Vietnam during northeast monsoon (Modified from Tkalich et al., 2009a)**

### 4.3.4 Sea level rise

For sea level rise, the value will depend on the year which the projection is carried out as the rise of sea level due to climate change is progressive and cumulative as the years pass. Hence the value of sea level rise projected by IPCC AR4 (IPCC, 2007) for the average of all emission scenarios is 34.3 cm over the 1990 levels by around 2100, will not be take into account as in the extreme water level estimation and its return frequency.

### 4.3.5 Extreme water level

The extreme value of each of the hydrodynamic influences on water level with uncertainty has been mentioned above. Figure 4.37 shows the computed extreme water levels by superimposition of surge, tide and SLA, and also the superimposed positive and negative uncertainties at each of the 13 stations. This water level is referenced to the local mean sea level.

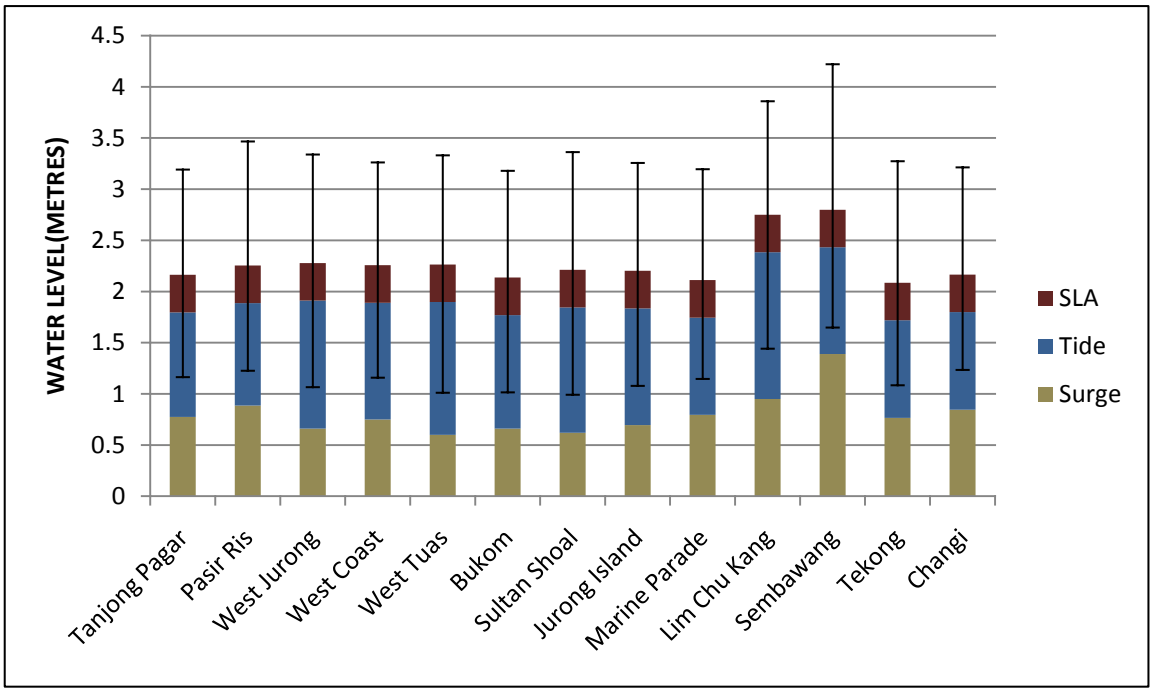


**Figure 4.37 Water level with its uncertainty resulted from the extreme scenario at 13 stations**

As observed in Figure 4.37, the water level is the highest in the Johor Strait which is where Lim Chu Kang and Sembawang stations are located; up to 2.8 m high. Other stations have water level of 2.0 m. High surge in the Johor Strait high risk of flooding in NE monsoon, surface runoff from the land may not be able to discharge effectively due to the high water level near the river mouth of Sungei Johor and Sungei Pulai, located in the east and west of Johor Strait respectively.

# 5 Conclusion and recommendations

## 5.1 Conclusions

1. The hydrodynamic condition in Singapore Strait is highly complex due to the influences of two large water bodies; Andaman Sea and South China Sea. In addition, the strait itself also has a unique topography with Malaysia Peninsular and Singapore in the north and several small islands including Pulau Bintan and Batam in the south, which makes this area a partially enclosed basin that further complicates typhoon-induced surge and its propagation.

2. Observation data at a number of stations showed that it is difficult to make a distinction between the water level variation induced by large scale meteorological phenomenon (SLA) and surge level produced by Vamei, as both levels have a same order of magnitude.

3. Despite this difficulty and lack of wind data for calibration of the typhoon winds, the surge induced by typhoon Vamei could be reasonably reproduced. The hindcast was achieved by slightly shifting the track northwards.

4. Extreme wind analysis based on 13.5 years wind data obtained from a station on Singapore Island did not support the 400 years recurrence interval of a typhoon mention by Chang et. al. (2003). The analysis showed that wind speed associated with 400 years recurring interval in this region is only 27 knots (considered as tropical depression). However, 13.5 years of wind data is too short to prove this conclusively. We think the wind speed assumption applied here (>33 knots) for the typhoon winds is not unrealistic.

5. The results of the sensitivity analysis on the typhoon parameters (track, forward speed and $RMW$) show that the surge is strongly influenced by the geographical topography of the region which directly affects the flow obstruction and water surface area (in contact with wind).

    - The track can significantly influence the surge propagation in that area. The forward speed of the typhoon can also enhance the cyclone winds on the right (relative to the forward motion).

    - In partially enclosed waters like the Singapore Strait which is surrounded by land; Malaysia Peninsular, Singapore and some islands of Indonesia, land obstruction to water flow affects the rate of receding surge.

    - $RMW$ determines the area containing high wind speed which leads to a longer duration of the surge.

6. The proposed extreme typhoon track (‘worst’ case) can cause a maximum surge of up to 1.6 m depending on location.

7. Typhoon induced surge during neap tide is greater than spring tide, supporting earlier findings from literature.

8. The estimated 1 in 400 years mean extreme water level condition which includes the typhoon-induced surge, high tide and SLA amounts to 2.0 to 2.8 m depending on location.

9. Based on the conclusions above, we can conclude that our aim to provide a quantitative assessment of the typhoon-induced surge and extreme water level conditions with a recurrence interval of 1 in 400 years has been accomplished in this study. Overall, considering this a first study of this kind for Singapore, this report provides a substantial information on the surge level and extreme water level which could be used to enhance public awareness for possible flooding occurrence in the future especially with the sea level rise due to global warming.

## 5.2 Recommendations

Improvements to this study can be made with more available data; denser network of wind stations, longer observation data, and more detailed and higher temporal resolution information of typhoon.

A more thorough statistical analysis of this extreme event can made to estimate a more accurate return frequency and water levels. In particular for the probability of various surge levels induced by typhoon; factors such as landfall (relative to tidal timing) and the chance of the typhoon to follow this worst track, which can greatly affect the level and propagation of surge induced, should be taken into account.

Also the interaction between the tide and surge; effect of hydrography and tide in different areas around Singapore especially in the Johor Strait, may have different impact on the surge and further studies are required for qualitatively conclusion.

Multiple extreme scenarios with various combinations of high/low tide and landfalls at different stations can be carried out to further investigate on the typhoon-induced extreme water levels in this region.

# 6 References


An, T. V., 2009. General Research and Solution to Stabilize Lai Giang Inlet. Key Laboratory of River and Coastal Engineering, Vietnam Institute for Water Resources Research (Vietnam Academic for Water Resources), Hanoi, Vietnam.

Anthes, A.R., 1982. *Tropical Cyclones: Their Evolution, Structure and Effects*. American Meteorological Socitety, Boston, USA.

Chambers, C. R. S. and Li, T., 2007. *Simulation of a near-equatorial typhoon Vamei (2001).* Meteorology and Atmospheric Physics, 97, 67–80.

Chan, E.S., Tkalich, P., Gin, K.Y.H., and Obbard, J.P., 2006. *The physical oceanography of Singapore coastal waters and its implications for oil spills*. The Environment in Asia Pacific Harbours, Chapter 23, edited by: Wolanski, E., Springer, Netherlands, 393–412.

Chang, C.P. and Wong, T.S., 2008. *Rare Typhoon Development near the Equator.* In Recent Progress in Atmospheric Sciences: Application to the Asia-Pacific Region. Lioi, K.N., Chou, M.D. and Hsu, H.H. (editors). World Scentific.

Chang, C.P., Liu, C.H. and Kuo, H.C., 2003. *Typhoon Vamei: an equatorial tropical cyclone formation.* Geophys. Res. Lett., 30, 1151–1154.

Charnock, H., 1955. *Wind stress on water surface.* Quart J. Roy. Met. Soc. 81, 639.

Chew, S.Y., 1974. *Waves at southeast coast of Singapore.* J. Inst. Eng. Singapore 14, 36-40.

Chew, S.Y., Wong, P.P. and Chin, K.K., 1975. *Beach development between headland breakers.* Proceedings of the 14th Coastal Engineering Conference. Copenhagen, Denmark.

Chia, L.S., 1998. *Coastal management in Singapore: institutional arrangements and implementation.* Ocean & Coastal Management Volume 38, Issue 2, 1998, 111-118.

Chia, L.S., Habibullah, K. and Chou, L.M., 1989. *The coastal environmental profile of Singapore.* Manila: International Center for Living and Management (ICARM).

Deltares | Delft Hydraulics (Zijl F. and Kernkamp HWJ.), 2004. *Further Hydraulic Model Studies for Pulau Ubin & Pulau Tekong Reclamation Scheme. Interim Report on Hydrodynamic Modelling - Model Set-up and Calibration.* Delft Hydraulics Report Z3437 for Housing and Development Board (HDB).

Deltares|Delft Hydraulics, 2009a. *Delft3D-Flow.* User Manual.

Deltares|Delft Hydraulics, 2009b. *Wind Enhanced Scheme (WES) for Cyclone Modelling*. User Manual Version 3.00.

Eskinazi, S. and Cramer, D.E., 1982. *Generalized characteristics and applicability of various probability distributions for wind energy applications.* J. Energy 6 (6), 384–391.

Garcia, A. J., Torres, L., Prieto, E. and De Francisco, A., 1998. *Fitting wind speed distributions: a case study.* Sol. Energy 62 (2), 139–144.

Gerritsen, H., de Vries, J.W. and Phillippart, M.E., 1995. *The Dutch continental shelf model*. Quantitative Skill Assessment for Coastal Ocean Models. Coastal Estuarine Studies, Vol. 47, 425-467.

Gerritsen, H., E.J.O. Schrama and H.F.P. van den Boogaard, 2003. *Tidal model validation of the seas of South-East Asia using altimeter data and adjoint modeling.* Proc. XXX IAHR Congress, Thessaloniki, 24-28 August 2003, Vol. D, 239-246.

Glaser, R., Haberzettl, P. and Walsh, R.P.D., 1991. *Land Reclamation in Singapore, Hongkong and Macau.* GeoJournal 24.4, Kluwer Academic Publishers.

Gray, W.M., 1968. *A global view of the origin of tropical disturbances and storms.* Mon. Wea. Rev., 96, 669-700.

Holland, G.J., 1980. *An analytic model of the wind pressure profiles in hurricanes.* Mon.Wea. Rev., 108, 1212-1218.

Holland, G.J., 1993. *"Ready Reckoner" - Chapter 9: Global Guide to Tropical Cyclone Forecasting.* WMO/TC-No. 560, Report No. TCP-31, World Meteorological Organization; Geneva, Switzerland.

Indonesia, Japan and Singapore, 1979. *Report on the joint tidal and current studies in the Strait of Malacca and Singapore*. Technical report, Tokyo.

IPCC, 2007. IPCC Fourth Assessment Report, Climate Change: Synthesis Report. [Online] Available at http://www.ipcc.ch/publications_and_data/publications_ipcc_fourth_assessment_report_synthesis_report.htm (Accessed 28 April 2010).

Johnson, R. J. and Chang C. P., 2007. *Winter Vortex: A Quarter-Century and Beyond.* American Meteorological Society, doi: 10.1175/BAMS-88-3-xxx [Online] Available at http://www.wmo.int/pages/prog/arep/tmrp/documents/WinterMONEX25MeetingReport.pdf (Accessed 18 February 2010).

Johnson, R.H. and Houze Jr, R.A., 1987. *Precipitation clouds systems of the Asian monsoon.* In Monsoon Meteorology, Chang, C.P. and Krishnamurti (edits), pp 298-353. Oxford Univ. Press, New York.

Joint Typhoon Warning Center, 2001. *Annual Tropical Cyclone Report.* Joint Typhoon Warning Center Pearl Harbour, Hawaii. [Online] Available at http://www.usno.navy.mil/NOOC/nmfc-ph/RSS/jtwc/atcr/2001atcr/pdf/2001atcr.pdf (Accessed 5 February 2010).

Lesser, G.R., Kester, J.Y., Roelvink, J.A. and Stelling, G.S., 2002. *Development and Validation of a Three-dimensional Morphological Model.* Coastal Engineering 51, 883– 915.

Maritime and Port Authority of Singapore (MPA), 2009. *Singapore tide tables and port information.* Singapore.

McBride, J. L., 1995. *Tropical cyclone formation*, in *Global Perspective on Tropical Cyclones*, R. L. Elsberry, ed., Tech. Docu. 693, World Meteorological Organization, 63-105.

NASA Earth Observatory, 2003. Equatorial Typhoon Observed by QuikSCAT 12/26/2001 UTC22:32:36 [Online] Available at http://earthobservatory.nasa.gov/images/imagerecords/3000/3441/vamei-strm-011226_lrg.jpg (Accessed on 10 May 2010)

Phillips, N.A., 1957. *A co-ordinate system having some special advantages for numerical forecasting*. Journal of Meteorology 14, 184-185.

Raghuraj, R., Gerritsen, H. and Babovic, V., 2010. *South China Sea winds as a triggering mechanism for sea level anomalies around the Singapore coast*. Proceedings of the 9th International Conference on Hydroinformatics HIC2010. Tianjin, China.

Rego, J.L. and Li, C, 2010. *Nonlinear terms in storm surge prediction: Effect of tide and shelf geometry with case study from Hurricance Rita.* Journal of Geophysical Research, Vol. 115. XXXXXXXX, dol: 10.1029/2009JC005285.

Singapore's National Climate Strategy, 2008. [Online] Available at http://app.mewr.gov.sg/data/ImgUpd/NCCS_Full_Version.pdf (Accessed 28 May 2010).

Statistics Singapore 2010. *Population & Land area.* [Online] Available at http://www.singstat.gov.sg/stats/keyind.html#popnarea. (Accessed 31 May 2010).

Swan, S.B.St.C, 1971. *Coastal geomorphology in A humid tropical low energy environment: the islands of Singapore.* J. Trops. Geogr. 33, pp 43-61.

Thomas, G.S.P, 1991. *Geology and Geomorphology.* In Biophysical Environment of Singapore. Chia, L.S., Rahman, A. and Tay, D.B.H (edits). Geography Teachers' Association of Singapore, Singapore.

Thurman, H. V. and Trujillo, A. P., 1999. *Essentials of Oceanograhy* (*6th edition).* Prentice Hall, Chicago, USA.

Tkalich, P., Vethamony, P., Babu, M.T. and Pokratath, P., 2009a. *Seasonal sea level variability and anomalies in the Singapore Strait.* Proceedings of third International Conference in Ocean Engineering. ICOE-2009. Subramanian, V.A., Nallayarasu, S. and Sannasiraj, S.A. (edits), IIT, Madras, India, 874-880.

Tkalich, P., Vethamony, P., Babu, M.T., Pokratath, P. and Zemskyy, P., 2009b. *Sea level anomalies in the Singapore Strait due to storm surges of the South China Sea: the monsoon regimes*. Unpublished manuscript.

Twigt, D., 2007. *MHBox: Seasonal, climatological boundary forcing for the Singapore Regional Model.* Report No. X0349 for WL|Delft Hydraulics.

Urban Redevelopment Authority of Singapore, 2008. *Singapore Master Plan*. [Online] Available at http://www.ura.gov.sg/MP2008/ (Accessed on 20 May 2010).

Vatvani, D.K., Gerritsen, H., Stelling, G.S. and Krishna Rao, A.V.R.,2002. *Cyclone-induced storm surge, flood forecasting system for India.* In Solutions to Coastal Disasters, Ewing L, Wallendorf L (eds). ASCE: San Diego, Reston, VA; 473–487.

Weibull, W., 1951. *A statistical distribution function of wide applicability.* J. Appl. Mech.-Trans. ASME 18 (3), 293–297.

Williams, J., 2004. *Why don't certain areas in Asia, like Singapore, have typhoons, tornadoes or other disastrous weather?* USAtoday.com [Online] http://www.usatoday.com/weather/resources/askjack/archives-hurricane-science.htm. (Accessed 18 February 2010).

Wong, P.P., 1985. *Singapore.* In The world's coastline. Bird, E.C. and Schwartz, M.L. (edits). Van Nostrand Reihold, New York.

# Appendix A. Return period of a near equatorial typhoon near Singapore derived by Chang et al. (2003)

Data used: NCEP/NCAR data 1951/1952-2001/2002 (**51 boreal winters**)

Three components required to form a tropical cyclone in this region:

1) **Strong persistent cold surge** which contribute to the "spinning top effect"
2) **Borneo vortex** which moves over to water (open sea region in the southern end of the South China Sea) and stay for **four days**
3) Other general factors contributing to the development of a tropical cyclone

## Strong persistent cold surge

The surge index (average of all northeasterly wind components) is calculated in the dash box in Figure A.1 (upstream from the region of Borneo vortex) and summarized in Table A.1. Considering the minimum duration of the persistent surge is **7 days**, there are a total of **61** persistent surge events which added up to **582 days** of persistent surges. With the assumption of a three day overlap between the vortex and the surge to develop into a tropical cyclone, the last 2 days of each surge will be sufficient, which then left with **460 days** (Table A.1). The total number of boreal winter days is **4590 days** (3 months x 30 days x 51 winters) between 1951/52 and 2001/02.

> Probability of persistent cold surge = 460/4590 = 0.10 = **10%** of boreal winter days

If the minimum duration of persistent surge is reduced from 7 days to 5 days,

> Probability of persistent cold surge = 625/4590 = 0.14 = **14%** of boreal winter days

## Borneo vortex

During the **51** boreal winters, there are only **six** occurrences of Borneo vortex centre stayed continuously for **4** days or more in the southern end of the South China Sea (southwest box in Figure A.1).

> Probability of a pre-existing Borneo vortex stayed in the open water region continuously for 4 days = 6/51 = 0.12 = **12%** in a given year

## Other general factors

For a pre-existing disturbance to develop into a tropical cyclone, several factors such as background shears of wind and vorticity, upper level divergence, and a variety of environmental factors (Anthes, 1982 and McBride, 1995). The percentage of pre-existing synoptic disturbances developing into tropical cyclones in the more favoured tropical cyclone basins of western Pacific and North Atlantic ranges between **10-30%** (average is **20%**) during their respective tropical cyclone seasons.

## Return period

Return period = P(cold persistent surge which can contribute to tropical cyclone development) x P(Borneo vortex staying on water long enough) x P(development of tropical cyclone due to other general factors)

For at least **7** days of persistent surge,

Return period = 0.10 x 0.12 x 0.20 = 0.0024 = 0.24% a year which is about **1 in 400 years**

For at least **5** days of persistent surge,

Return period = 0.14 x 0.12 x 0.20 = 0.0034 = 0.34% a year which is about **1 in 300 years**

To be more conservative, the criterion for the duration of the vortex staying on water is reduced from 4 days to 3 days and the occurrences during the 51 boreal winters are increased to **21**.

P(Borneo vortex on water) = 21/51 = 0.41 = **41%** in a given year

For at least **7** days of persistent surge,

Return period = 0.10 x 0.41 x 0.20 = 0.0082 = 0.82% a year which is about **1 in 120 years**

For at least **5** days of persistent surge,

Return period = 0.14 x 0.41 x 0.20 = 0.0115 = 1.15% a year which is about **1 in 90 years**

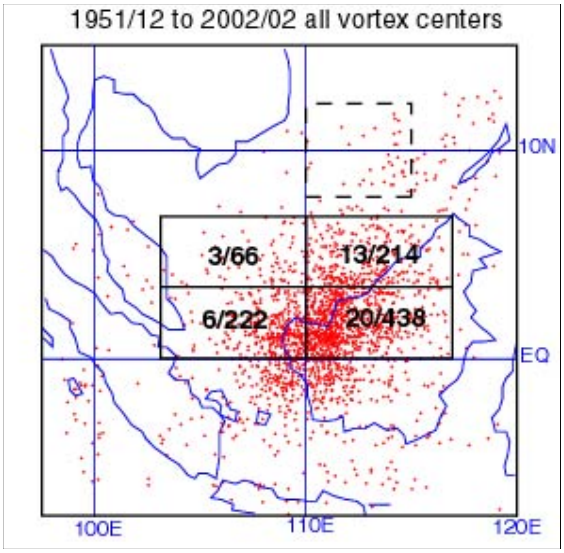


**Figure A.1 Location of NCEP/NCAR 925 hPA counterclockwise circulation centers during the 51 boreal winters. The four sub-regional boxes are enclosed by equator - 7°N, and 103°E – 117°E. The internal partitions are 3°N and 110°E. The first number in each box indicates the frequency of persistent 925 hPA cyclonic circulation center that lasted for 4 days or more, based on the 1951/52-2001/02 DJF NCEP/NCAR 2.5 x 2.5' reanalysis. The second number is total number of days a center is identified. The heavy dashed box indicates the area in which the northeasterly component of QuikSCAT winds to produce the surge index.**

**Table A.1 The frequency of surge durations. The first column is the number of consecutive days (duration) that the northeast surge index ≥ 10 ms-1 at least once during each day of the duration. The second column is the total number of events associated with the duration. The third column is the cumulative number of events that lasted for at least the duration, and the fourth column is the maximum value of surge index among surges of the duration.**

| Surge duration | Number of events | Cumulative no. events | Max. Surge index | Surge duration x number of events for duration ≥ 7 days | Surge duration x number of events for duration ≥ 5 days |
|---|---|---|---|---|---|
| 1 | 151 | 449 | 13.0 | | |
| 2 | 87 | 298 | 13.6 | | |
| 3 | 62 | 211 | 14.3 | | |
| 4 | 40 | 149 | 15.3 | | |
| 5 | 27 | 109 | 15.0 | | 135 |
| 6 | 21 | 82 | 15.8 | | 126 |
| 7 | 11 | 61 | 14.2 | 77 | 77 |
| 8 | 13 | 50 | 16.5 | 104 | 104 |
| 9 | 15 | 37 | 15.1 | 135 | 135 |
| 10 | 6 | 22 | 15.4 | 60 | 60 |
| 11 | 6 | 16 | 15.1 | 66 | 66 |
| 12 | 4 | 10 | 16.0 | 48 | 48 |
| 13 | 2 | 6 | 15.2 | 26 | 26 |
| 14 | 1 | 4 | 14.3 | 14 | 14 |
| 15 | 0 | 3 | 0.0 | 0 | 0 |
| 16 | 1 | 3 | 14.6 | 16 | 16 |
| 17 | 1 | 2 | 14.6 | 17 | 17 |
| 18 | 0 | 1 | 0.0 | 0 | 0 |
| 19 | 1 | 1 | 14.9 | 19 | 19 |

# Appendix B. Holland's model (1980)

The wind profile in Holland's model is expressed as

$$V_g = \sqrt{\frac{AB(p_n - p_c)\exp\left(-\frac{A}{r^B}\right)}{\rho_a r^B} + \frac{r^2 f^2}{4}} - \frac{rf}{2} \quad \text{(B.1)}$$

where $V_g$ is the gradient wind at radius $r$, $f$ is the Coriolis parameter, $\rho_a$ is the density of air (assumed to be constant at 1.10 kg/m$^3$), $p_c$ is the central pressure, $p_n$ is the ambient pressure (theoretically at infinite radius, however in this model the average pressure over the model domain is used), and $A$ and $B$ are scaling parameters. Physically, $B$ defines the shape of the profile and $A$ determines its location relative to the origin (Figure B.1). With the same $B$ and $v_{max}$ values, the $RMW$ can vary with different $A$ and $RMW$; $A$ basically determines the wind gradient along the profile (gentle or steep sloping), while $B$ gives rise to the width of high wind near $RMW$ (thickness of eyewall).

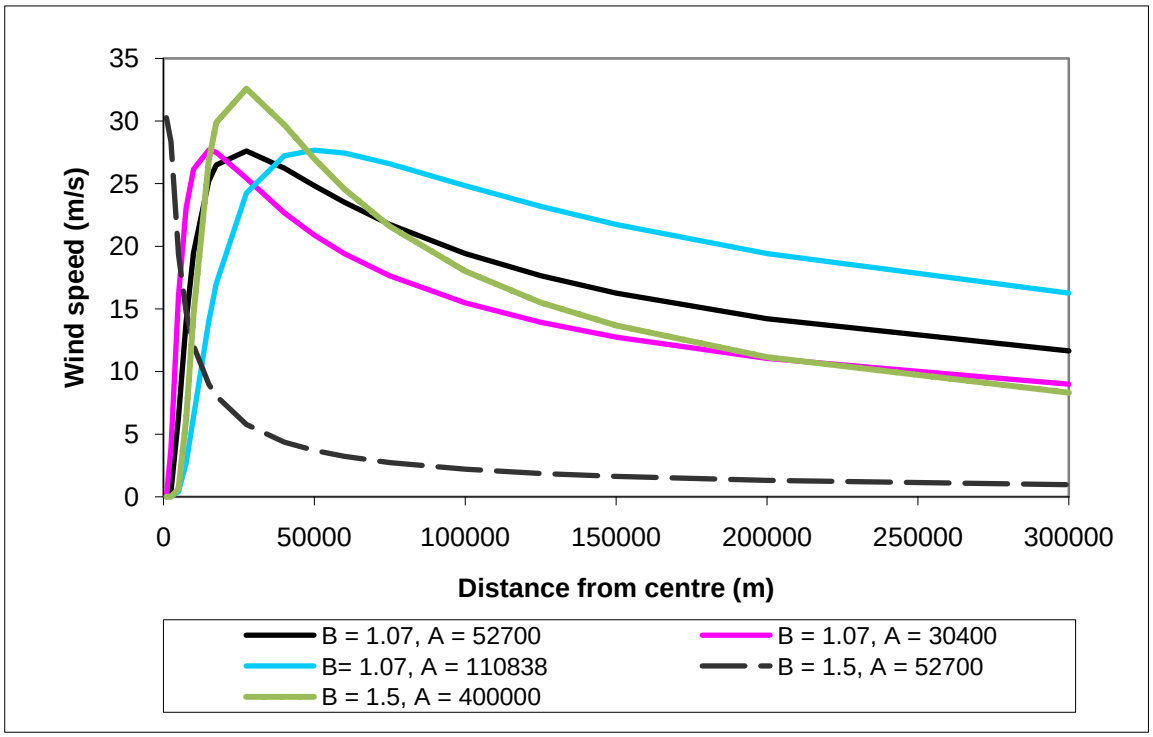


**Figure B.1 Example of computed wind speed with various B and A combinations**

In the region of maximum winds, the Coriolis force is small in comparison to the pressure gradient and centrifugal forces and the air is in cyclostrophic balance. Equation B.1 then becomes

$$V_c = \sqrt{\frac{AB(p_{drop})\exp\left(-\frac{A}{r^B}\right)}{\rho_a r^B}} \quad \text{(B.2)}$$

to express these cyclostrophic winds. The pressure drop term $p_{drop}$ is introduced to represent $(p_n - p_c)$ for simplicity. By setting $dV_c/dr$ equals to zero, the radius of maximum winds ($RMW$) is

$$(RMW) = A^{1/B} \quad \text{(B.3)}$$

The $RMW$ is independent of the relative values of ambient and central pressure and is defined entirely by the scaling parameters $A$ and $B$. Substituting equation 3.3 back into equation B.2 yields an expression for maximum wind speed as

$$v_{max} = \sqrt{\frac{Bp_{drop}}{\rho_a e}} \tag{B.4}$$

where $e$ is the base of natural logarithm. Parameters $A$ and $B$ can now be expressed as functions of measurable quantities;

$$A = (RMW)^B \tag{B.5}$$

$$B = \frac{v_{max}^2 \rho_a e}{p_{drop}} \tag{B.6}$$

and the central pressure drop is given by

$$p_{drop} = \frac{\rho_a e v_{max}^2}{B} \tag{B.7}$$

## Synthesis of cyclone wind and pressure field in WES

In order to predict a storm surge, measured or forecasted physical quantitative properties of the cyclone (usually reported by the cyclone advisories) have to be provided to compute the wind and pressure fields. Based on these properties, the parameters $A$ and $B$ will be determined and the wind and pressure drop will be synthesized using the Holland's model on a circular polar co-ordinate or 'spiderweb' type grid (Figure B.2).

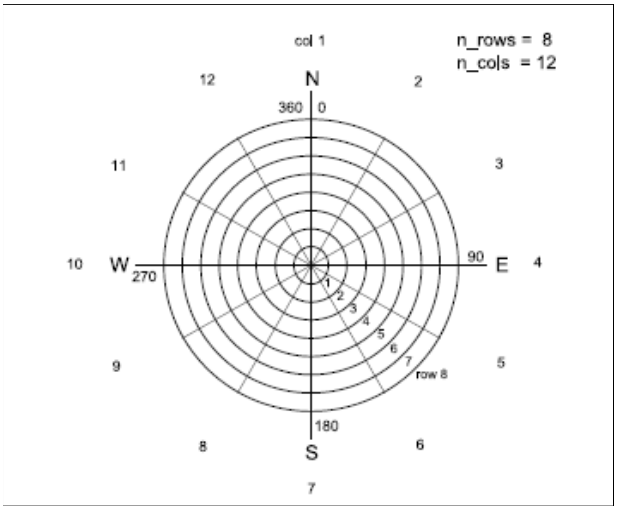


**Figure B.2 shows the definition of the spiderweb grid (Adopted from Deltares|Delft Hydraulics, 2009b)**

The displacement of the cyclone in the simulation is demonstrated by the position change of the entire circular grid in the Delft3D-FLOW model. This elegant technique has helped to minimize data storage by adopting the required data on a moving polar co-ordinate grid centred on the centre of the cyclone.

According to (Deltares|Delft Hydraulics, 2009b), there are three options to specify the cyclone parameters to synthesize the wind and pressure field of the cyclone.

1. $v_{max}$ and $p_{drop}$

2. Radius of 35, 50 and 100 knots wind
3. $v_{max}$ and Holland's parameter $A$ and $B$

Options 1 and 2 require values that are usually provided by cyclone advisories, especially for the strong cyclone. As for option 3, the value of $B$ may be already determined from climatological data of some regions and the value of $A$ is very unlikely to be known. Option 3 is useful if one wants to synthesize an arbitrary cyclone of a certain radius of maximum wind which will be applied later in Section 3 and 4.

# Appendix C. Tidal constituents used in tidal prediction

| | |
|---|---|
| MSM | M2 |
| MM | MSP2 |
| MSF | MKSW |
| MF | M2(KS)2 |
| SNU | 2SN(MK)2 |
| SN | SNM2 |
| MFM | L2 |
| 2SM | T2 |
| 2SMN | SW |
| NJ1 | R2 |
| SIGMA1 | K2 |
| Q1 | MSNU2 |
| NUK1 | MSN2 |
| O1 | ETA2 |
| MP1 | 2SM2 |
| NO1 | SKM2 |
| PI1 | MQ3 |
| P1 | MO3 |
| SE | SO3 |
| K1 | MK3 |
| RP1 | SK3 |
| KP1 | MN4 |
| J1 | M4 |
| SO1 | 2MKS4 |
| OO1 | 3MN4 |
| 2NSW | MS4 |
| O2 | MK4 |
| MU2 | 2MN6 |
| SNK2 | M6 |
| N2 | 2MS6 |
| NU2 | 2MK6 |
| 2KN2SW | 2SM6 |
| MA2 | |

# Appendix D. Hindcast using Option (2) Vmax and RMW (by inputting Holland's parameter A and B)

This option gives unrealistic surge (very high) results (Figure D.1) especially for JTWC. This is due to the impractical value of $B$ (less than 1) yielded by the $RMW$ with the reported $v_{max}$ and $P_{drop}$ (Equation B.5 and B.6). Also the typhoon eye's radius (directly proportional to $RMW$) given by JMA is too large; 200 km which is unrealistic in this region.

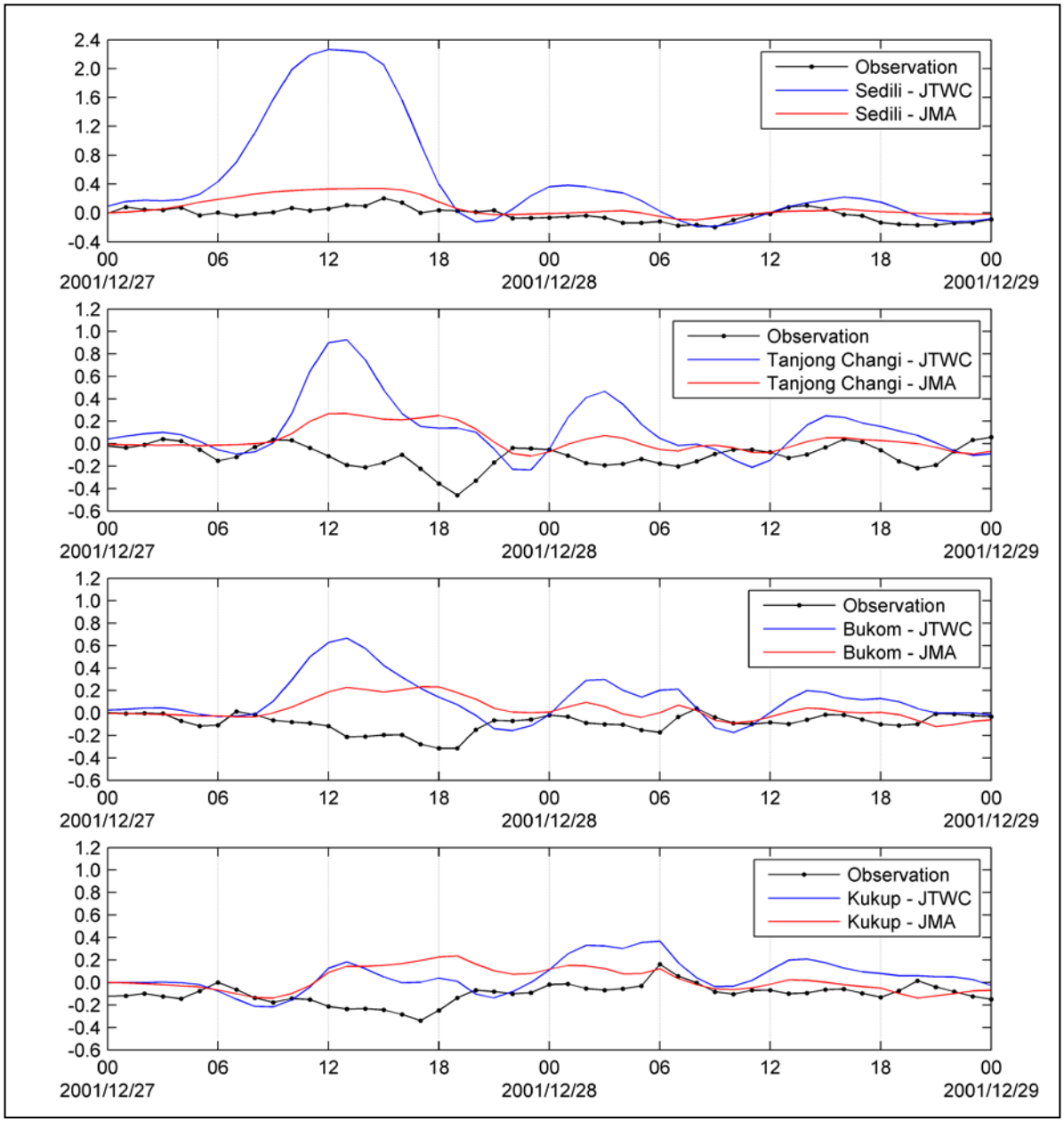


**Figure D.1 Simulated surge level (metres) using typhoon information provided by JTWC and JMA using WES Option (2)**

# Appendix E. Surge propagation in the hindcast of typhoon Vamei Simulation(4)

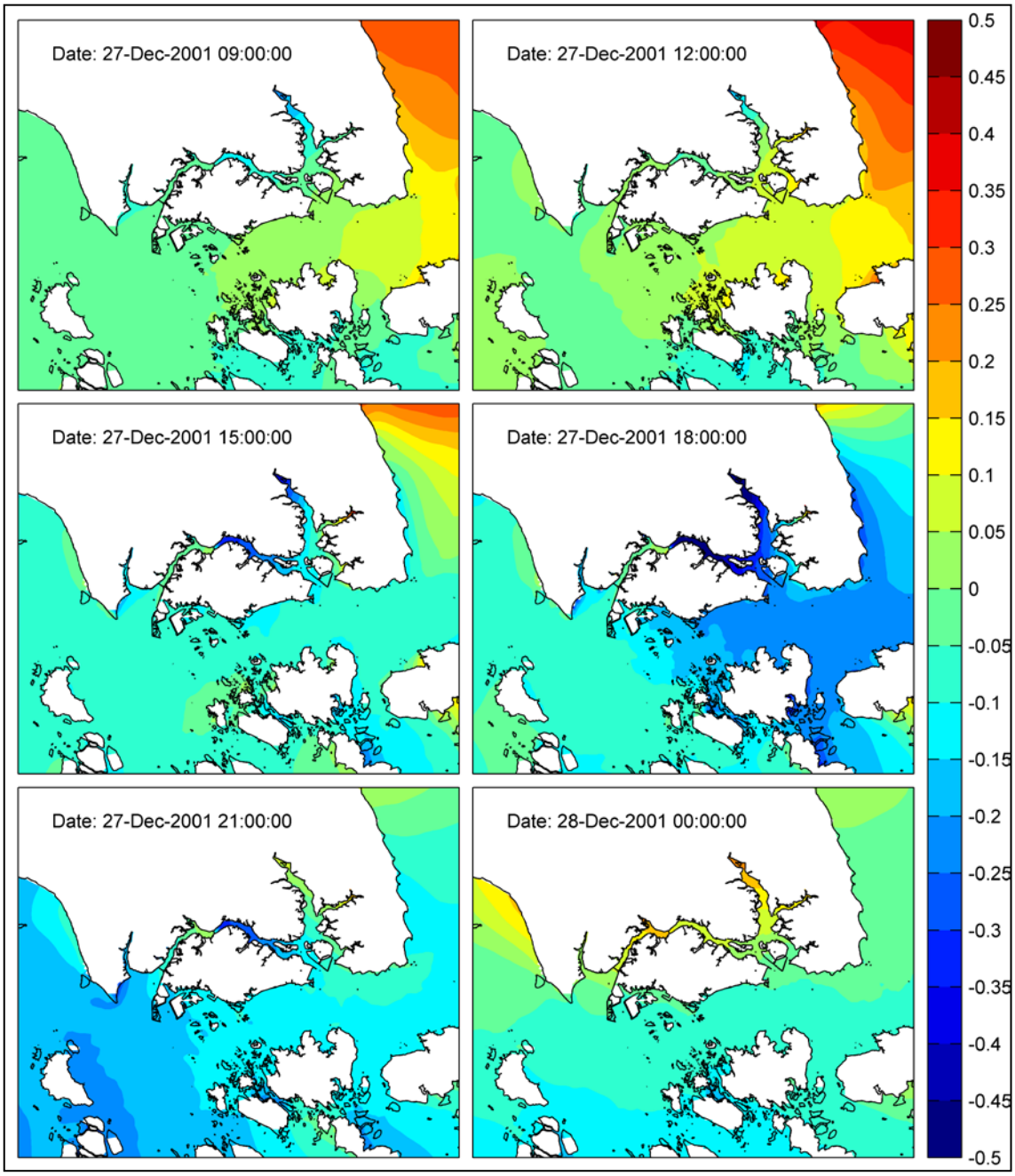


**Figure E.1 Surge level in metres 09:00 27th to 00:00 28th December of Simulation (4)**

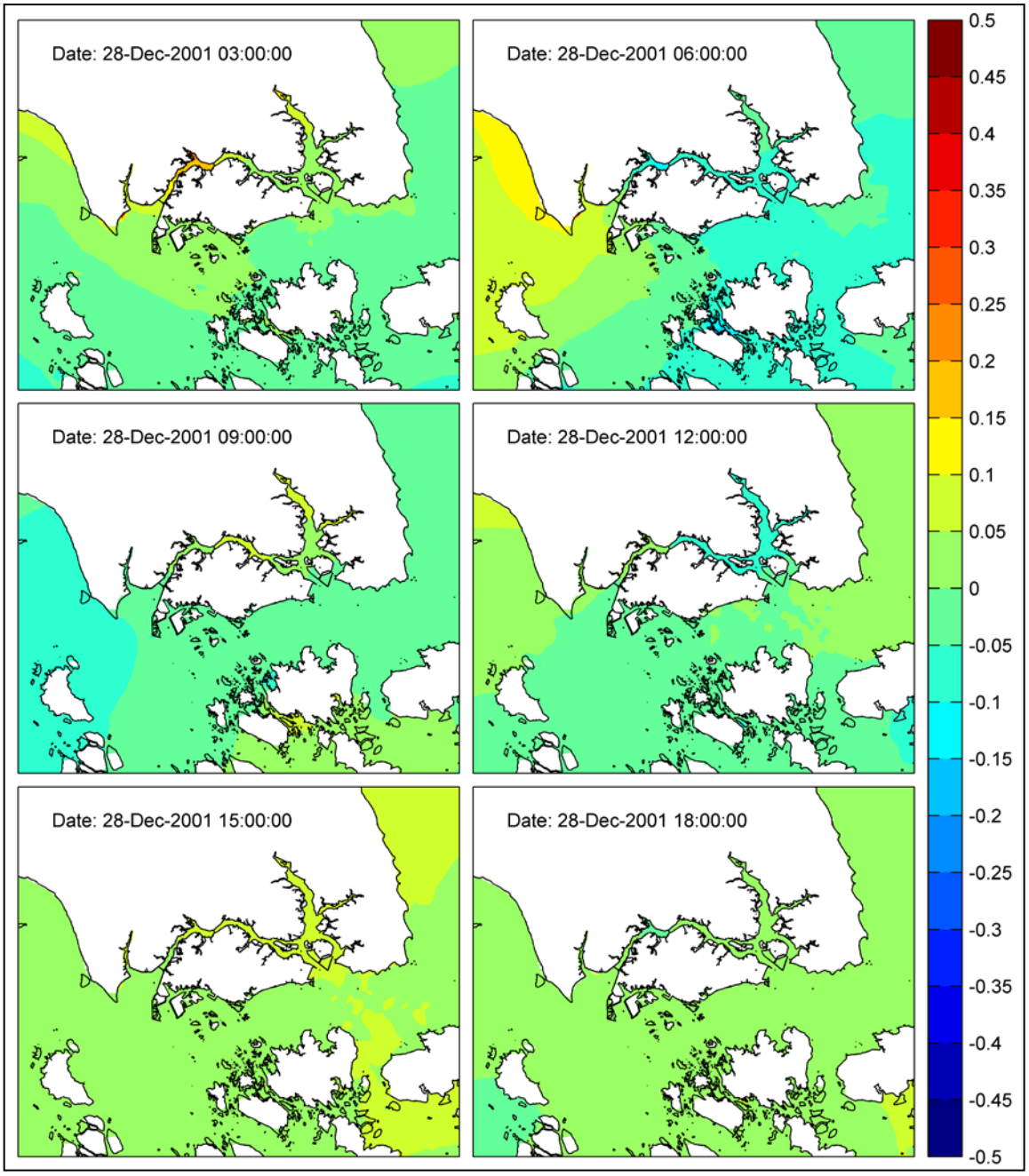


**Figure E.2 Surge level in metres 03:00 to 18:00 28th December of Simulation (4)**